

Chapter 1 Introduction

1.1 Summary

Geophysical data acquired at Vinton Dome, a piercement dome located in Calcasieu Parish, southwest Louisiana (Figure 1), in 1997 included a 3-D surface seismic, two 3-D vertical seismic profiles (VSP), and other geophysical data. Complementing the geophysical data are over a hundred well logs. The large database provided me with an excellent opportunity to investigate geophysical problems that exist in the Vinton Dome survey. The surface seismic data were processed commercially in 1998. The final processing step was to prestack time migrate (PSTM) the data. Data quality was regarded as meeting, if not exceeding, industry standards yet the data lacked the fidelity to accurately image the flanks of the salt dome and small, compartmentalized faults that had been mapped using well logs. A motivation for the study was poor image fidelity.

Image fidelity as it relates to this study refers to issues concerning the correct spatial placement of seismic events and the resolution of those events. Reasons for a lack of high fidelity typically relate to both geology and processing. PSTM is best suited for layer cake geology with constant lateral velocities. The Vinton Dome 3-D surface seismic survey contains relatively flat strata, i.e. layer cake, with a salt dome and steeply dipping strata in the center of the survey. Steeply dipping strata and salt are the types of geology that invoked a reassessment of the processing, especially the migration, as a cause of less than optimal fidelity.

At Vinton Dome, where salt approaches the surface to within a few hundred feet, P-wave seismic velocities can double in the salt compared to the adjacent sediment. Strong lateral velocity changes in a seismic survey require prestack depth migration (PSDM) (Yilmaz, 1987), illustrating the coupling of geology and processing. I used PSDM to achieve improved fidelity and applied a basic pre-migration processing flow to the data that was structured to maintain a broadband characteristic to the data. Data were PSDM using a Kirchhoff migration. In any PSDM the accuracy of the image depends on the velocity model used in the migration, so I designed an innovative approach to velocity modeling and compared it to the conventional method of velocity modeling. Attribute analysis, velocity analysis, and the use of well data as quality control (QC) helped to insure achievement of the goal of this study. The goal of this study was to assess and improve the spatial fidelity of seismic imaging through a deterministic evaluation of surface seismic data with velocity modeling and attribute analysis.

1.2 Overview of the Study

The study is divided into seven chapters, an introduction, a discussion of the geology of Vinton Dome, a description of the pre-migration processing, velocity modeling and migration, attribute analysis used for QC, a chapter on interpretation and conclusions and discussion.

1.2.1 Geology

Vinton Dome is a piercement salt dome located in the upper continental margin of the Gulf of Mexico. Sediments surrounding the dome range in age from Oligocene to Miocene. Salt tectonics and deposition have influenced the structural characteristics surrounding the dome. Issues of interest are the depositional environments, salt tectonics and structure associated with the dome. Even though this is a mature basin with over one hundred years of geologic investigation, there are a number of geologic issues to be resolved.

1.2.2 Processing

An examination of shot gathers from the field data revealed the need for pre-migration processing. The most profound problem was high amplitude low frequency noise. To focus the study on velocity modeling and depth migration I used a simplistic approach to pre-migration processing. My main objective in processing was to maintain as high a bandwidth as possible and eliminate the noise. Testing and filtering data provided a data set to apply deconvolution and to calculate a residual static. Data were common mid-point (CMP) sorted and I used stacking velocities calculated using the velocity field from the PSTM. I gained CMP sorted data using a spherical divergence gain control and had both the datum static and residual static applied. Static corrected data were amplitude balanced using automatic gain control (AGC). These data then had a shot deconvolution applied and were filtered using a 5-6-70-80 filter. Filtered data had the first breaks muted and amplitude balanced again using AGC. These data were the input for the PSDM.

1.2.3 Velocity Modeling and PreStack Depth Migration (PSDM) of 3-D Surface Seismic Land Data

Since the early 1990's prestack depth migrations (PSDM) have been routinely applied to 3-D seismic data but almost exclusively to marine data. There are several reasons for this, uniform acquisition, long offsets, and generally higher data quality. Essential to achieving the robust character of PSDM applied to 3-D surface seismic land data is the ability to derive an initial sediment velocity model that minimizes the adverse effects of degraded data quality. An accurate initial sediment velocity model is necessary for several reasons but primarily because it is the most critical step in PSDM. I used a novel, non-seismic approach to generate an initial sediment velocity model. I assessed this method by a comparison of the fidelity of the PSDM volume generated in both a PSTM volume and a PSDM volume migrated using a traditional seismically derived initial sediment model.

Differences between 3-D marine data and 3-D surface seismic land data result in marine data that are generally higher quality. Acquisition issues range from the uniform grid used to acquire marine data that allows for more accurate processing to the variety of cultural influences that adversely impact land data. Geology can be an issue as demonstrated in the complexity of deriving the refraction static for land data. Differences in deriving a refraction static are apparent when considering the impact of the weathering

layer in land data that in extreme cases is profound compared to marine data that are impacted less severely, if at all, by a weathering layer. As a result, acquiring higher quality data in the marine setting means that marine data tend to be more accurately processed yielding superior data.

1.2.4 Velocity Modeling

One processing application derived nearly exclusively from marine data is velocity modeling for PSDM. With computing expenses no longer an issue it is economically reasonable to investigate innovative velocity modeling for 3-D surface seismic land data. Deriving an accurate initial sediment velocity model was my main objective in this study. Investigating current practices, identifying problems with 3-D land surface seismic data, and devising an approach that integrates the efficiency and accuracy of current methods that overcomes the limitations imposed by data quality were some of the issues I pursued to achieve this objective. Using sonic logs acquired over Vinton Dome I derived an initial sediment velocity model. I improved the final migrated volume by building the initial sediment velocity model from sonic logs and was able to show improvements in the fidelity over both the PSTM volume and a volume migrated with a seismically derived velocity model.

1.2.5 Attribute Analysis

Coherence is an attribute typically used for interpretation. I used coherence as both an interpretation tool and a QC tool. In the PSTM volume the fidelity began to diminish in

the coherence cube after about one second. Based on this observation I used coherence to qualitatively assess the fidelity of data to determine the most accurate velocity model.

My objective was to assess the value of attributes as a QC tool.

1.2.6 Interpretation

I used the interpretation of the well-based PSDM to gain a better understanding of the geology. One of my objectives was to verify improved fidelity by providing a more detailed interpretation and to gain new insights into the geologic processes associated with Vinton Dome. I used well ties and synthetics to assess the accuracy of interpretations. Coherence also aided in my interpretation of salt and faults, and as a QC tool.

Improved resolution of the Vinton Dome 3-D surface seismic data demonstrates the value of PSDM using a well-based velocity model in 3-D land surveys with piercement salt domes to provide a greater understanding of geology. Improved resolution translates to better interpretations that are necessary for understanding the evaluation of salt tectonics, structural details, and complex stratigraphy.

1.3 Conclusions and Discussion

Assessing and improving the spatial fidelity of seismic imaging through a deterministic evaluation of surface seismic data with velocity modeling and attribute analysis was the goal of this study. I demonstrated a novel approach to modeling velocities using well

logs as being an effective approach to PSDM where the flanks of the dome were the primary imaging objective.

I evaluated the effectiveness of the approaches used on the fidelity of the data. I used various data such as well logs and attributes to aid in the interpretation of the seismic data. Benchmarks to determine the effectiveness were the ability to improve imaging close to the salt flanks, the ability to image small compartmentalized fault blocks, detailed faults, and stratigraphic features such as stream channels that were not imaged using PSTM.

To achieve the stated goal of this study I fulfilled objectives in processing, velocity modeling, interpretation and use of attributes as a QC tool. My conclusions are that using well logs to derive an initial sediment velocity model used for a PSDM provided greater fidelity in 3-D surface seismic land surveys with strong lateral velocity variations. I also concluded that the higher fidelity resulted in a greater signal to noise ratio, and improved interpretations over PSTM and standard PSDM. I used the enhanced fidelity for a more accurate interpretation to improve the understanding of the Vinton Dome geology.

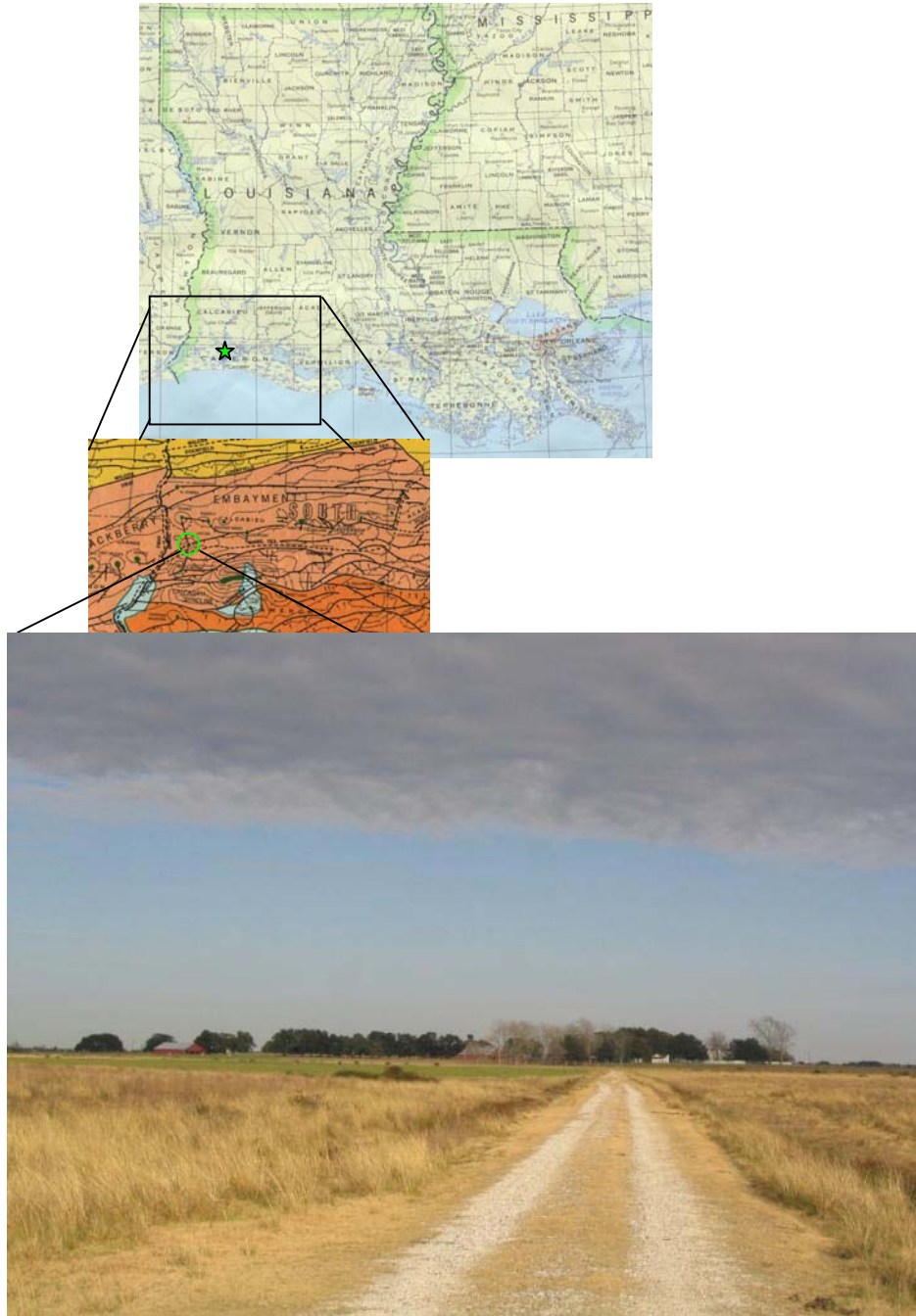


Figure 1. Location map of Vinton Dome, Calcasieu Parish, southwest Louisiana.

Chapter 2 Geology of Vinton Dome

2.1 Introduction

Vinton Dome is a large faulted salt diapiric structure located in southwestern Louisiana on the Upper Continental Margin of the Gulf of Mexico Basin. Strongly influencing the character of this structure, and the region, is tectonics, differential depositional history, salt deformation and fault development. With over one hundred years of drilling, and subsequent subsurface exploration, a large volume of information is available to resolve the geological setting that has influenced the creation of and unique character of the Vinton Dome area.

Salt bed deformation has produced a large part of the structural fabric of the northern gulf margin (Martin, 1976). The occurrence and movement of salt resulted in the formation of numerous syndepositional and post-depositional swells and diapiric structures (Humphris, 1978) that are of great economic importance to petroleum exploration in the region. Different mechanisms for salt movement have been proposed (Nelson, 1991) that impact sediment deposition and structural dynamics.

Deposition of clastic sediments is also fundamental to understanding the geology. High porosity sands with high permeabilities, like those that exist in the Vinton Dome area, are especially interesting because they can be prolific petroleum reservoirs. Deposition of

sediments is also important because it modifies the movement of salt and the movement of salt will alter sediment deposition.

One of the more challenging aspects to describing the geology of Vinton Dome is properly identifying the cross-cutting relationships between regional-scale structures and salt bodies. Unraveling the relative timing of the structures is necessary to understanding the relationship between faulting and emplacement of salt bodies.

The Neogene was a period of significant salt tectonics, growth fault development, and maximum clastic deposition along the outer shelf and upper slope that occurred in the northern Gulf of Mexico Basin (Lowerie, 1994). All of these processes took place synchronously (Lowerie, 1994), possibly linking them.

2.2 Basin Formation

Bounding the Gulf of Mexico Basin to the east is the Florida Carbonate Platform, to the south by the Yucatan Carbonate Platform (Figure 2) (Ewing, 1991), to the west by the Chiapas massif, the Sierra Madra Oriental, and the eastern edge of the Coahuila Platform in Mexico. Northern limits are defined, from west to east, by the structural limits of the Marathon uplift, the Ouachita orogenic belt, the Ouachita Mountains as delineated by the Mexia/Talco fault, the Central Mississippi deformed belt, and the southern extent of the Appalachian Mountains. There is no distinct structural limit to define the boundary between the southern Appalachians to the Atlantic Ocean.

The Gulf of Mexico Basin contains Upper Triassic to Holocene sediments. Modifying the Upper Triassic to Holocene sediments are second-order structural elements such as arches and uplifts. Upper Triassic to Holocene sediments forms an unconformity with the pre-Triassic basement. The understanding of this contact is poor because of a lack of outcrops around the basin and little drilling information from within the basin.

Geophysical data indicates that sediments overlying an oceanic-type crust reach depths of 12-16km. The basement is also composed of transitional crust, rifted and stretched continental crust, and continental crust composed of a variety of igneous, metamorphic and sedimentary rocks. Documentation of basin formation from the late Paleozoic through the beginning of the Mesozoic is thorough (Winker and Buffler, 1988) (Salvador, 1987) (Galloway, 1989).

Characterizing the Cenozoic history in the northwest Gulf of Mexico Basin is rapid ongoing sediment input and thick prograding depositional sequences with extensive gravity deformation (Galloway, 1989). Structural development, clastic sediment deposition, and salt tectonics in the Cenozoic were interrelated. Prograding sediments were deposited over the underlying autochthonous Jurassic salt and produced a variety of structural styles controlled by the distribution of salt structures, varying depositional environments, and the amount of salt withdrawal from displaced allochthonous salt sheets (Diegel *et al.*, 1995).

2.3 Stratigraphy

Salt accumulated into the large Paleo-Gulf of Mexico basin during the Jurassic. Basin analysis suggests the region subsequently divided into two separate basinal features (Humphris, 1978) (Figure 3). By the end of the Jurassic, all of the structural and stratigraphic features seen today were in place, but accentuation and modification of these features continued over time (Salvador, 1987).

During the late Jurassic, the northern Gulf of Mexico Basin evolved from a dominantly progradational setting to late-stage aggradation. The complexity of the Mesozoic GOM basin has resulted in differing models to describe it. Some aspects of the early GOM development are still not fully understood as can be seen by the theoretical problem that exists in explaining the mechanisms for drowning carbonate margins and platforms (Schlager, 1981). Another issue of interest is the relationship between the carbonates and salt. Growth faulting and rapid subsidence of the shelf margin results from bathymetric relief over a mobile belt (Winker, 1982), yet Winker's (1982) model appears to be incompatible with underlying sequences of mobile evaporates (Winker and Buffler, 1988). Such issues illustrate the need for a more detailed understanding of the interrelationships of salt, stratigraphy and structure.

Thick prograding depositional sequences deformed by gravity loading characterize the Cenozoic history of the northwestern Gulf of Mexico Basin. Stratigraphic sequences

developed from repetitive episodes of basin-margin offlap bracketed by transgressive events that produced widespread depositional platform flooding. Typical sequences observed include the progradational depositional systems, associated subaerial erosional surfaces, and syndepositional structural discontinuities. Related to first-order depositional episodes of the Paleogene and many episodes of the Neogene are large-scale North American plate tectonic events such as the Laramide Orogeny. These episodes affected the changes in the paleogeography of the northwest Gulf of Mexico coastal plain. Later Neogene successions in the depositional history were eustatically controlled. Although often obscured, the short-term eustatic changes in sea level may overprint the first-order stratigraphic events (Galloway, 1989). As the underlying thick sediment wedge prograded southward, loading deformed the salt and squeezed it into a distal wedge (Salvador, 1987) (Figure 4).

The Vinton Dome contains stacked sequences of Cenozoic sediments surrounding an intensive Jurassic salt diapir. Of primary importance to this study is Tertiary system Oligocene and Miocene series. Formations in the Oligocene, in ascending order, are the Vicksberg Group, the Frio Formation, and the Anahuac Formation. Miocene formations are simply designated as the Lower, Middle, and Upper Formations.

Sediments deposited during the Oligocene formed in marginal marine and shallow marine environments. Sediments in flux came from the Ouchita Mountains, the southern Cordillera, and the southern Appalachians. The Vicksberg Group includes sediments

between the underlying Jackson Group and the overlying lower Frio. This interval varies from 200 and 300 feet thick in the Vinton Dome area and is composed of dark gray, calcareous shale with occasional streaks of siltstone deposited in an outer neritic environment. A characteristic faunal marker for the Vicksberg is the *Textularia warreni* (Tabbi-Anneni, 1975).

Overlying the Vicksberg Group is the Frio Formation. Sediments in the Frio have an average thickness of 1500 feet and are composed of dark shale and silt with occasional massive sand beds. The Frio subdivisions are the lower, middle and upper members. Both the lower and middle Frio is composed primarily of bathyal shale deposited on the continental slope. The lower Frio is approximately 400 feet thick and is composed of thin sand stringers. The middle Frio is approximately 300 feet thick and has thick sand stringers. Three faunal markers in the lower Frio are, in ascending order, *Discorbis "D"*, *Nodosaria blanpiedi*, and *Nonion struma*. An index fossil, *Marginulina texana* marks the top of the middle Frio.

Deposition of the 800 feet thick upper Frio occurred in both an inner neritic environment, consisting of coarse sands, inter-fingered with an outer neritic environment composed of shale. Two characteristic microfossils found in the upper Frio include *Cibicides hazzardi*, found in the lower part, and *Camerina "A"*, typical of the upper part of the section. A shale zone overlain by a continuous sand bed characterizes the lower portion

of the upper Frio. Overlying the lower portion of the upper Frio are two thick sand beds separated by a shale bed (Tabbi-Annani, 1975).

At the upper Oligocene series, the Anahuac Formation overlies the Frio Formation and underlies the lower Miocene. Deposition of the 1400 feet thick Anahuac occurred in an outer neritic environment. Sediments are composed of calcareous shales with sporadic alternating sand (Tabbi-Annani, 1975). There are three biostratigraphic units in the Anahuac. In ascending order, these include the *Marginulina*, the *Heterostegina*, and the *Discorbis* zones (Tabbi-Annani, 1975).

Overlying the Anahuac formation is the Miocene Series. Deltaic and continental environments typify this 7000 - 7500 feet thick interval. Sediments are composed mainly of massive sands with periodic shale breaks. Common microfossils found in the Miocene are *Operculinoides* sp. and *Amphistegina* sp. (Tabbi-Annani, 1975).

2.4 Salt Tectonics

Understanding mechanisms for salt emplacement and movement are important to understanding the formation and dynamics of individual salt bodies such as Vinton Dome. Developing a comprehensive model requires accurate evaluation of events that led to the current salt geometry. Another important aspect of model development is proper identification of key stress, loading, tectonic mechanisms, and ways to distinguish which mechanisms were factors at what times. Geologic processes such as depositional

loading and faulting are the major processes that typically affect the evolution of salt bodies. Shown in Figure 5 (see below) are types of salt features recognized in the Upper Continental Margin of the Gulf Coast Basin.

Salt body formation is generally in restricted basins and deposited as sub-horizontal beds. Salt has a low density and yield strength, and will flow in the solid state by gravity alone. Factors influencing flow are temperature, pressure, and the presence of impurities. Water will increase diffusive flow and non-evaporite minerals will reduce plasticity. Salt flow will result in the transformation of a tabular body into a variety of geometric structures. Salt beds generally deform into concordant low-amplitude structures such as salt anticlines, rollers and pillows that may evolve into discordant high-amplitude diapiric structures such as salt walls, stocks, nappes, and detached teardrop units, and may eventually form into extrusions (Figure 5) (Jackson and Talbot, 1986). Deformation can stop at any time and reactivate at a later period. A diapiric structure is the reference to a salt body that either pierces or appears to have pierced the overburden. A salt dome is the term applied to diapirs such as salt pillows or stocks and their surrounding arched strata (Jackson and Talbot, 1986).

Based on experimental modeling, one classification system of diapirs is in three stages. Reactive diapirs that initiate and grow under grabens formed by extension of the overburden, active diapirs that rise by pushing aside thinned overburden, and passive diapirs that grow by downbuilding (Vendeville and Jackson, 1992). Downbuilding

structures form by the differential sinking of some of the unconsolidated water-saturated overburden until it becomes denser than salt (Talbot, 1995). These three stages of diapirism often represent various stages of the development of a salt body, or if the overburden is thin or uneven the entire process may be passive (Rowan, 1995).

Dips of salt-sediment contacts are a function of two processes, the net accumulation of overburden and the net relief of overburden. Net accumulation of overburden, A , is equal to deposition minus compaction and net increase in relief of salt structures, R , is equal to salt rise minus dissolution. Using a method developed by Talbot (1995), measurement of the dip of salt sediment contacts is a means to calculate a kinematic ratio of A/R and R/A (Figure 6). Using the calculated ratio is a method to identify the stage of diapirism (Figure 7). Talbot studied an example of calculating A and R to estimate the R/A ratio around domes, 1995, in East Texas. By increasing the resolution around the sediment salt interface, the potential for unraveling the history of dome development increases.

2.5 Structural Development

The structural evolution of the Upper Continental Margin of the Gulf of Mexico Basin is a function of the early tectonic history beginning in the Triassic, later salt formation, salt movement, and Tertiary depositional history. Processes involved in the structural development include the formation of salt bodies, extension updip in the form of growth faults, and downdip contraction. Describing the regional structural development of the

northern Gulf margin provides insights into the local structures in areas such as Vinton Dome.

Structures that developed in the stratigraphic interval from the Upper Jurassic through the Cenozoic formed resulting from sediment-driven gravity loading resulting from salt displacement and resulting from gravity spreading. Many of these structures have been imaged with 2-D seismic and interpreted from well data to include listric normal down-to-basin growth faults, roll over structures, en echelon faults, counter regional faults, and localized radial faults. Salt displacement has been modeled to be primarily driven by vertical sediment movement and is characterized by withdrawal and diapirism on the shelf and upper slope and by canopy emplacement and withdrawal on the middle to lower slope. Manifesting basinward gravity spreading is by large-scale updip growth faulting and downdip contraction (Peel, *et al.*, 1995).

Growth faults are listric normal faults that show an expansion or thickening of basin fill in their hanging walls as loading continues and the fault becomes displaced.

Identification of the displacement resulting from growth faults in the northern Gulf of Mexico Basin is by different contraction features at the base of the continental margin. Toe thrust-faults, fold belts, salt canopies, and salt deformations are the principal contraction features.

Dividing the Gulf of Mexico Basin into four provinces is the method of describing the structural components (Figure 8). Division of provinces is according to the timing of extension (Peel, *et al.*, 1995). Vinton Dome falls within the Central Province, dominated by isolated structural systems such as fault compartments and radial faulting associated with diapirs surrounded by areas of relatively simple structures such as extensional normal faults.

Understanding the relationships between salt flow and listric normal faults is essential in deciphering the complex structure of Vinton Dome. Pressure gradients resulting from the weight of overlying sediments are the source for salt flow in nonorogenic environments. Basinward movement of sediments above some decollement surface generates listric normal faults. In the Gulf of Mexico Basin, salt flow is a function of either differential sediment loading or the creation of a density gradient produced by denser sediments on top of less dense salt resulting in buoyant salt rise. Differential loading refers to the situation that occurs when two adjacent vertical columns of sediment of different mass cover a common level of salt and result from depositional variations. If sediments are less dense, then salt will tend to move out from under the salt high into the adjacent salt. Equal salt and sediment densities result in no salt movement. Higher sediment densities drive salt out of the salt bed into the salt high (Figure 9). Lateral extension will spread the salt and sediment layers over a larger area (Nelson, 1991).

Characterizing an early stage of active piercement is the development of thick sediment covering the salt with a normal fault bounding one side of the rising salt. As the diapir rises an elongate anticline forms on the footwall side of the fault in response to the intruding salt. As the dome continues to grow radial faulting will develop on the footwall side with subparallel faulting on the hanging wall side (Figure 10). Passive piercement or down building is characterized by structures that result from salt withdrawal. A common feature forms from the dragging due to sediment compaction around the dome and as a result, the dip of sediment beds around passive domes tends to be less than seen around active domes. Passive domes tend to form circular geometries as they develop. Faults around passive domes radiate out at high angles and tend to be largest near the salt (Figure 11). Radial faults forming in this manner are a response to the relative uplift of the sediments flanking the dome. Relative uplift is a response to the combination of the withdrawal of salt from its source layer, relative rise of the salt with respect to the source, and compaction and subsidence of sediments around the salt plug. Extensional stresses generated by the relative uplift around the circular plug tend to be oriented parallel to the salt sediment interface. Resulting faults that formed in response to this stress are perpendicular to this interface. If an active piercement structure phases into a passive piercement structure, the radial faults that develop in the passive phase generally have their footwalls toward the withdrawal flank that developed during the active phase (Nelson, 1991).

2.6 Geologic Modeling

Historically, models of the Gulf of Mexico Basin have progressively developed as new information has become available implying that detailed information has been acquired basinward. For example, to describe Gulf Coast salt structures the updip basin margin is a progression of low-relief structures that become high-relief salt stock structures on coastal Louisiana, and then develop into the salt structures found in the outer shelf and slope. A different approach is to analyze the salt structures in a reverse manner, start with the abyssal plain and work toward the coastal areas. Starting from the abyssal plain and working updip has the advantage of providing analogs of the early history of structures buried deeper updip from structures imaged on the modern slope. There are several reasons for using this approach. Starting from the most recent geology and moving towards the older geology provides the impetus to reevaluate less recently studied areas, such as the Vinton Dome area, and other inner shelf and onshore areas of the Gulf Coast. Such an approach also provides a modern perspective to establish a consistent comprehensive tectono-stratigraphic framework of the Gulf of Mexico Basin (Diegel, *et al.*, 1995).

In order to construct a regional framework of the Upper Gulf of Mexico Basin the complexity of structures must be resolved. The mechanisms of gravity spreading or gliding associated with the progressive tilting of the margin and gravity spreading of the salt layer under differential loading by prograding deposits (Letouzey, *et al.*, 1995) have helped to create the complexity of structures that vary both along strike and dip. There

are descriptions of eight distinct tectono-stratigraphic regions (Figure 12). These eight provinces are, from downdip to updip, the contractional foldbelt, tabular salt-minibasin, Pliocene-Pleistocene detachment, salt dome minibasin, Oligocene-Miocene detachment, Oligocene Vicksberg detachment, upper Eocene detachment, and Wilcox growth fault provinces. Areas dominated by listric growth faults soling on subhorizontal detachments and the large salt dome minibasin province divide the shelf and onshore areas.

Geographically the salt dome minibasin province subdivided into updip, eastern, and mid-shelf sectors (Diegel, *et al.*, 1995). Vinton Dome is located in the updip sector.

Intervening shelf minibasins bounded by large displacement, arcuate, with predominate counter-regional growth faults is the description of the minibasin province.

Distinguishing the updip sector are isolated structural systems surrounded by areas of relatively simple structures. Characterizing these structures as isolated minibasins rimmed by arcuate faults and flanking salt domes formed during evacuation of isolated allochthonous salt bodies. Working from the deep water Gulf of Mexico to the inner shelf, where the updip minibasin sector is located, is a model of shelf margin progradation of southern Louisiana (Figure 13). Coalescing of allochthonous salt formed a continuous canopy resulting in the development of a salt-based detachment system and salt-floored minibasins formed where the salt bodies were isolated. These mechanisms produced structures described as salt-based detachments and stepped counter regional fault systems (Diegel, *et al.*, 1995).

2.6.1 Vinton Geology

Analysis of seismic data was of the top four seconds so deposition relevant to this study began on the Vicksburg formation during the Oligocene and continued through the Miocene. Oligocene stratigraphic units consist of the Vicksberg, the Frio, the Hackberry a subsurface wedge of the middle Frio, and the Anahuac formations. Miocene units are the lower Miocene, middle Miocene, and the upper Miocene (Figure 14). Stratigraphy of the Oligocene Frio formation in Calcasieu Parish is complex, due in part to the tectonic history of the lower Frio and the depositional variation in the middle Frio and the chronostratigraphic equivalent Hackberry. Transgressive and regressive cycles dominated the Oligocene with a shore zone environment present during the regression and a marine environment present during the transgression (Figure 15). Oligocene geology consists of eight stages that could have overlapped or occurred at slightly different times in different places along the upper Gulf of Mexico Basin (Paine, 1968). Miocene deposition shifted to a deltaic environment and back to a broad sandy strand plain (Galloway *et al.*, 2000).

Sediments deposited in the Oligocene were in marginal marine and shallow marine environments in the Vinton Dome study area. A complex eight stage depositional history of the Oligocene began with deposition of the Vicksberg and lower Frio. Shale comprising the Vicksberg formation represents a neritic environment. Characterizing early lower Frio sedimentation is a lowering of sea level along the northwest Gulf of Mexico Basin resulting in the deposition of sand stringers. Following early lower Frio

sedimentation is the second major event, a depositional hiatus producing an unconformity updip from the Vinton Dome area. Continuation of the lower Frio deposition after a marine transgression and deepening of marine environment was the third event. A bathyal environment along the continental slope is an interpretation of the primarily shale upper portion of the lower Frio (Figure 16). Uplift, folding, and erosion resulted in the formation of the pre-Hackberry unconformity that marks the fourth major stage of the Vicksberg-Frio-Anahuac events along the northwestern Gulf of Mexico Basin. Possibly related to this stage is the movement of salt resulting in the uplift and folding.

The pre-Hackberry unconformity represents a depositional hiatus making downcutting of channels into the pre-lower Hackberry possible and the truncation of these beds over local salt domes (Figure 17). There are two mechanisms used to explain subcropping of lower Frio and older sections interpreted from well data. One is due to domal uplift resulting in non-deposition of Vicksburg through middle Frio and the other is uplift and truncation following deposition of the base of the middle Frio. Either mechanism indicates that closely spaced salt masses became loaded by contrasting sediment densities that caused passive diapirism to produce salt domes. Contemporaneous to the passive diapirism was the formation of rim synclines and interdomal withdrawal basins as the salt pushed basinward, creating depressions in the pre-Hackberry surface (Figure 18) (LeVie, 1986). These topographic differences of interdomal ponds and salt domes can account for the presence submarine canyons formed by turbidity currents channeled through the interdomal areas (LeVie, 1986). Erosion renewed after tilting of the unconformity

surface and a number of small submarine canyons formed for the fifth depositional event. These events marked the middle Frio Hackberry transgression period (Paine, 1968). Collapse of the Hackberry (Figure 19) was by subsidence resulting in the retrogradation of the continental margin (Galloway *et al.*, 2000). Eroded channels filled forming a flat surface. The sixth major depositional event was deposition of the basal Hackberry on this flat surface.

The Vinton Dome study area is in the Hackberry embayment that formed during the middle Frio after a major drop in sea level (Winker, 1982). Characterizing the major drop in sea level is large-scale syndepositional down-to-the-basin faulting and diapiric displacement (Galloway, *et al.*, 1982). In the Vinton Dome survey the middle Frio is absent and has been replaced by the Hackberry (Figures 16 and 17). One of the major controlling factors of the Hackberry was prominent, positive paleotopographic highs on the slope and sea floor that had formed from differential loading and sediment ponding from salt withdrawal, Vinton Dome being one of these highs (LeVie, 1986). A more prominent structural feature in the Vinton Dome and surrounding areas is the essentially east-west trend of salt domes with Starks and Vinton Domes on the west and Jennings to the east (Paine, 1966). Connecting these domes is a large regional fault (Figure 20) suggesting the preexistence of the salt domes influenced the initiation of the fault and even controlled its location (Winker, 1982). As sea level increased through deposition of the Hackberry the Vinton Dome area became a bathyal, continental slope (Figure 21). Structure mapped in the Hackberry (Figure 22) indicates an extension regime as would be

typical of the shelf margin. Because of the strong extensional component of the faults and the movement of salt, the geometry as described by Nelson, 1991 (Figure 10) indicates that during Hackberry deposition Vinton Dome continued to form as an active diapir. Active diapirism could have resulted from the prograding margin pushing salt basinward initiating faulting. As the fault developed in response to salt movement, the salt pushed upward into the zone of weakness.

Finally, the eighth and last event was the deposition of the remaining Frio and the early Anahuac (Paine, 1968). Upper Frio represents a regressive phase and lowering of sea level as is evident from the numerous sand sequences found in the upper Frio (Figure 23). Mapping of two of these sand units on 3-D PSTM (Figure 24) data indicate that a transition from active to passive diapirism as described by Nelson (1991), Figures 10 and 11 began by the upper Frio. Anahuac sedimentation represents a late Oligocene transgression when the shelf margin was probably mud dominated (Figure 25) (Winker, 1982). Structural interpretation of 3-D PSTM surface seismic data (Figure 26) indicate that diapirism continued to be passive at the end of Anahuac deposition based on the interpretation of radial faulting and the lack of a major growth fault using Nelson's model Figure 11.

Miocene deposition shifted to a deltaic environment and back to a broad sandy strand plain (Figure 27) (Galloway *et al.*, 2000). The early Miocene shelf-margin depocenter located in southwestern Louisiana remained active through the Quaternary and

established the Mississippi delta as the largest sedimentary source for the Gulf of Mexico Basin (Winker, 1982). Migration of the ancestral depocenter was towards the east beginning in the early to late Miocene (Curtis, 1970). At the same time, replacing the Houston sediment dispersal axis was the Red River axis on the Texas/Louisiana border (Manning, 1990). During this phase the fluvial-dominated Calcasieu delta prograded onto the collapsing continental margin creating the principle lower Miocene depocenter (Figure 28). These deltas advanced the continental margin up to 80km seaward (Gallaway *et al.*, 2000).

Middle Miocene in the Vinton Dome area was a shore-zone system connecting the Corsair Delta to the west with the Mississippi Delta to the east (Figure 29). Like the middle Miocene the late Miocene was a shore-zone system (Figure 30) with sediments supplied by the Mississippi Delta and other smaller deltas such as the diminishing Corsair Delta. Both the middle Miocene and upper Miocene have the structural components of radial normal faulting and the absence of a major growth fault (Figures 31) to suggest passive diapirism based on Nelson Figure 11.

2.8 Conclusions and Discussion

Several questions remain concerning Vinton Dome geology. Among these questions are the timing of active and passive diapirism. Improvements in resolution and fidelity of the 3-D seismic enhanced imaging of the salt flanks. High fidelity also provides the ability to measure the slope of the salt flanks. Using such measurements is Talbot's method to

determine the stage of diapiric growth. Other issues deal with the structures associated with Vinton Dome. One question that higher fidelity data can address is the complexity of smaller faults that require higher resolution to image. A stratigraphic question of interest is to image the lower Hackberry where ponding of channel sands may have occurred. These and other issues regarding the geology point to the importance of improving the fidelity of the 3-D surface seismic data.

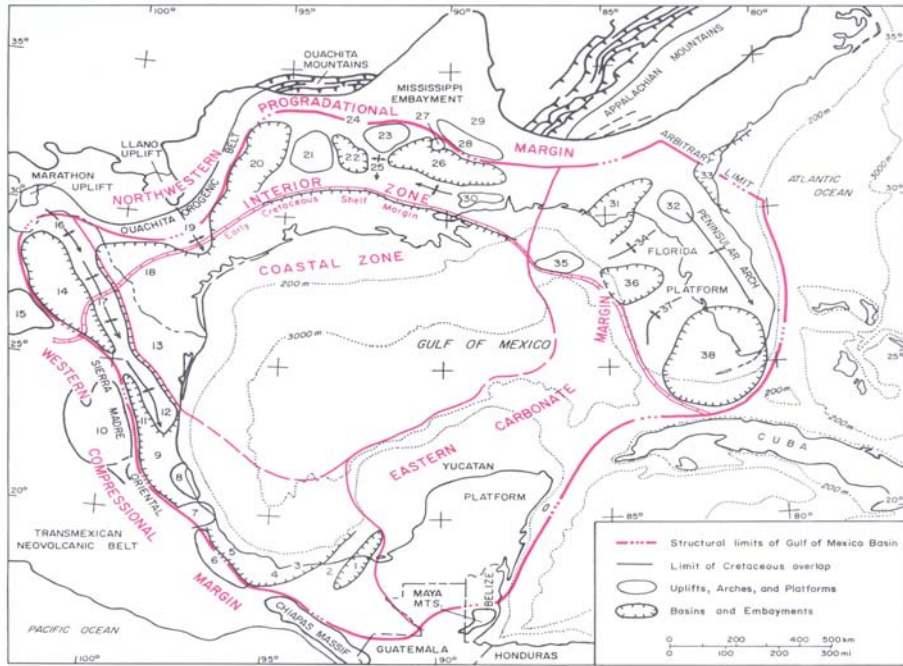


Figure 2. Outline of the extents of the Gulf of Mexico Basin (Ewing, 1991).

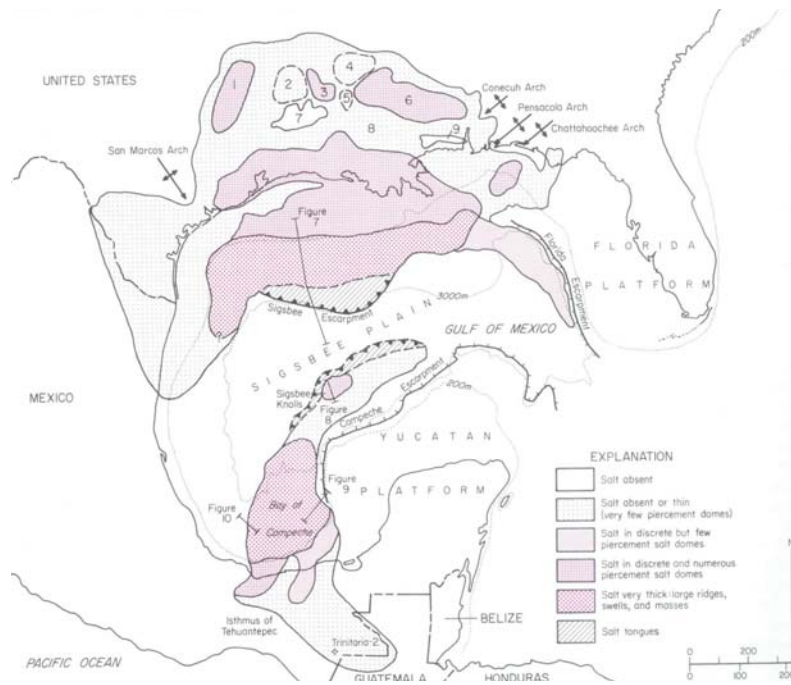


Figure 3. Distribution of salt in the Gulf of Mexico Basin (Salvador, 1987).

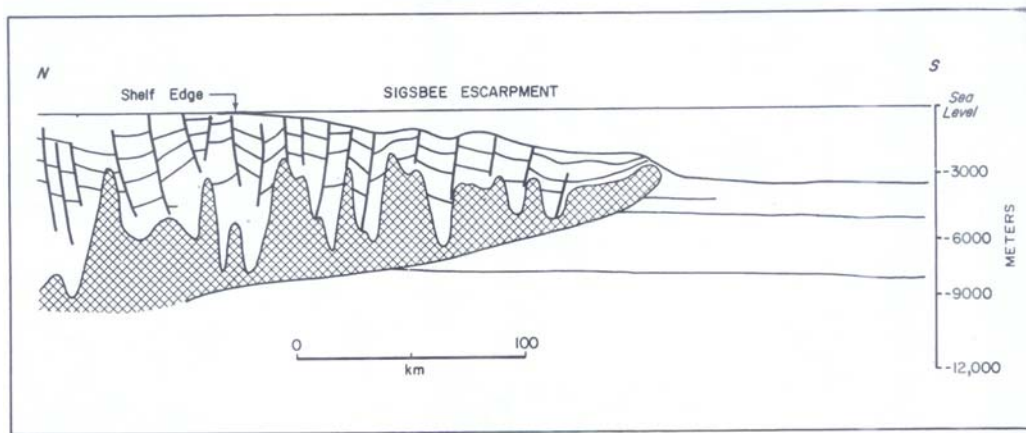


Figure 4. Prograding sediments squeezing salt ahead (Salvador, 1987).

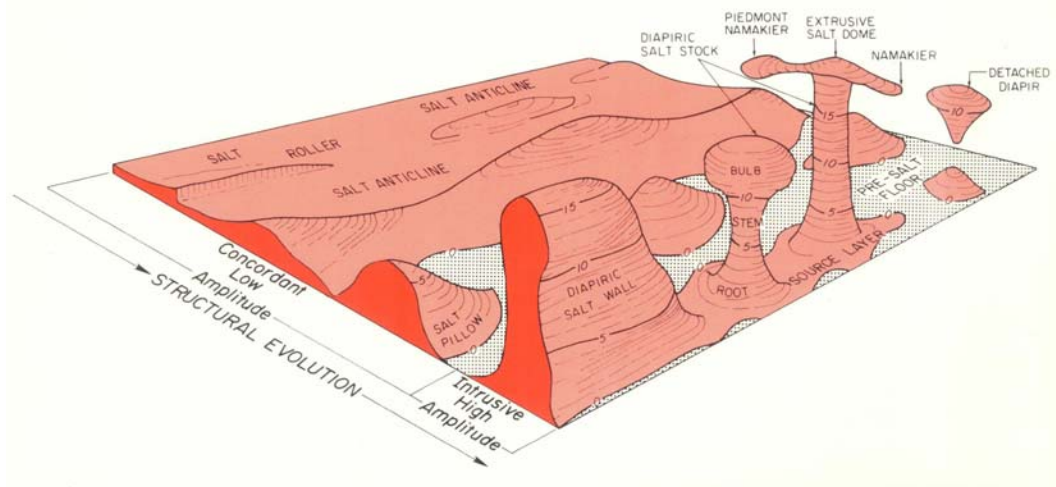


Figure 5. Various different salt structures (Jackson, and Talbot 1986).

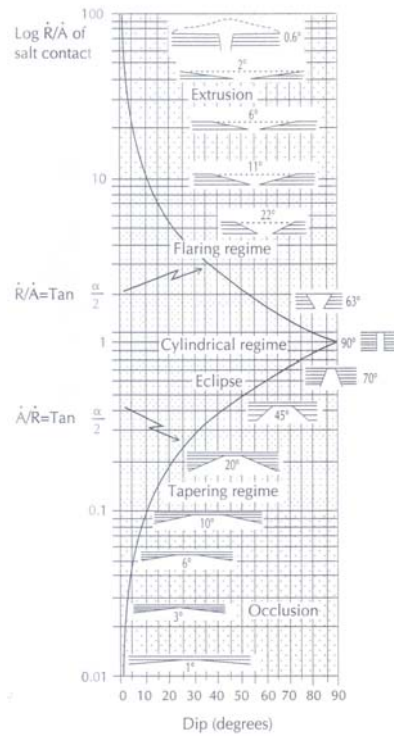


Figure 6. Salt sediment contacts used to calculate kinematic ration of A/R and R/A (Talbot, 1995).

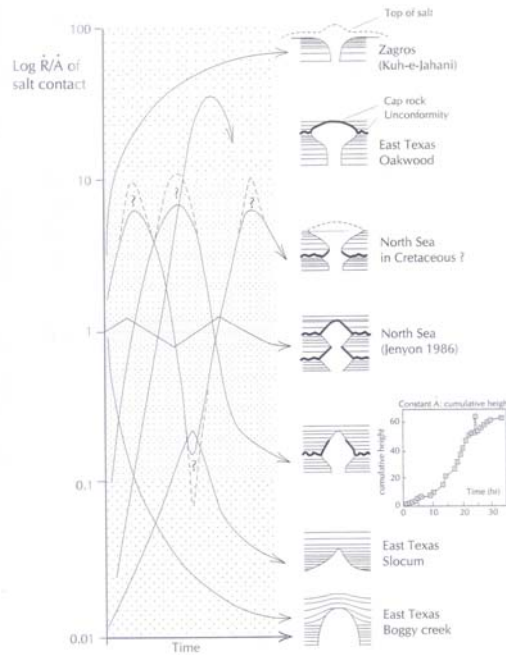


Figure 7. Chart to identify type of growth stage of salt based on kinematic ratio (Talbot, 1995).

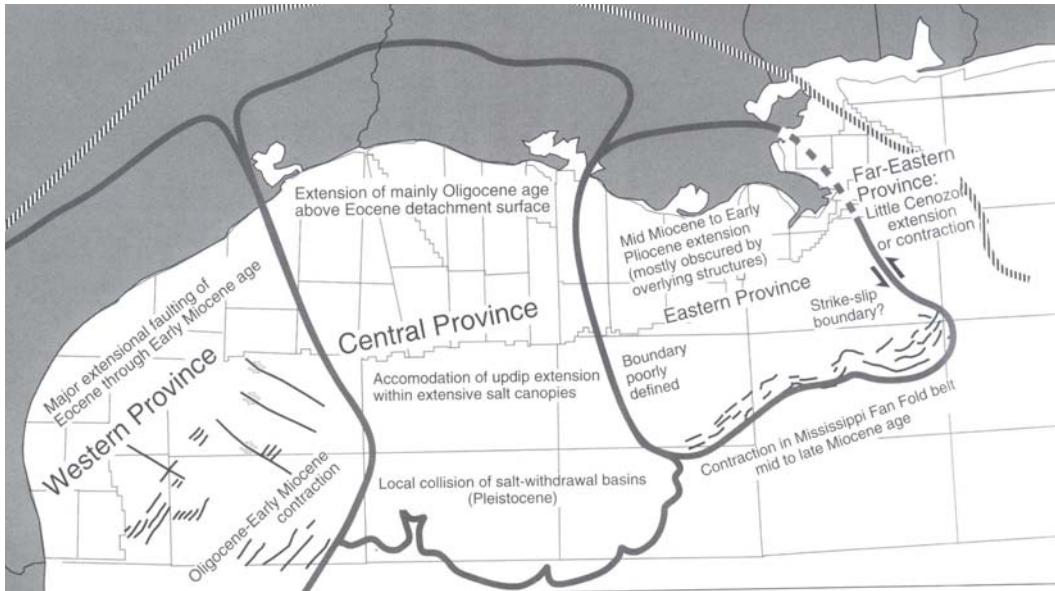


Figure 8. Northern Gulf of Mexico Cenozoic structural provinces (Peel, *et al.*, 1995).

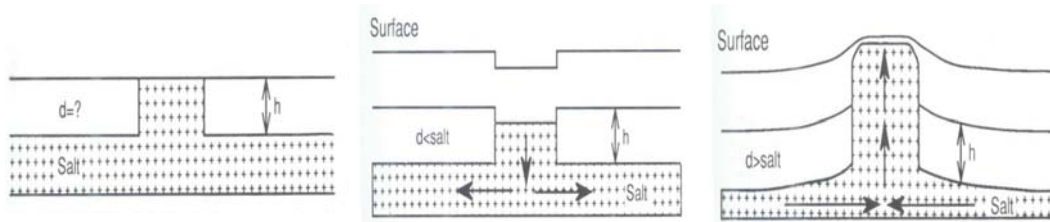


Figure 9. Illustration of mechanisms for salt movement (Nelson, 1991).

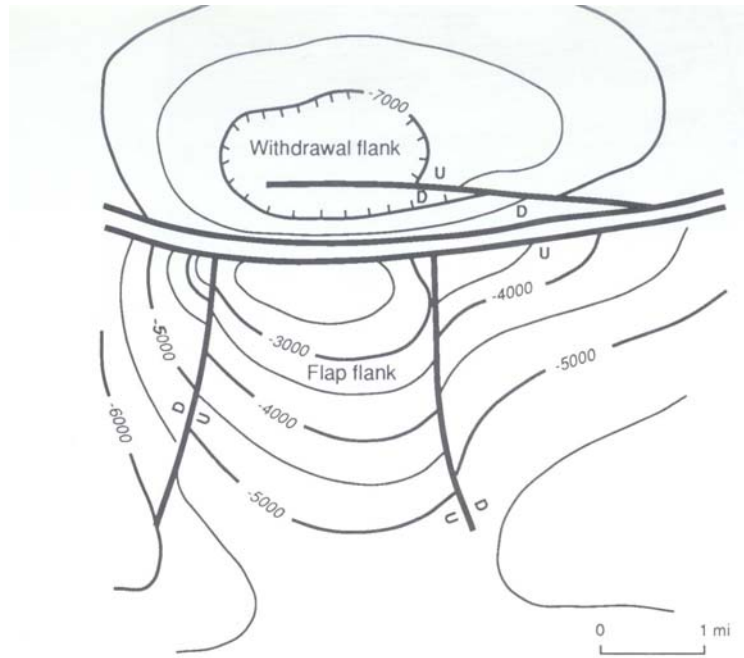


Figure 10. Fault pattern representative of active piercement (Nelson, 1991).

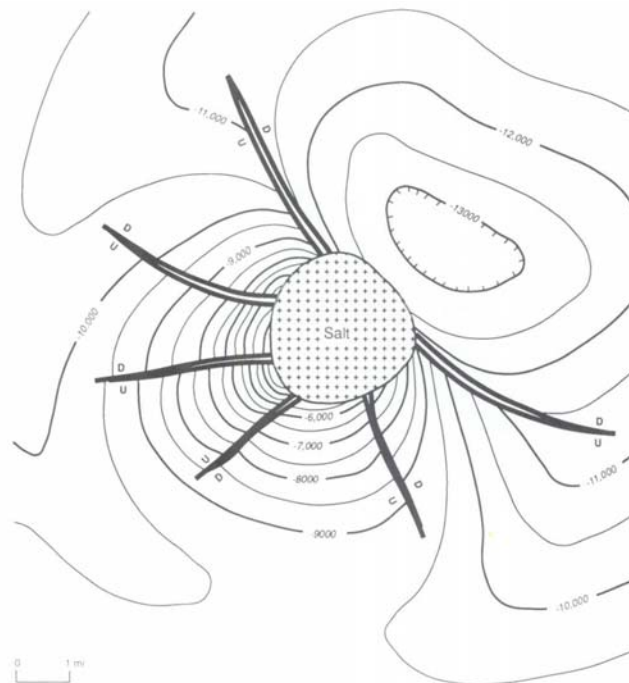


Figure 11. Fault pattern representative of passive piercement (Nelson, 1991).

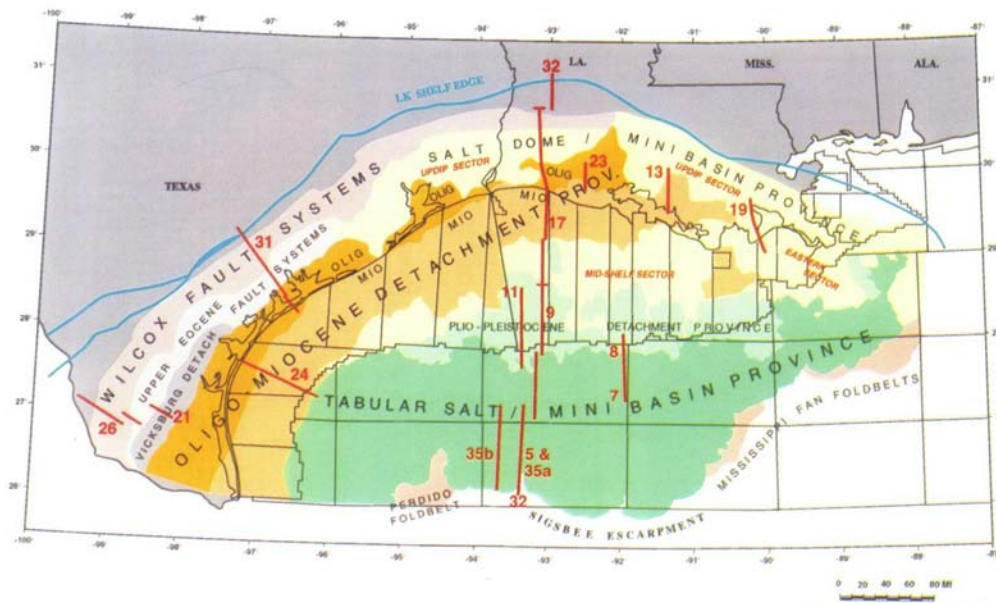


Figure 12. Eight tectono-stratigraphic regions of the Upper Continental Margin of the Gulf of Mexico Basin (Diegel, *et al.*, 1995).

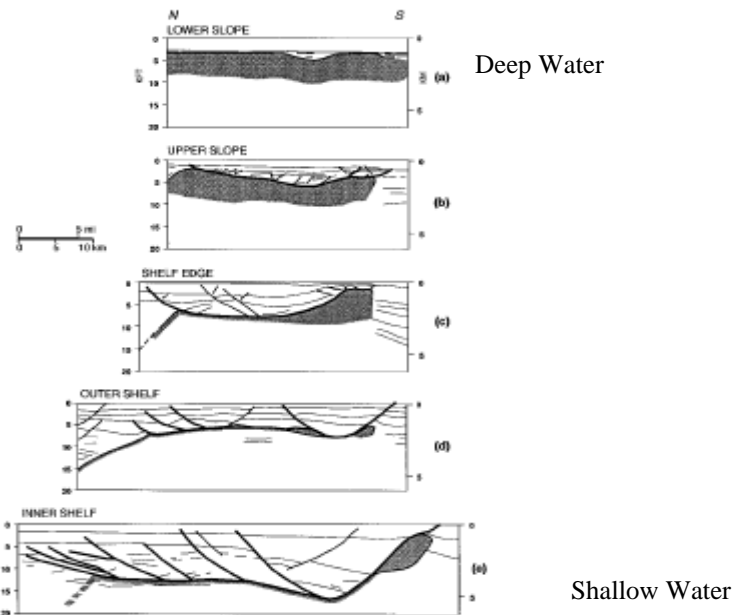


Figure 13. Model of shelf margin progradation showing the evolution of salt structures using deep water up through onshore to represent the developmental stages as the continental margin prograded across the allochthonous salt (Diegel, *et al.*, 1995).

MIOCENE	GRAND GULF	UPPER			
		MIDDLE			
LOWER					
OLIGOCENE	ANAHUAC	DISCORBIS ZONE		<i>Discorbis nomada</i> <i>Discorbis gravelli</i>	
			HETEROSTEGINA ZONE	HET LIME	<i>Heterostegina texana</i> <i>Bolivina perca</i>
		MARGINULINA ZONE	FIRST MARG SAND		<i>Marginulina idiomorpha</i> <i>Marginulina vaginata</i>
			SECOND MARG SAND		
			THIRD MARG SAND		
		FRIO	UPPER	WELCH SAND	<i>Camerina - Cib. 10</i> <i>Cibicides hazzardi</i>
				ORTEGO SAND	
				KLUMPP A, B, C, & D SANDS	
			MIDDLE	BURLEIGH SAND	<i>Marginulina texana</i>
				BOAGNI SAND	
	HOMESSEEKER A SAND				
	LOWER	FIRST NODOSARIA SAND (SAND A-1)	<i>Nonion struma</i> <i>Nodosaria blanpiedi</i>		
		SECOND NODOSARIA SAND			
		THIRD NODOSARIA SAND			
		FOURTH NODOSARIA SAND (SAND 3-1)			
			TWEEDEL SAND (HOMESSEKERS SAND AT SAVOY)	<i>Discorbis D</i>	
	VICKSBURG			<i>Textularia warreni</i>	
	RED BLUFF				

Figure 14. Stratigraphic column of the Vinton Dome study area (Tabbi-Annani, 1975).

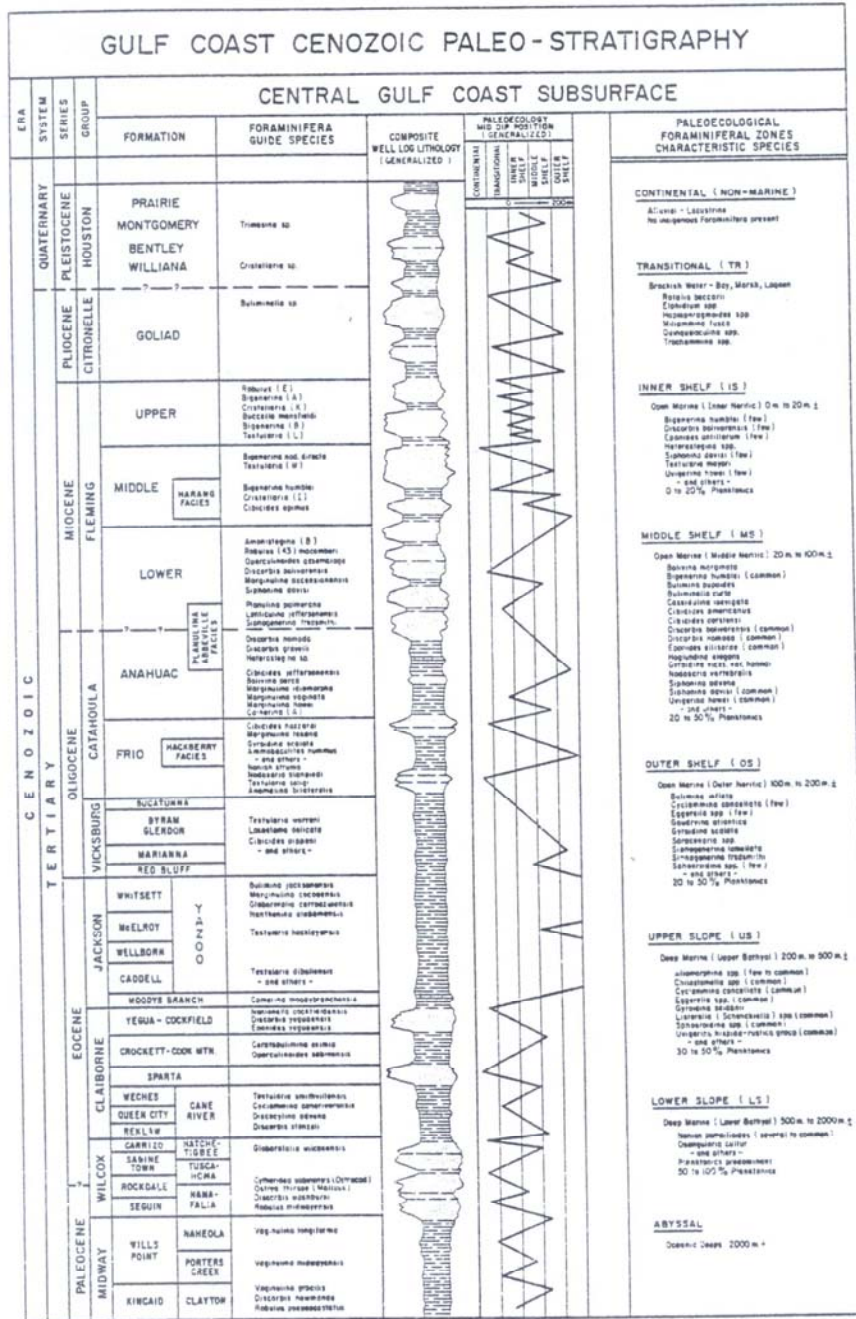


Figure 15. Sequence stratigraphy of upper Gulf of Mexico sediments with paleontologic markers through the Cenozoic (Tipsword *et al.*, 1966).

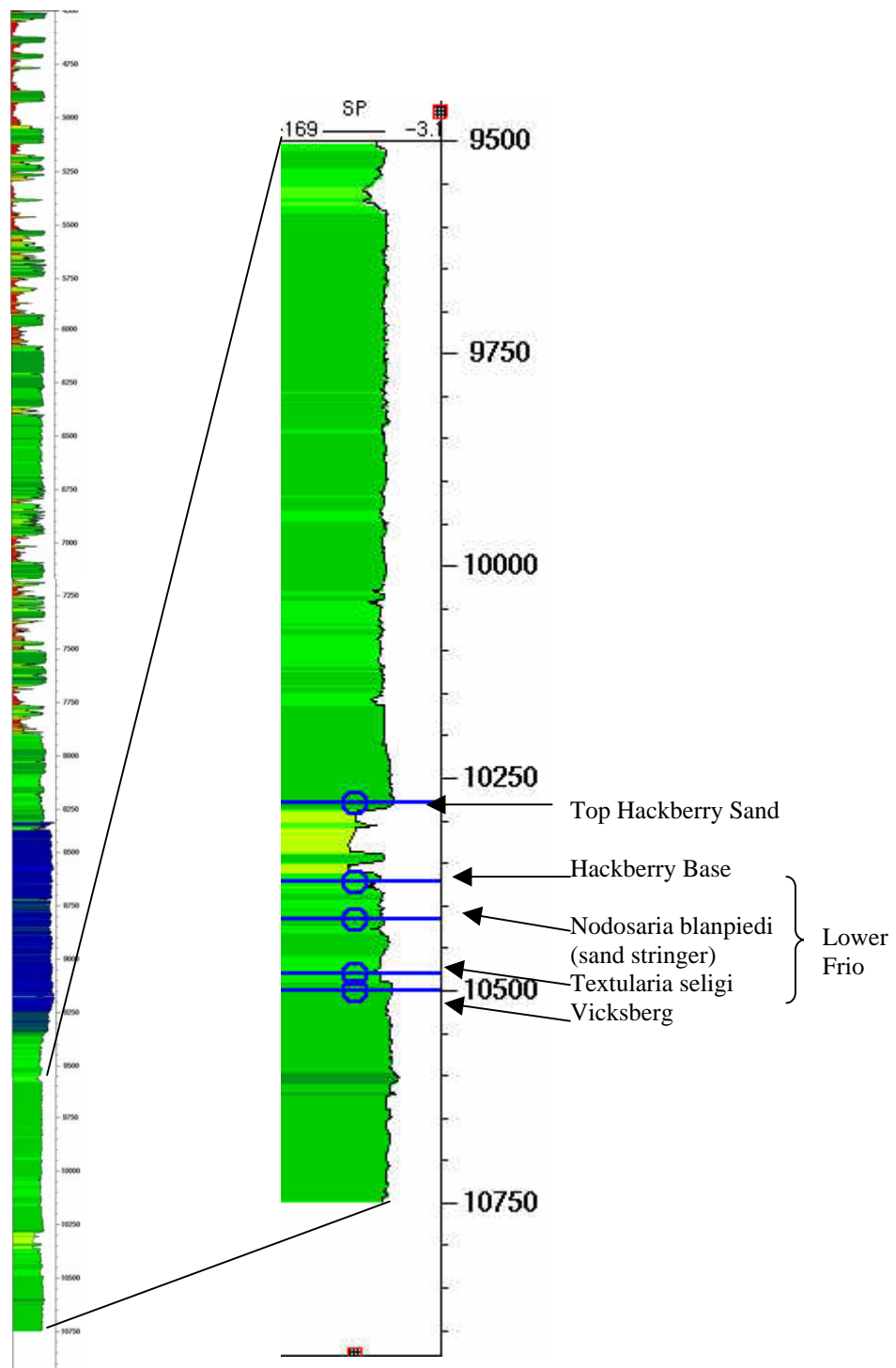


Figure 16. Spontaneous potential log of Oligocene section from the Seig well in the Vinton Dome survey showing the transgressive phase from the Vicksburg through the lower Frio and the channel sands of the Hackberry (OPEX).

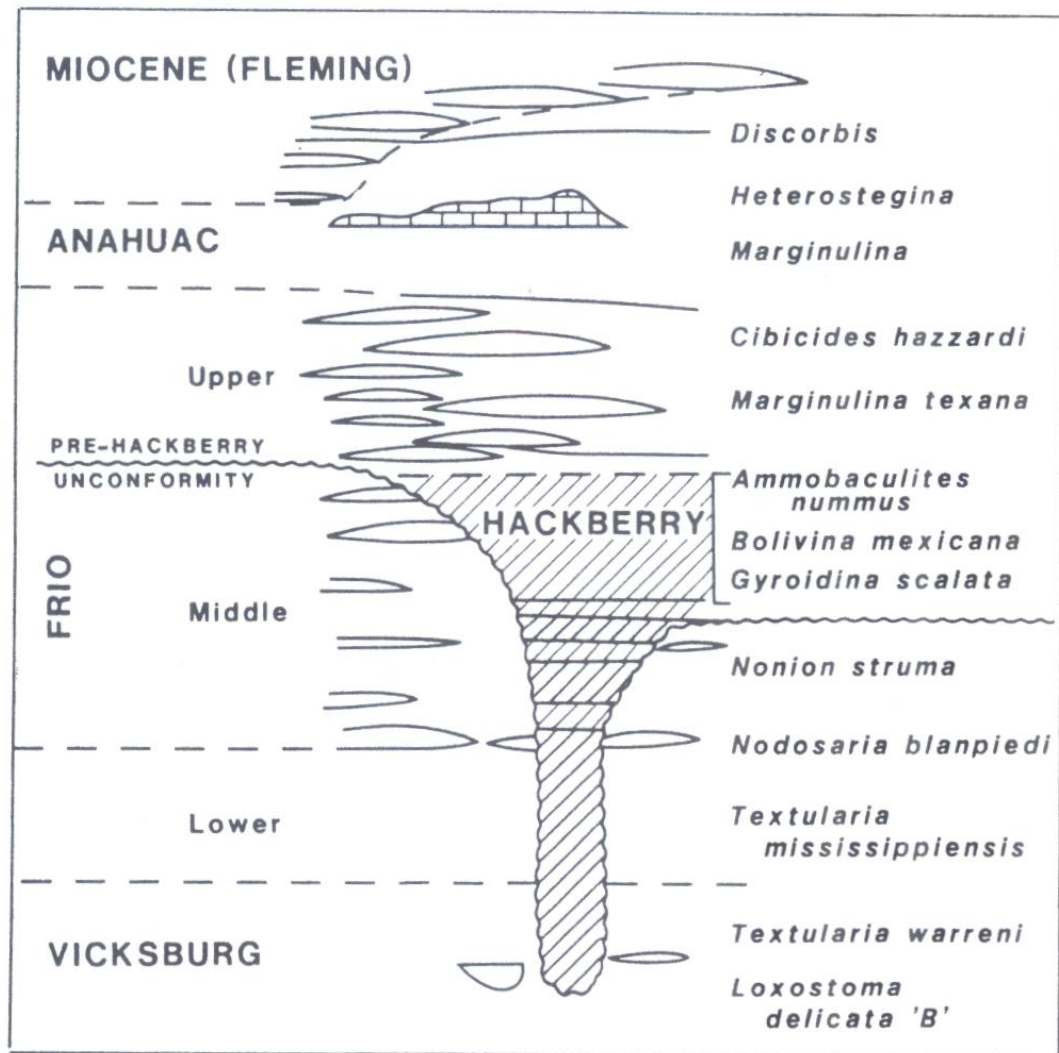


Figure 17. Downcutting through the middle and lower Frio produced submarine channels that were filled with turbidite sands and shale (Eubanks, 1987).

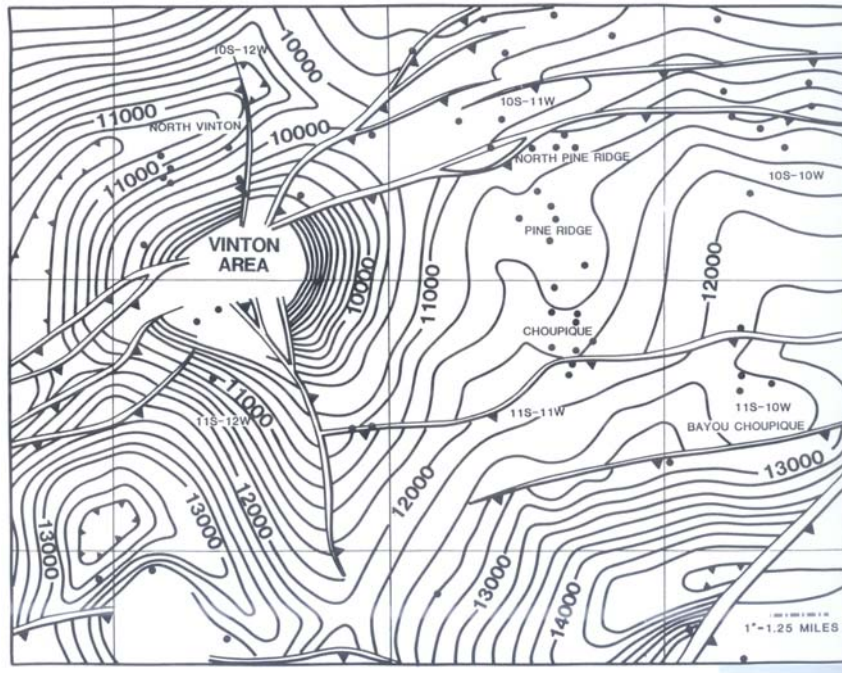


Figure 18. Structure map contoured to the lower Hackberry (LeVie, 1986).

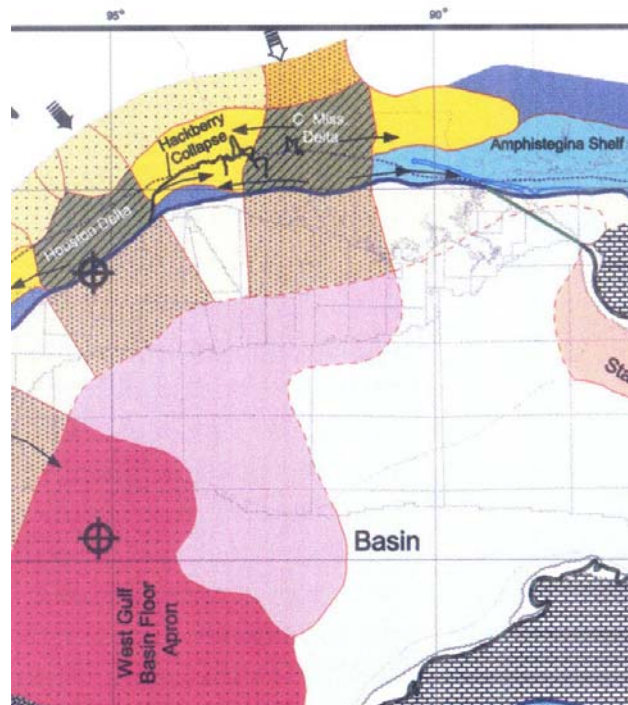
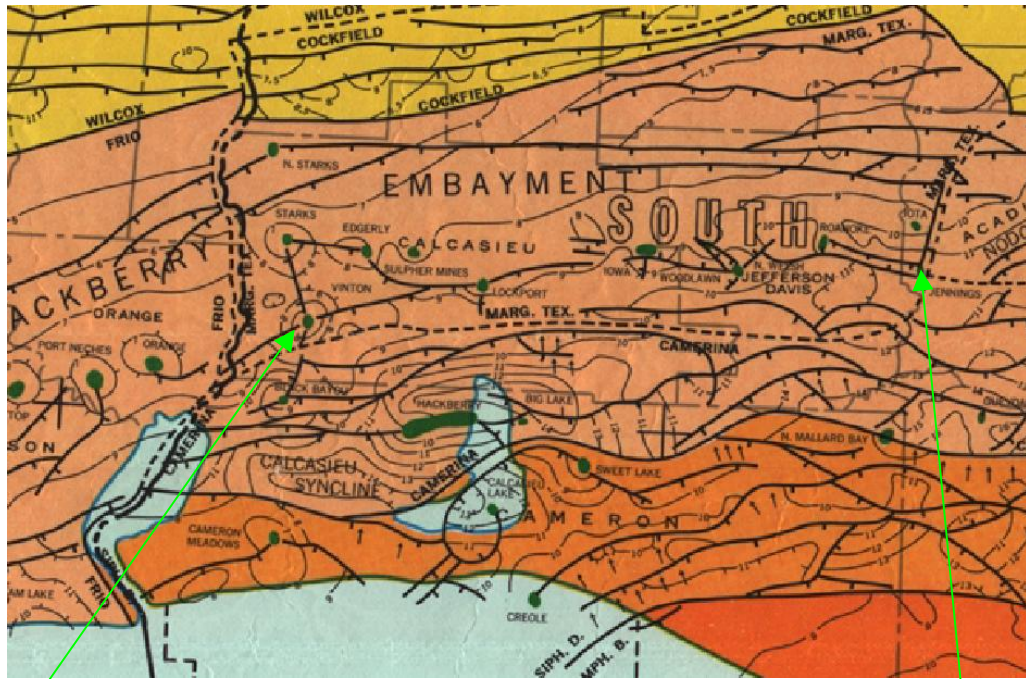


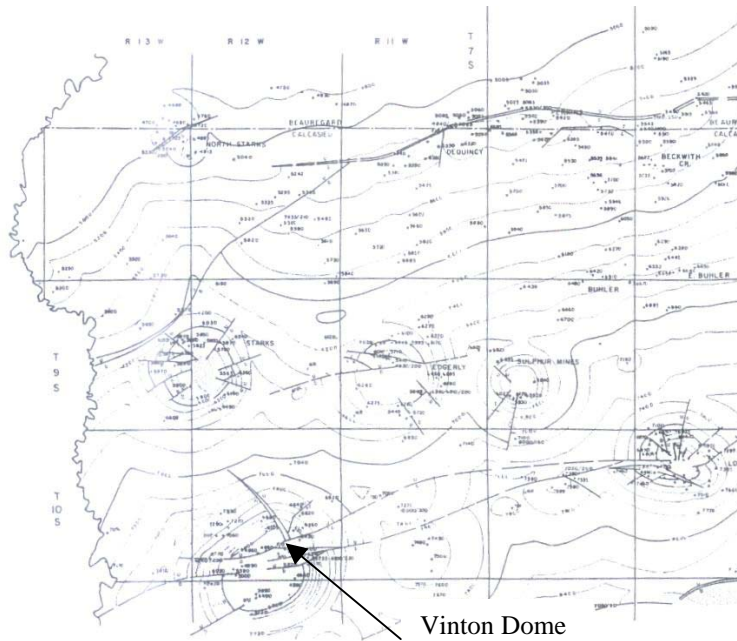
Figure 19. Map showing area of Hackberry collapse, Vinton Dome study area is located in the middle of the collapse (Galloway, *et al.*, 2000).



Vinton

Jennings

(a)



(b)

Figure 20. (a) Large regional down-to-basin fault connecting Vinton and Jennings domes (AAPG, 1972) (b). Structure map of the Anahuac showing detailed structural relationships of salt domes in the Vinton Dome study area (Paine, 1966).

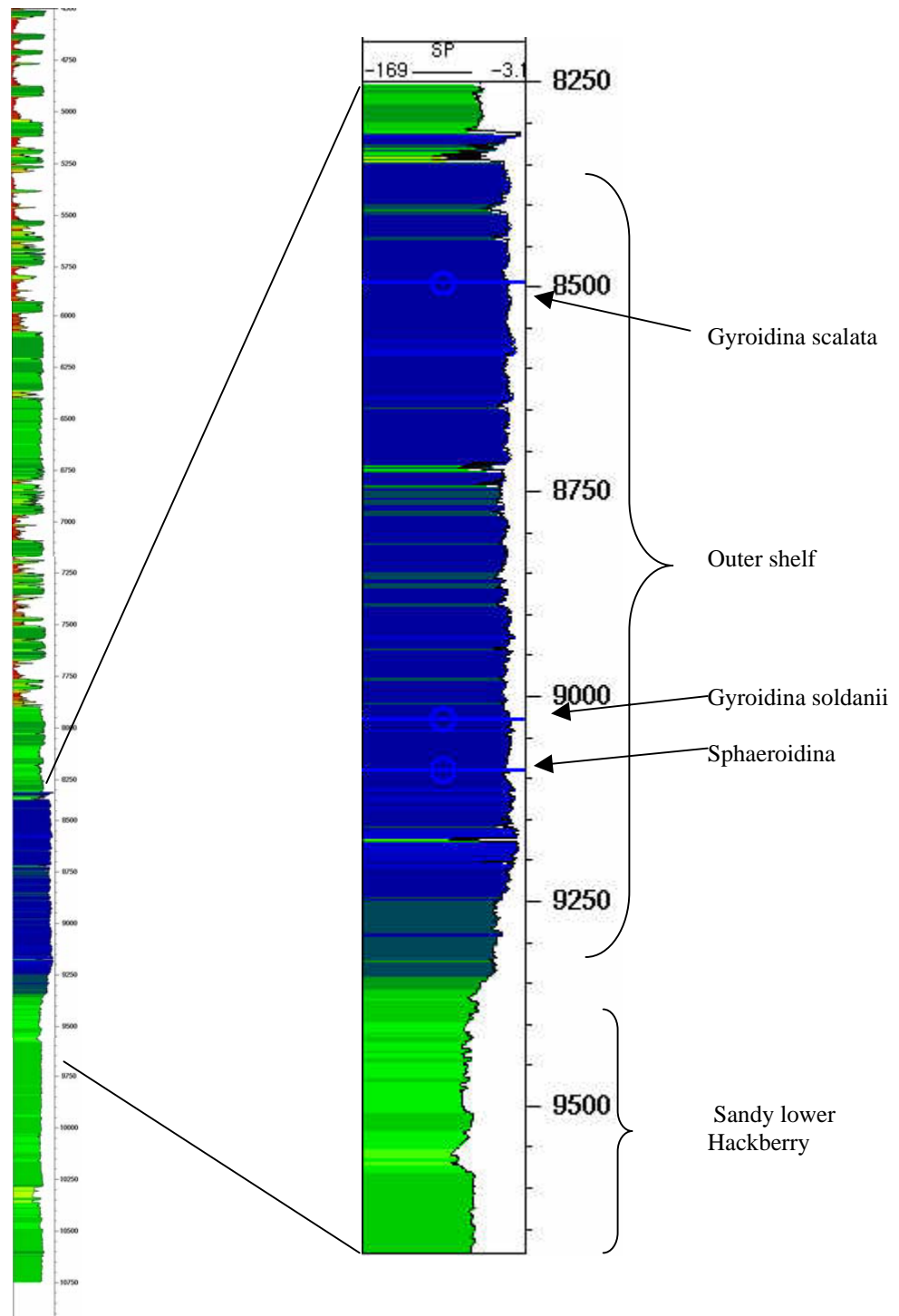


Figure 21. Spontaneous potential log showing shale-dominated facies in upper Hackberry overlying sandier lower Hackberry (OPEX).

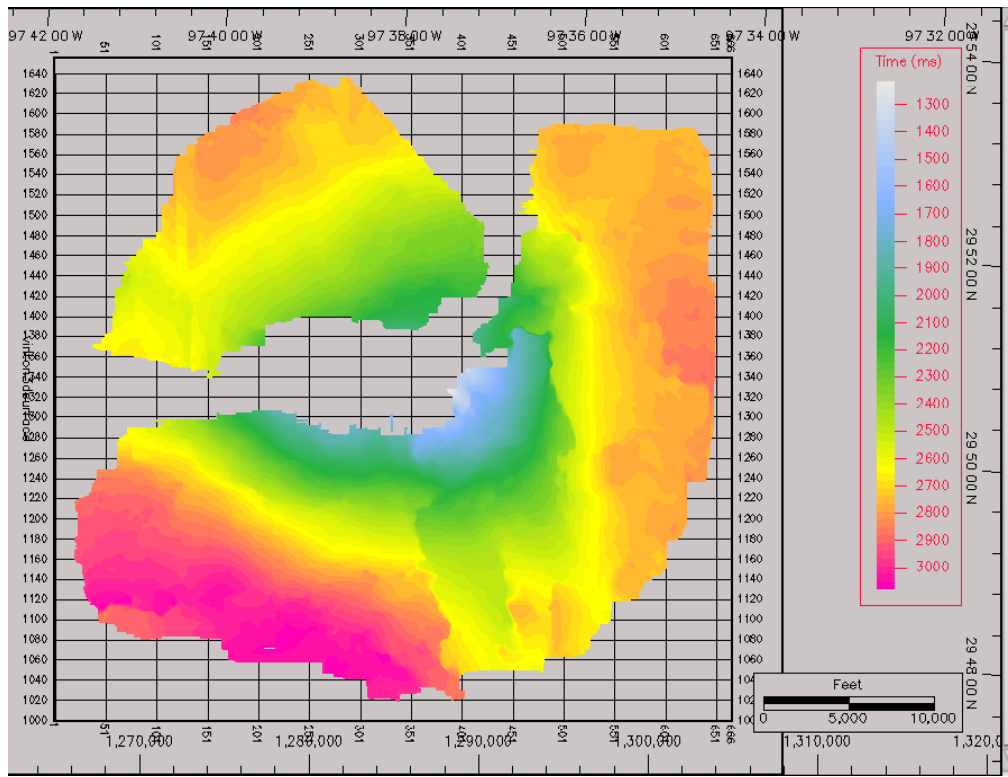


Figure 22. Interpretation of by OPEX of the Hackberry formation showing the extensional nature of the major fault and what appears to be active diapirism as modeled by Nelson.

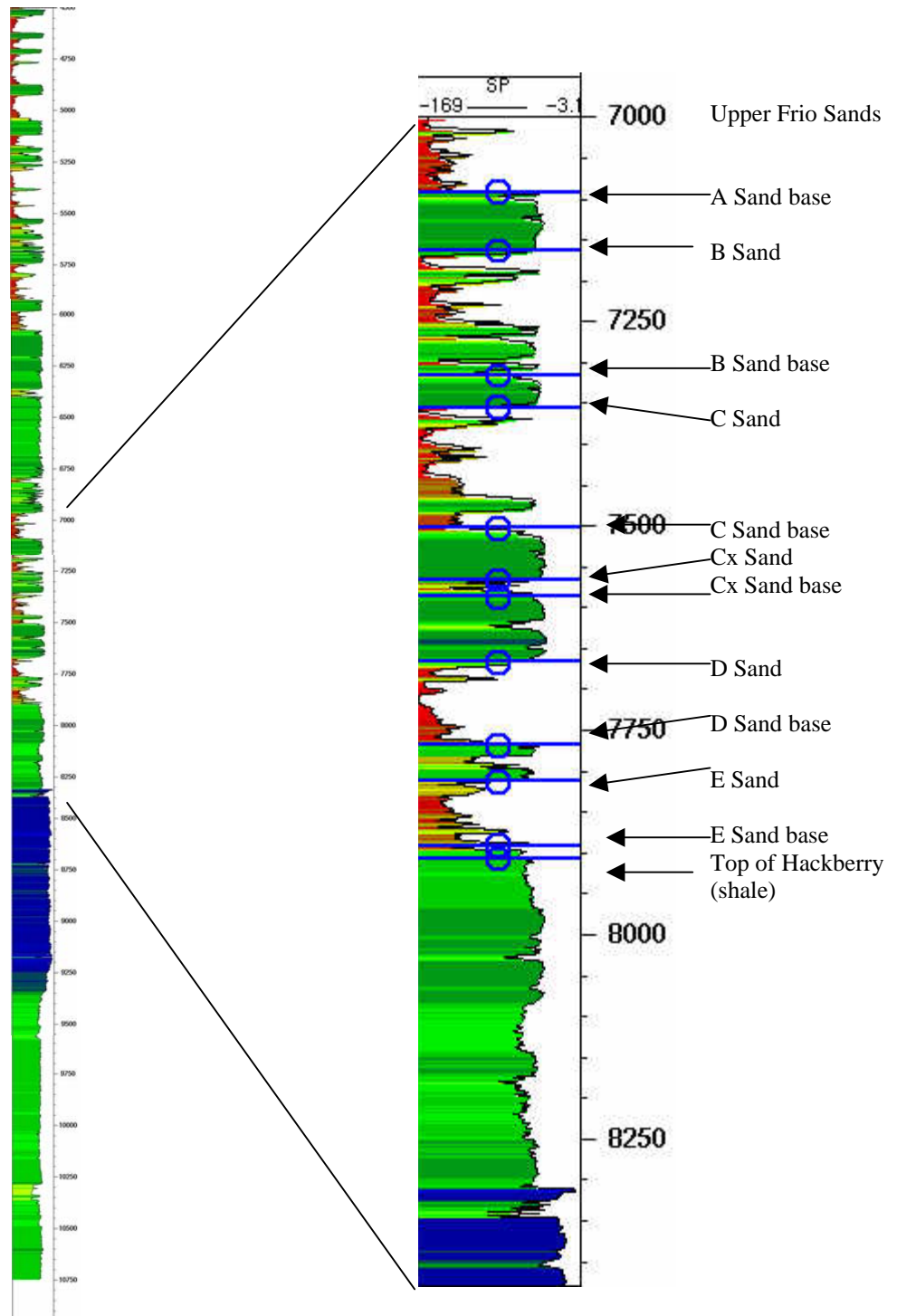
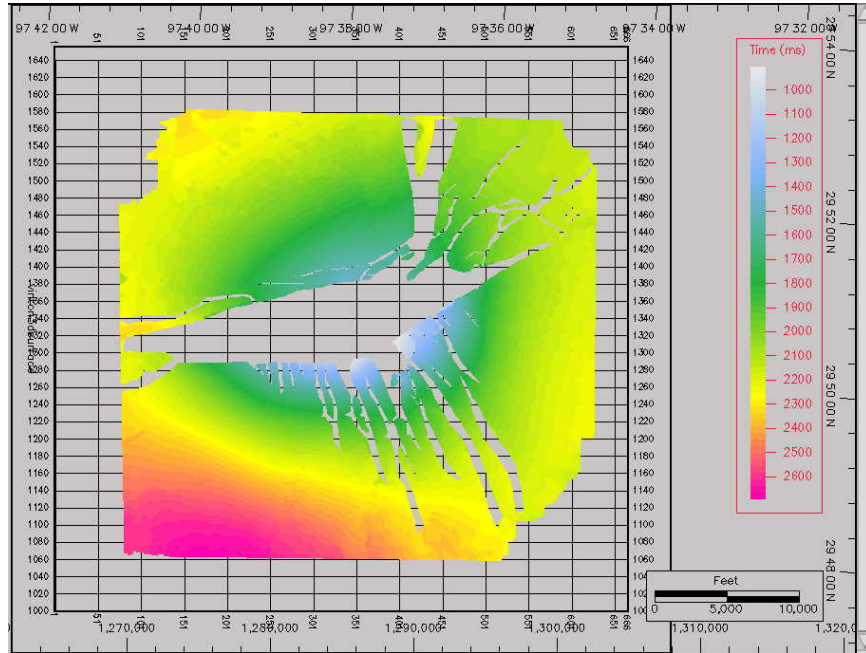
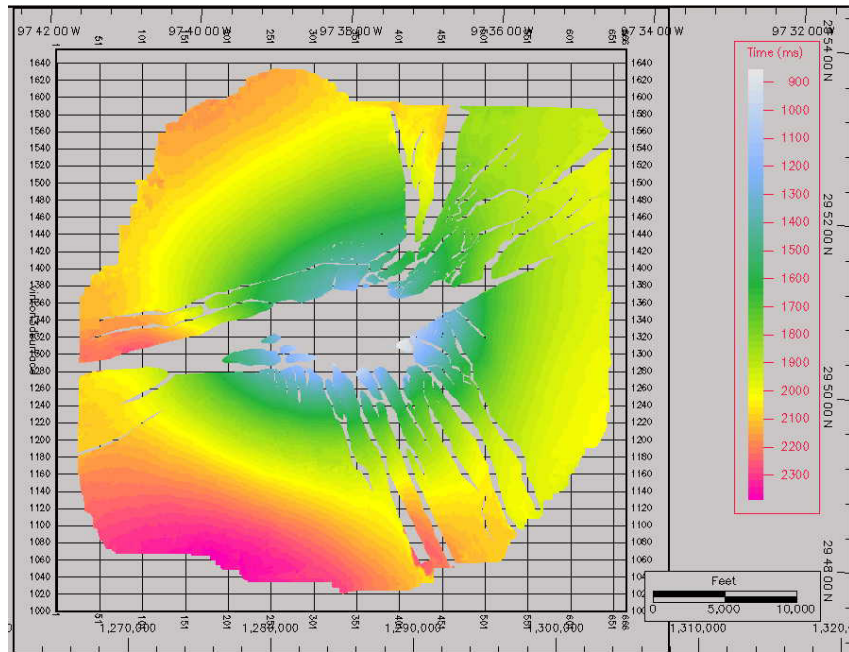


Figure 23. Section of the upper Frio spontaneous potential log used to interpret sand units in the upper Frio (OPEX).



D Sand Frio



A Sand Frio

Figure 24. Maps of the D and A-Sands of the upper Frio formation as interpreted by (OPEX). Structures mapped indicate active diapirism based on the large fault cutting through and extending beyond the dome as modeled by Nelson.

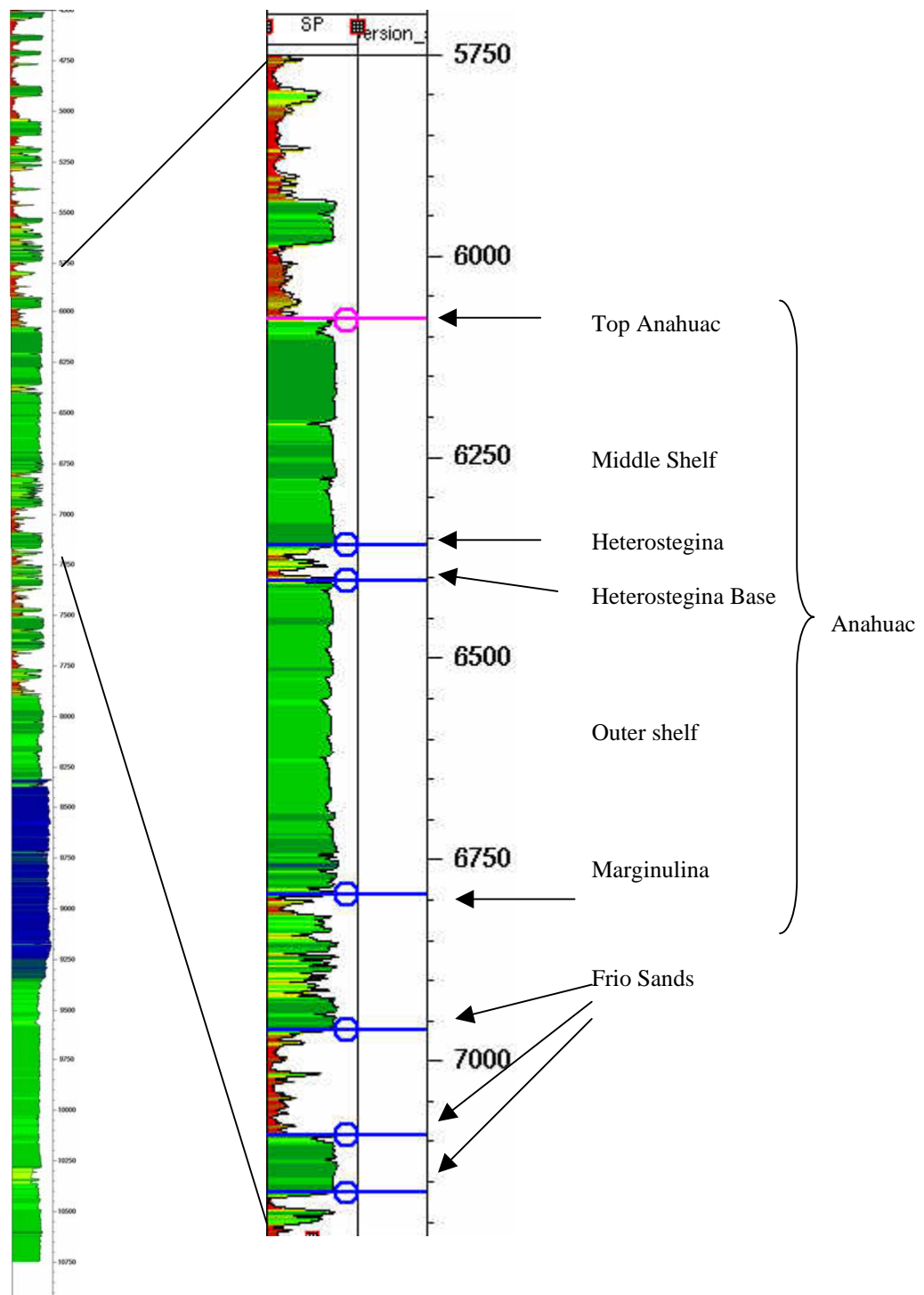


Figure 25. Spontaneous Potential log with the Anahuac enlarged showing a mud-dominated shelf (OPEX).

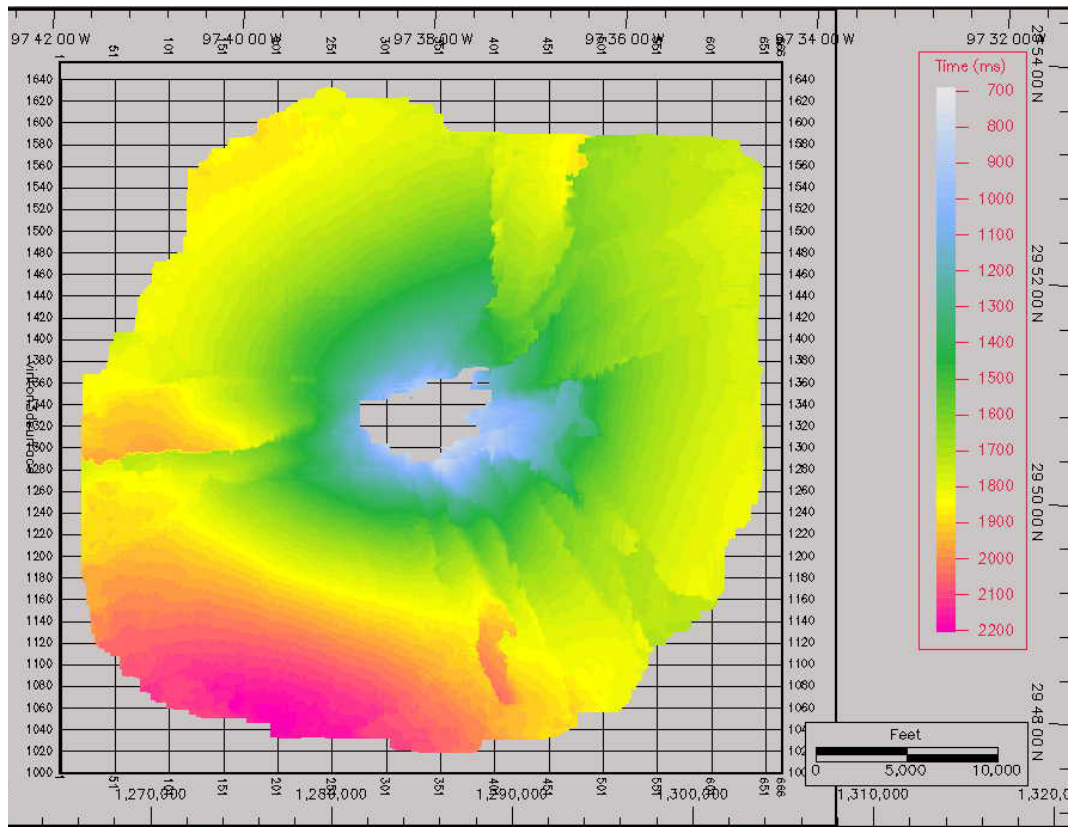


Figure 26. Top Anahuac interpretation by OPEX. Structures indicate passive diapirism using Nelson's model.

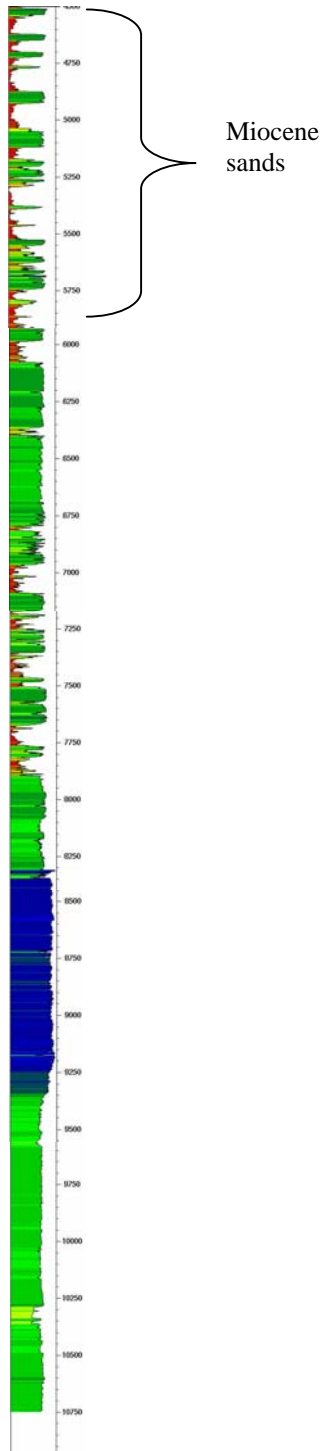


Figure 27. Spontaneous potential log showing Miocene sands.

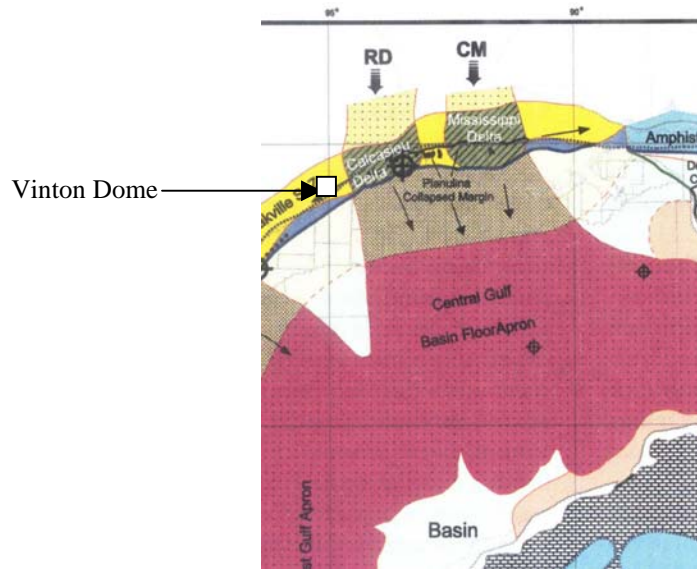


Figure 28. Lower Miocene depocenter in the Vinton Dome study area (Galloway *et al.*, 2000).

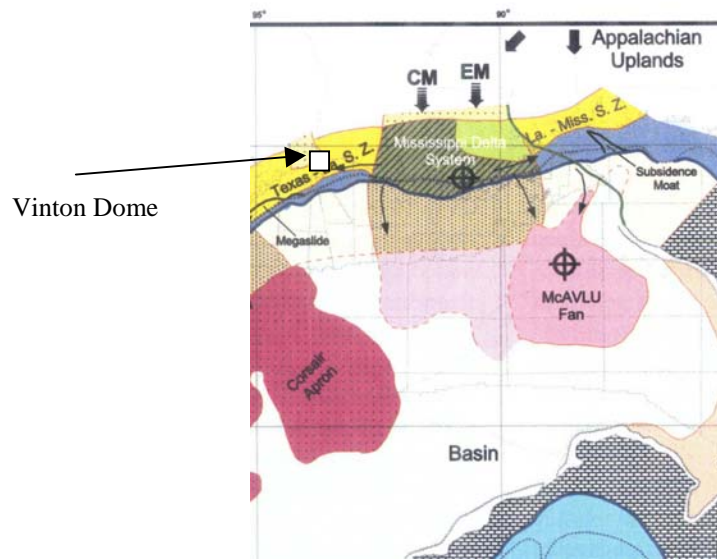


Figure 29. Middle Miocene depocenter in the Vinton Dome study area (Galloway *et al.*, 2000).

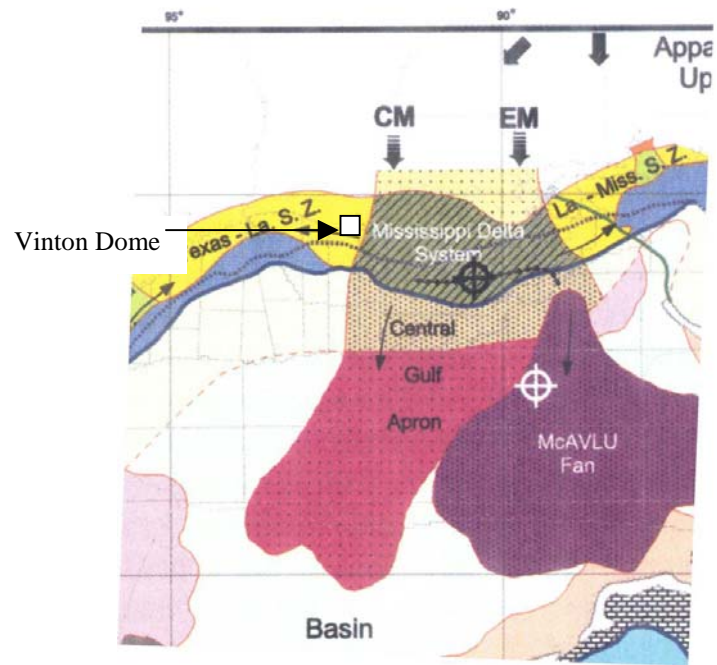
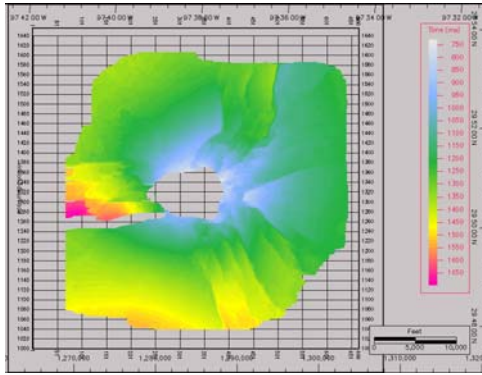
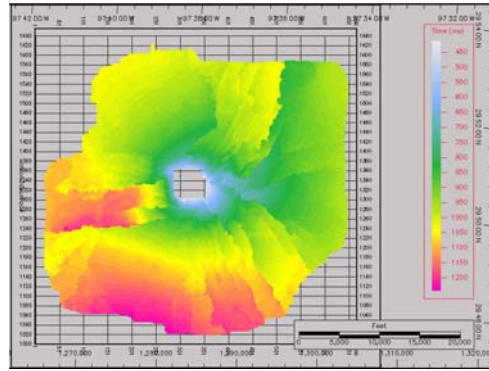


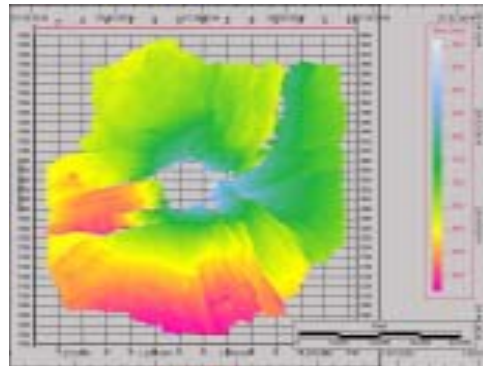
Figure 30. Late Miocene depocenter in the Vinton Dome study area (Galloway *et al.*, 2000).



Middle Miocene



Upper mid-Miocene



Upper Miocene

Figure 31. Interpretation of Miocene Sands by OPEX. Fault patterns indicate passive diapirism according to Nelson's model.

Chapter 3

Processing to Account for Non-Traditional Acquisition

3.1 Introduction

Attention to detail during the planning and implementation of acquisition and processing is required to insure the best possible imaging parameters are in place, but difficulties often arise with 3-D land surveys. Problems of improper spatial sampling often result because of issues such as right of ways, obstacles, and permits (Evans, 1997). In the plan there should be accounting for geologic factors such as the regional dip, structures, and target depths. After data acquisition, it is necessary to apply the proper processing to insure a high quality image. Surface seismic data acquired at Vinton Dome using innovative methods were prestack time migrated (PSTM). My objective in processing was to find an effective pre-migration processing flow that was easily implemented and reduced noise without drastically affecting the data, especially the bandwidth of the data.

3.2 Acquisition

A radial receiver grid with concentric source lines, differing from the typical brick pattern, was the acquisition pattern at Vinton Dome (Figure 32). The Vinton Dome survey design was to accomplish maximum fold and have a survey aperture to focus on the salt structure (Gibson and Tzimeas, 2002). Seismic sources were 5.5 pound pentolite charges that were detonated at a depth of 60 feet (18m). The survey used seventy-two receiver lines in the survey. Half of these lines extended from the predicted perimeter of the salt dome to the distal edges of the survey and the other half were short lines extending from about half the length of the long lines to the distal edge of the survey.

Five degrees separated each line with the long line separated by ten degrees, and the short lines with a ten degrees separation. Lines were closely spaced near the dome and spread apart as they radiated away from the dome. Receiver station spacing was 165 feet (50m) along each line segment. At each station was a six-element array using 10-Hz geophones. Source locations approximated concentric circles and had a shot spacing of 165 feet (50m) along the arc. Most disruptions in the shot pattern were due to cultural obstacles located in the north and west portions of the survey (Constance *et al.*, 1999). Obstacles included power lines, roads, and Interstate Highway 10 cutting across the northern portion of the survey (Figure 32).

A 90° sector of the 360° coverage was active for each shot with 19 active receiver lines per shot, which was between 1400 and 2000 active channels. For each active 90° receiver sector the center rack of source locations, forming an arc through the receiver lines, was detonated and recorded. Since the entire receiver line was active, there was no radial roll. After each shot the active receiver spread was advanced 10° or two receiver lines and the next sequence of shots were recorded (Constance *et al.*, 1999).

Innovative acquisition such as this has several benefits both recognized and many likely not realized. One aspect is the fold (Figure 33). Higher fold close to the dome was to enhance illumination of steeply dipping beds and illuminate areas of complex structure. Another intention of this acquisition design was to keep raypaths from passing through the salt so that depth imaging would not be necessary (Constance *et al.*, 1999).

3.3 Processing

My primary objective of the pre-migration processing phase of this study was noise suppression with minimal processing. I assessed field data to determine the appropriate processing steps that would limit the impact of processing on the migration as described by Yilmaz, 1987. The basic steps were: 1) to QC the geometry, 2) static corrections, 3) deconvolution, 4) velocity analysis, 5) normal moveout (NMO) correction, and 6) stack. I tested the impact of minimal processing by QCing the geometry, applying a datum static correction, running deconvolution, applying NMO and stacking the data. An automatic gain control (AGC) applied to the migrated volume revealed that noise manifested as migration swirls (Figure 34) was an issue that would require more aggressive processing.

One of my major concerns with the data was noise that is common with land data. Sources of noise in land data can result from poor receiver coupling and outside noise sources such as traffic and power lines. An additional noise source common to land data is ground roll (Figure 35). Low-frequency high-amplitude ground roll can have a significantly adverse effect on the migration. Ground roll consists of Rayleigh waves, air-coupled waves, and other guided waves propagating within the low velocity surface layers resulting in coherent noise (Al Hussein *et al.*, 1981). I believed ground round roll was a contributing factor to the noise present in the initial migration test. Examination of

the raw field data and the initial migrated volume led to the conclusion that a more comprehensive processing flow would be required to reduce the noise.

Examining the coherence of brute stacks and the uniform moveout on super shot gathers was a QC used to determine if both the geometry and field static were correct (Figure 36). Common mid-point (CMP) sorted shot data with datum static shift had spherical divergence gain applied. I ran these data through deconvolution. Using several band pass filters, I tested the filters to determine the best one to remove the ground roll (Figure 37). Data without ground roll that maintained the broadest bandwidth, the 16-17-70-80 filter, were then used to calculate the residual static (Table 1). This required using a detailed velocity field. In order to maintain continuity with the commercially processed PSTM data, I used the velocities used for the PSTM for calculating the residual static.

After calculating and applying a residual static, I reevaluated the data to determine additional processing steps needed to improve the signal. I designed a second processing flow to improve the signal-to-noise ratio for migration. The new processing flow consisted of taking CMP sorted data, applying both the field static and the residual static and boosting the gain using spherical divergence. These data had a shot deconvolution applied and were filtered. Shot deconvolution calculates a wavelet for both the source and the receiver. After each processing step, I applied an NMO using the same velocity as used to calculate the residual static. I applied the NMO along with a mute (Figures 36a,

38-42). For QC I would brute stack the data. I recognized attenuation of the data, especially in the eastern half of the survey (Figure 40).

To balance the amplitudes I applied automatic gain control (AGC) after the data were filtered. I also used a second application of AGC before migration. By balancing the amplitudes, the stack eliminated what had been higher amplitude low frequency noise caused by ground roll before the second application of AGC. Improvement of the signal justified opening the filter to 5-6-70-80, increasing the bandwidth and further improving fidelity. Another issue was the presence of high amplitude first breaks. These appear to have been creating artifacts (Figure 43). I muted these before the filter (Figure 44).

Results of this processing flow (Table 2) show reduction in migration swirls (Figure 45). Those that remain are possibly the result of sedimentary velocity model that lacked the detail to precisely model the velocities at the salt/sediment interface. A comparison of data processed with the minimal parameters and those with the more aggressive approach show differences in both the sections (Figure 46) and in the depth slices (Figure 47). I used improvements I recognized from these comparisons to select the processing flow from Table 2.

3.4 Conclusions and Discussion

Processing 3-D land surveys present several challenges with respect to noise. In the Vinton Dome survey these challenges are compounded by nontraditional acquisition parameters. My goal was to improve the fidelity of the 3-D seismic data by using an

innovative method to model the velocity field for a 3-D PSDM. Non-traditional seismic acquisition poses several challenges to the pre-migration processing. My focus was on velocity modeling so a simple pre-migration processing approach was taken. To achieve the goal of this study, one of my objectives was to maintain as high a bandwidth as possible and eliminate the noise. I demonstrated achievement of this objective in the QC of the processing steps.

One of the problems associated with processing land data is ground roll. There are several approaches to removing ground roll. These methods include low cut frequency filtering, FK moveout filtering, signal-noise separation with local slant stacks, signal noise separation of NMO-corrected CMP gathers, and τ - p moveout filtering (Alvarez, 1995). Removal of ground roll is an area of active research and some promising methods have potential in addressing this issue. One such method is to model the ground roll and then subtract it from the data. Specifically the ground roll is flattened, a median filter is applied, then the flatten portion is restored to its original position and subtracted (DeAgusto, 2003).

The method I used to reduce the effects of ground roll was to apply AGC to the data and use the stack to cancel the noise. Reduction of ground roll also provides a significant area for investigation of pre-migration processing. Examination of other innovative approaches, such as those mentioned, can use this study as a baseline.

Another significant issue was to identify the proper processing flow. I used a standard processing flow in this project implying a brick acquisition pattern design for the processing steps. Acquisition of the Vinton Dome data was in a radial pattern, so differences in the acquisition pattern may have an impact on the processing.

Table 1.

Flow chart of initial processing to calculate residual static

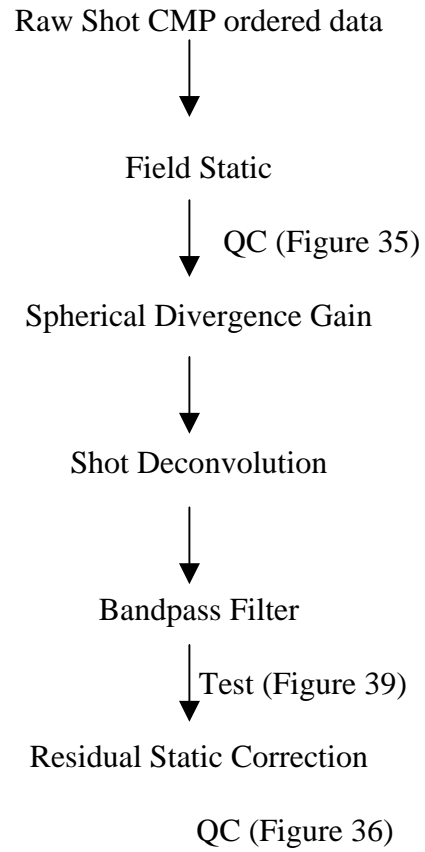
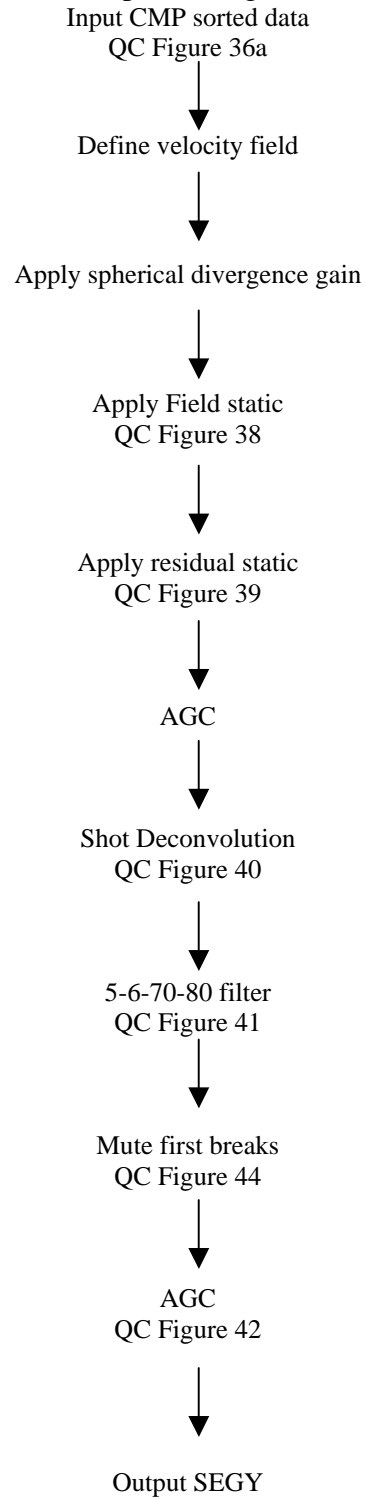


Table 2

Final processing flow



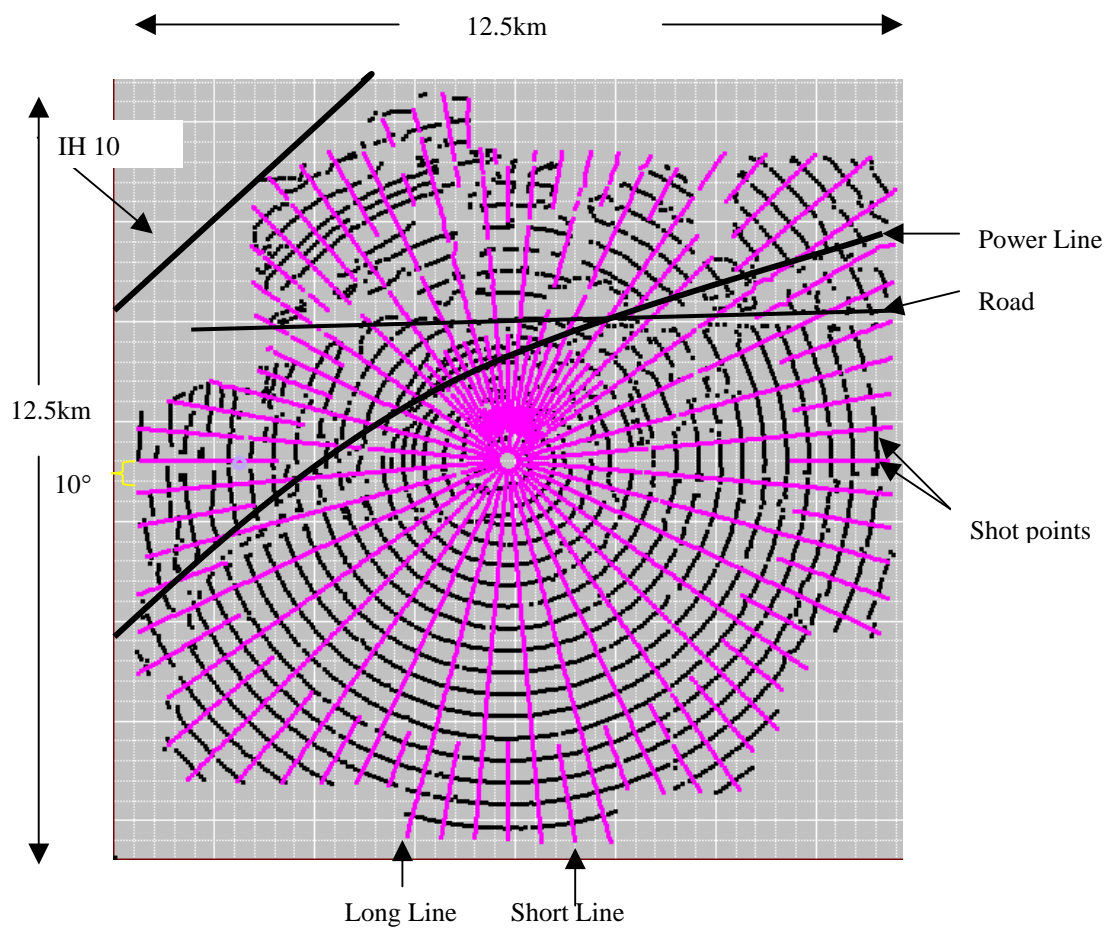


Figure 32. Acquisition pattern for the Vinton Dome Survey. Receivers are radial lines extending out from the center, shot points are roughly concentric circles Interstate Highway 10 shown running along the northern side of the survey (Constance *et al.* 1999).

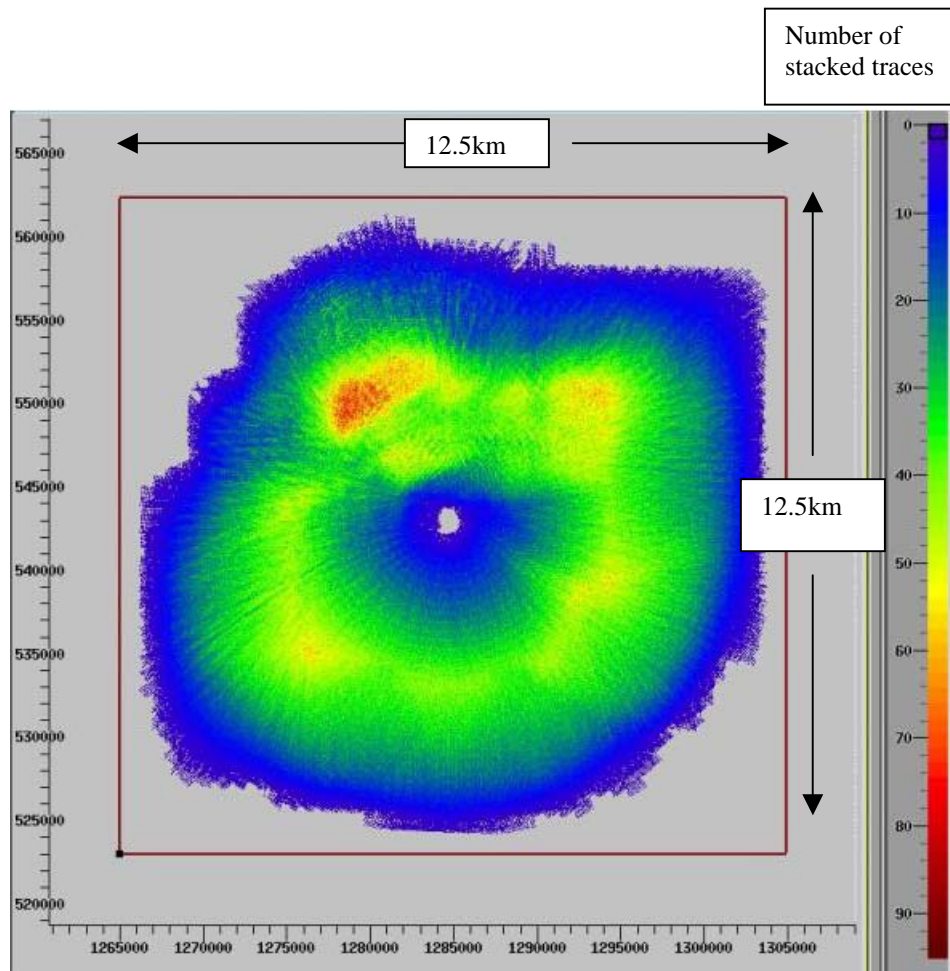


Figure 33. Fold map of the Vinton Dome Survey.

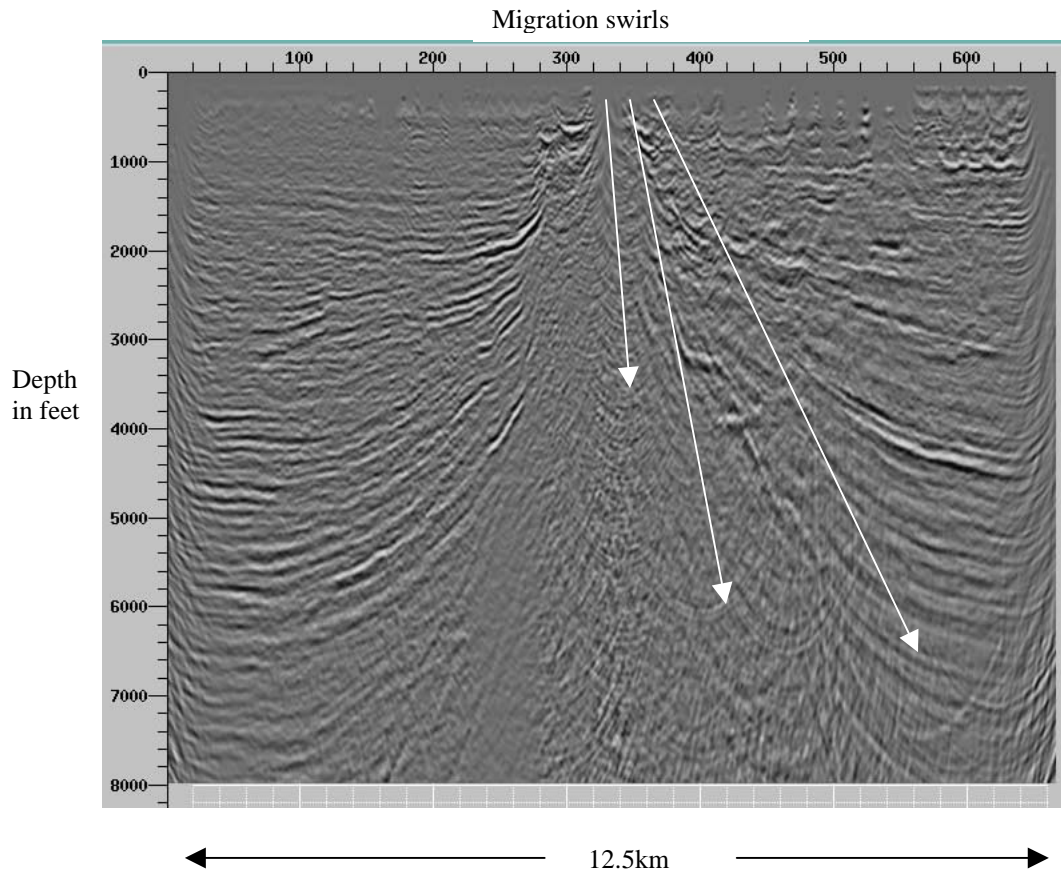


Figure 34. Migrated section of minimally pre-migration processed data with large migration swirls.

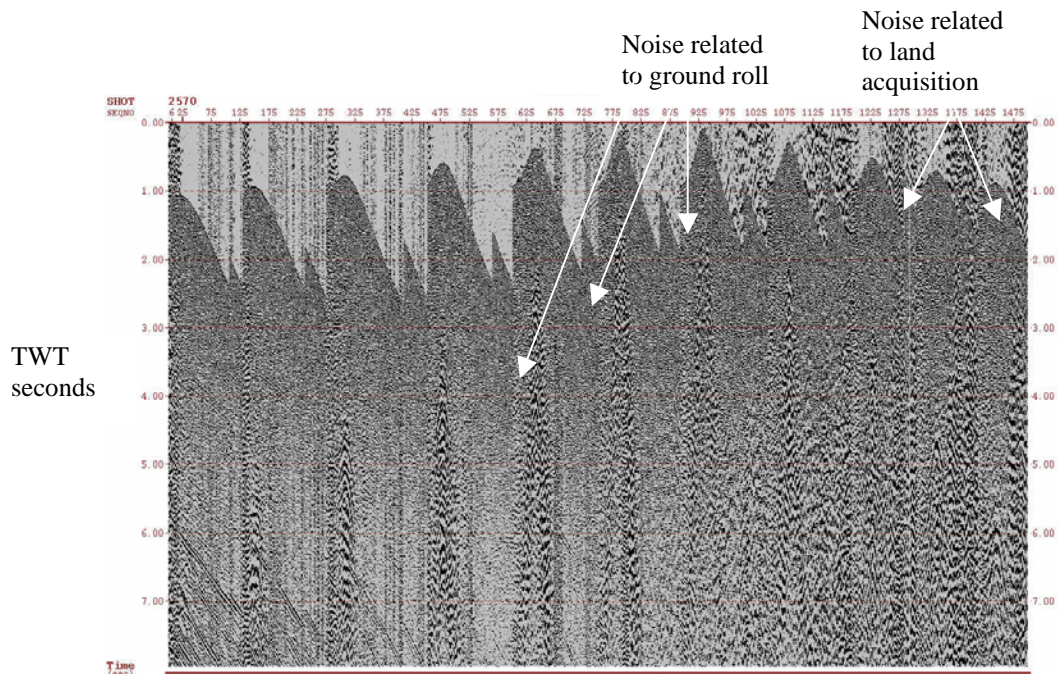


Figure 35. Shot gathers illustrating noise.

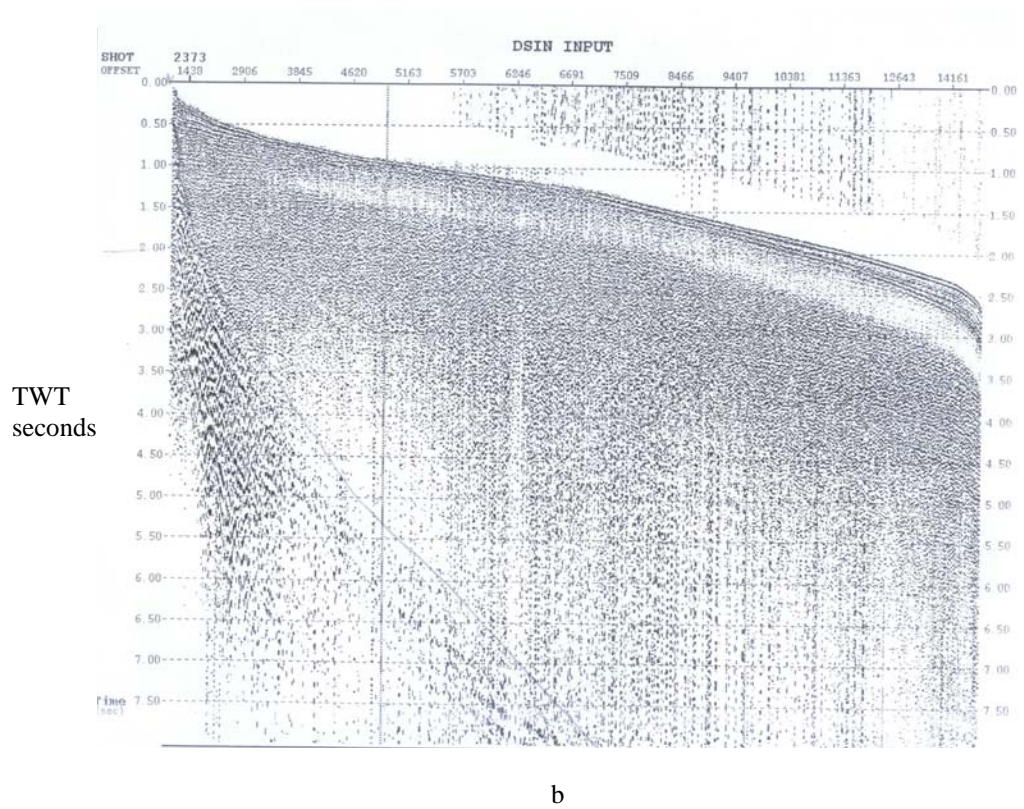
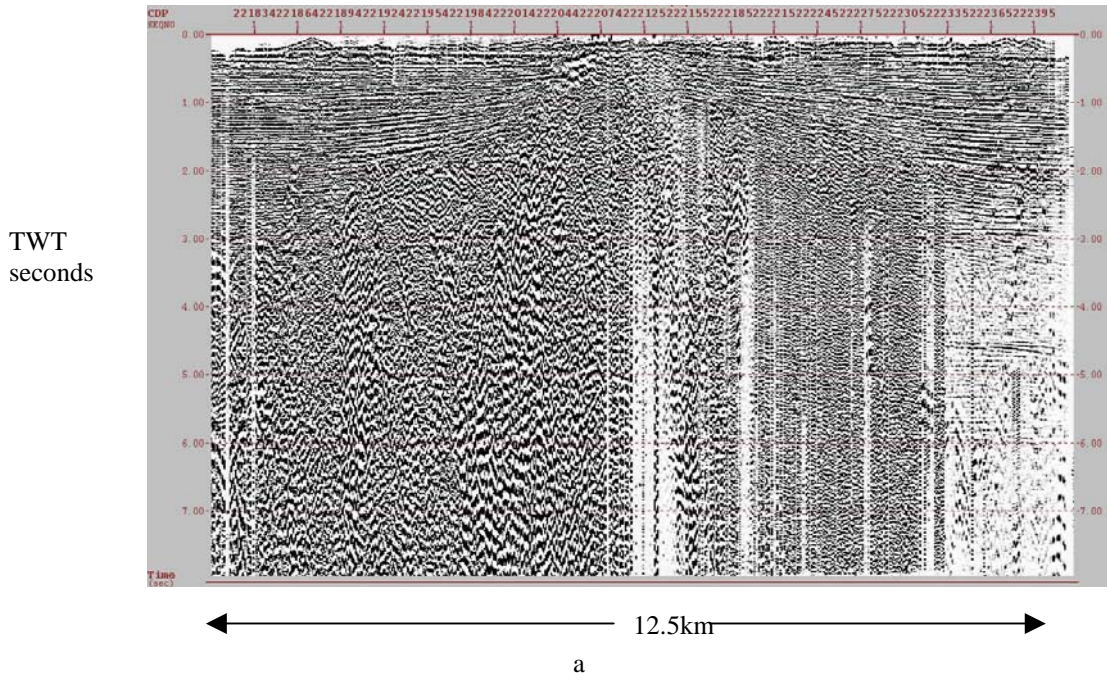
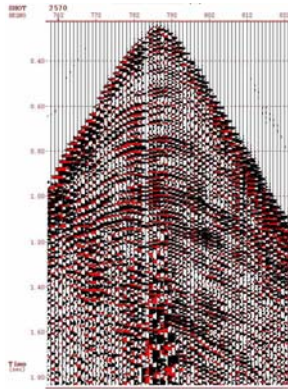
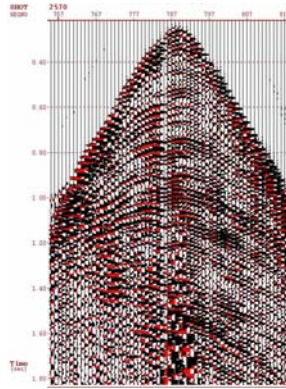


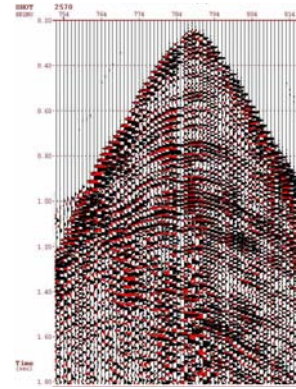
Figure 36. Stack of common midpoint sorted (CMP), (a) used to verify correct geometry based on coherent events and uniform moveout of the first arrival of a supergather, (b).



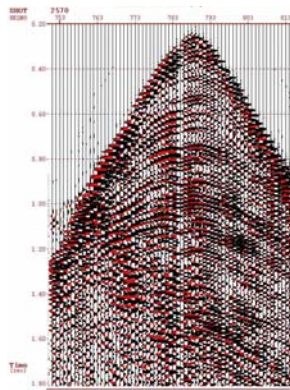
0-0-70-80



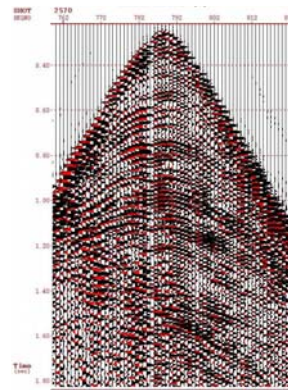
5-6-70-80



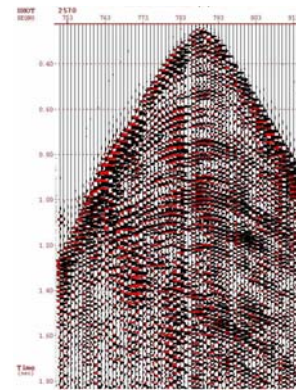
10-11-70-80



12-13-70-80



16-17-70-80



20-21-70-80

Figure 37. Filters tested to decided on the 16-17-65-75 Hz filter to remove the ground roll

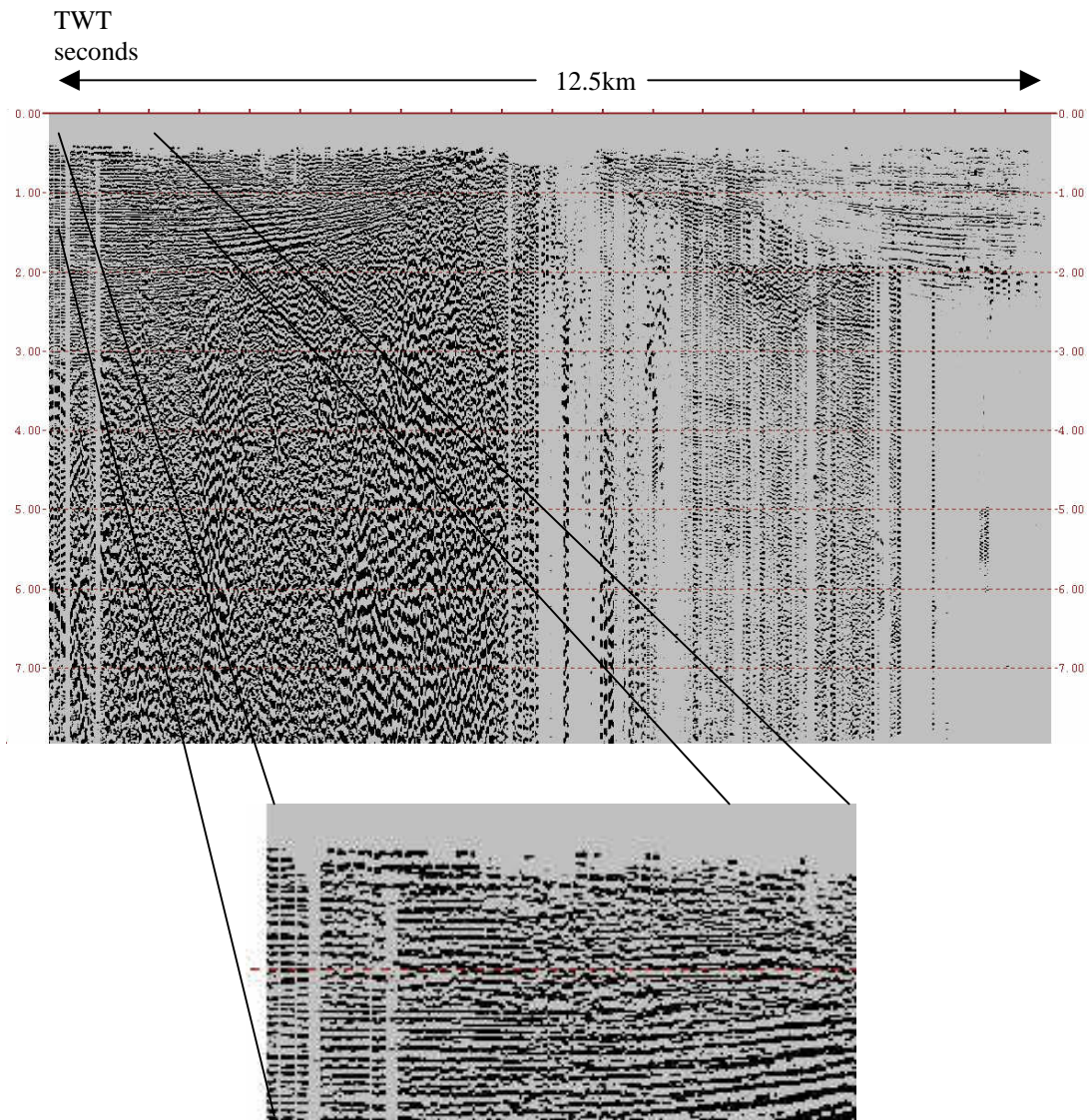


Figure 38. Brute stack of CMP sorted data with a datum static applied.

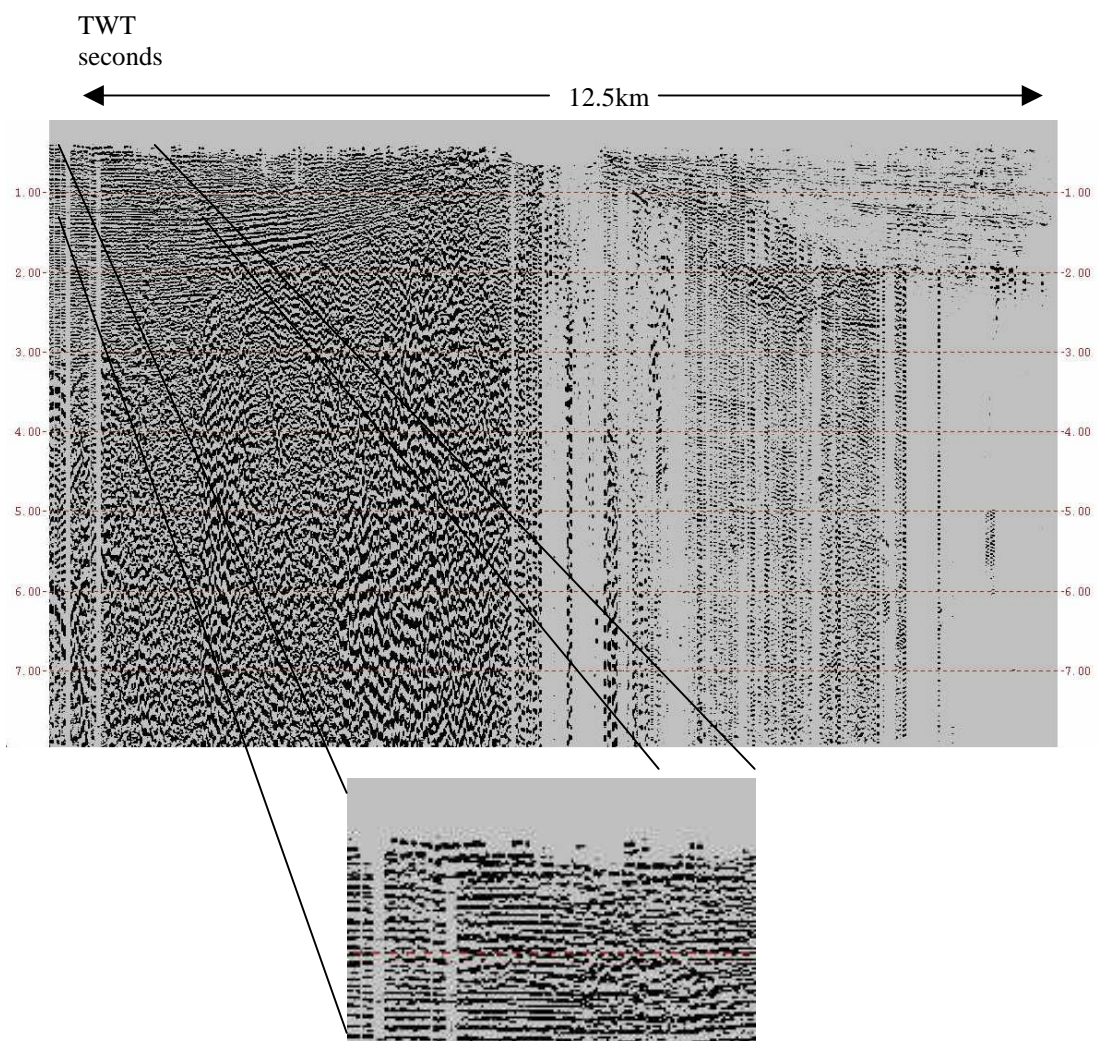


Figure 39. Brute stack of CMP sorted data with a datum static and residual static applied.

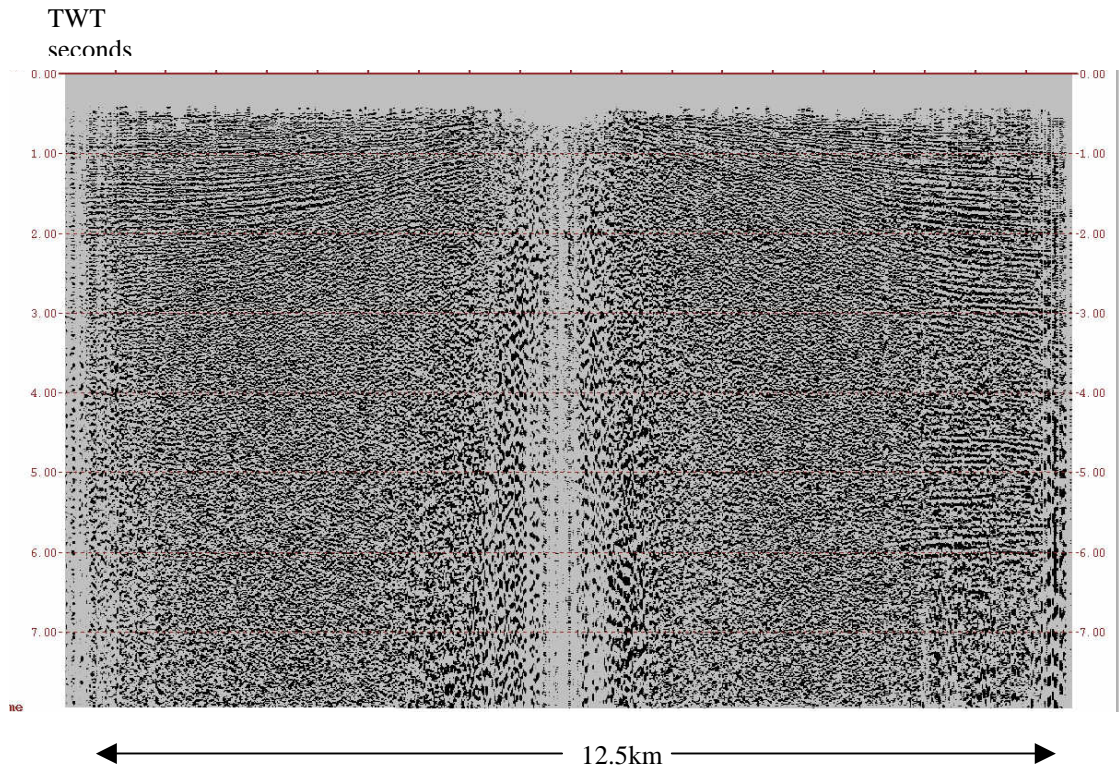


Figure 40. Brute stack of CMP sorted data with a datum static and residual static and deconvolution applied.

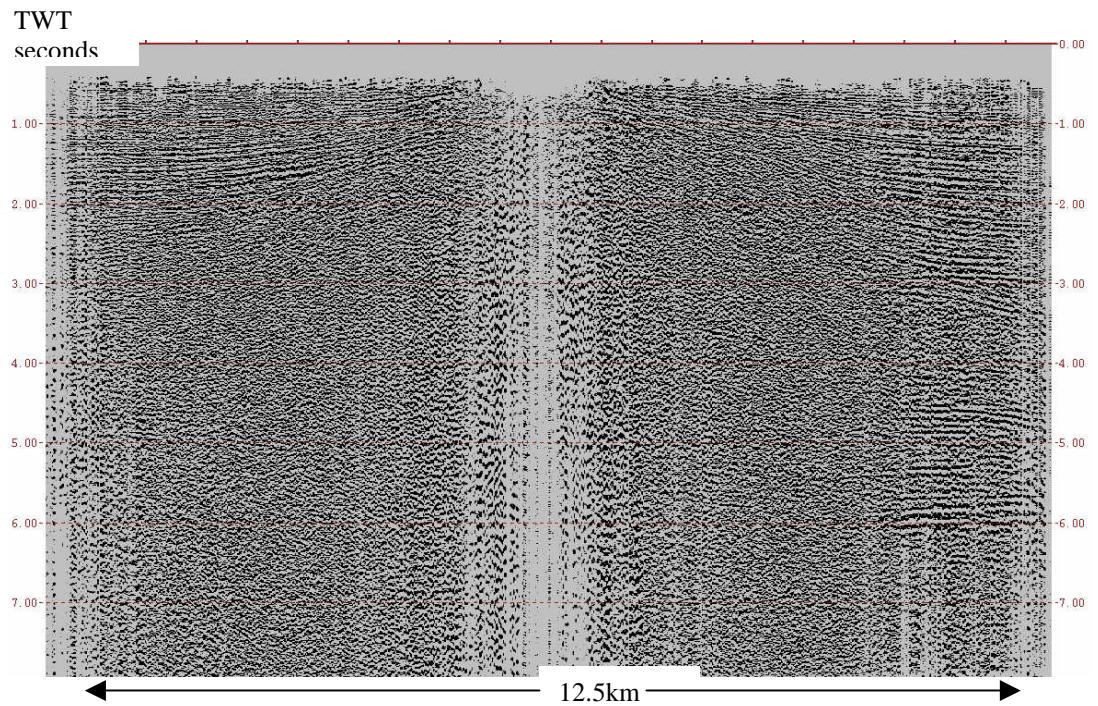


Figure 41. Brute stack of CMP sorted data with a datum static and residual static and deconvolution filtered with a 5-6-70-80 Hz filter applied .

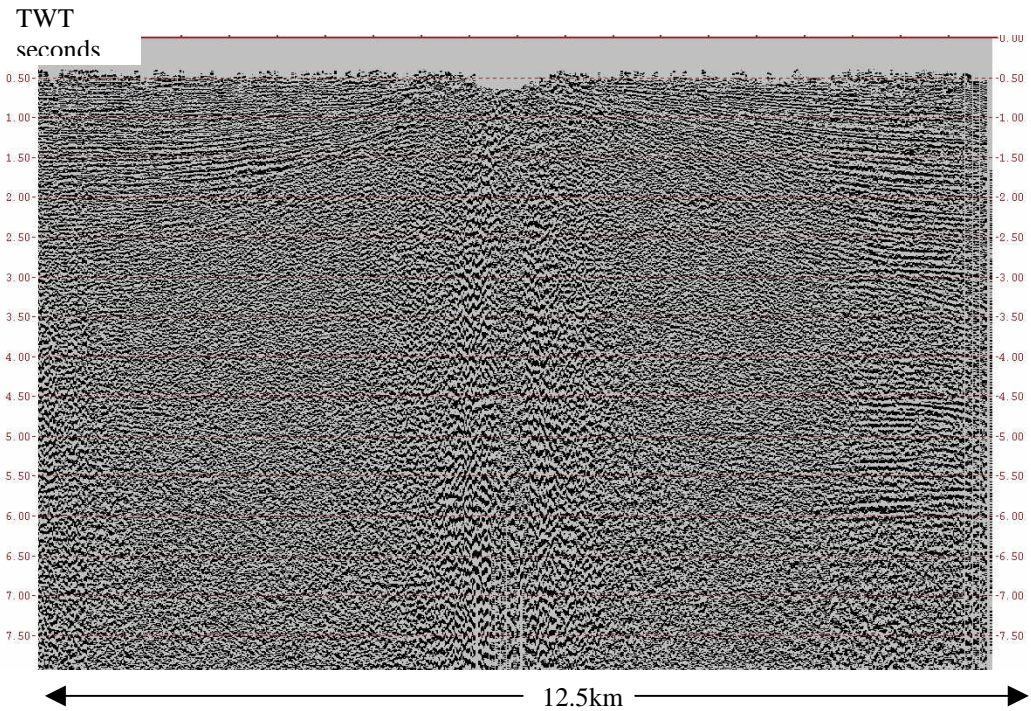


Figure 42. Brute stack of CMP sorted data with a datum static and residual static and deconvolution filtered with a 5-6-70-80 Hz filter and automatic gain control (AGC) applied .

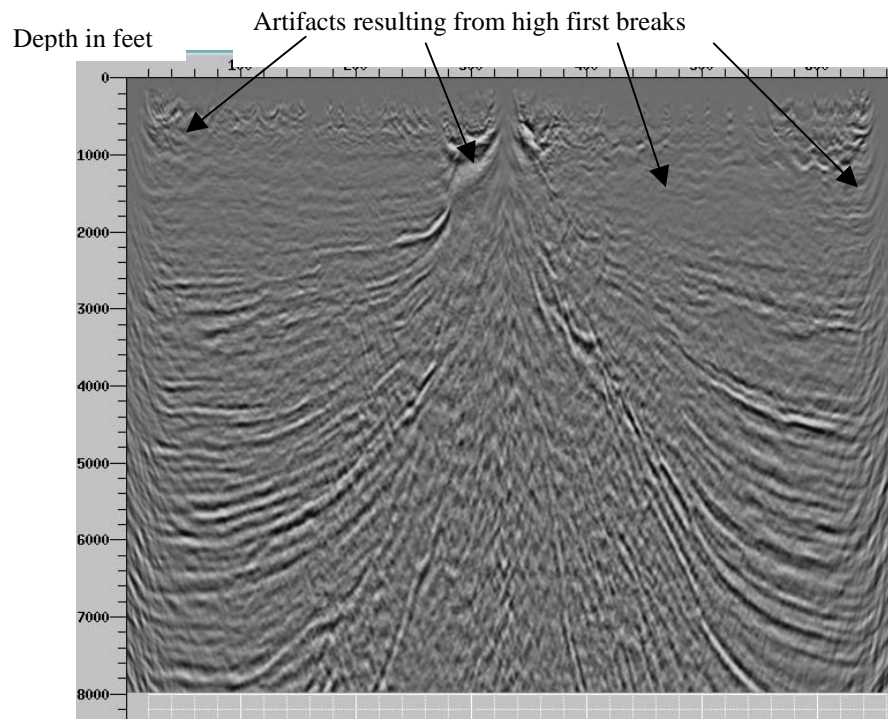


Figure 43. Migrated section showing artifacts resulting from first breaks.

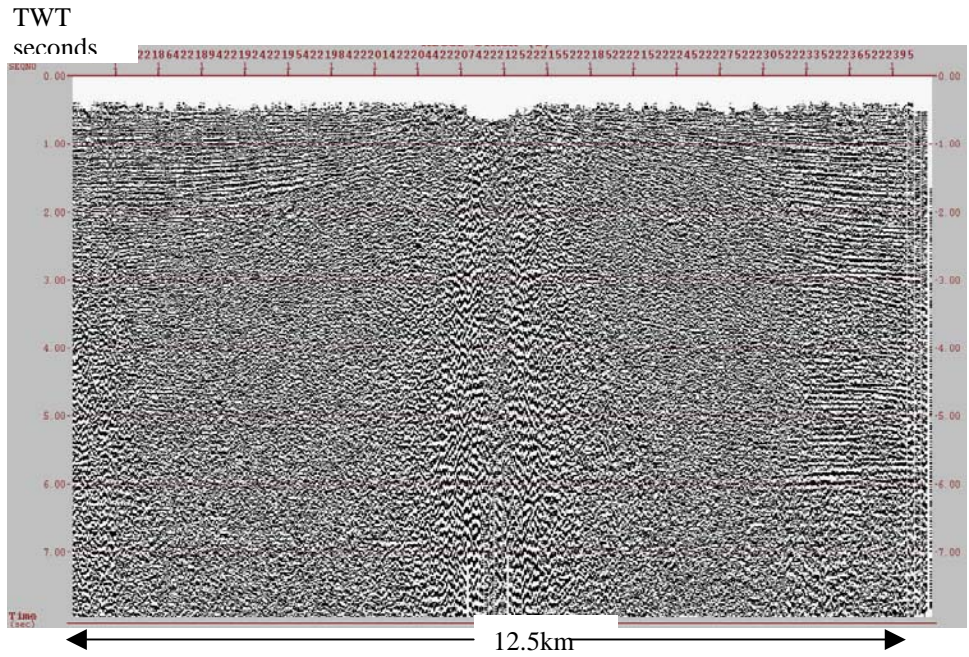


Figure 44. Brute stack of CMP sorted data with a field static and residual static and deconvolution filtered with a 5-6-70-80 Hz filter and automatic gain control (AGC) applied and first breaks muted .

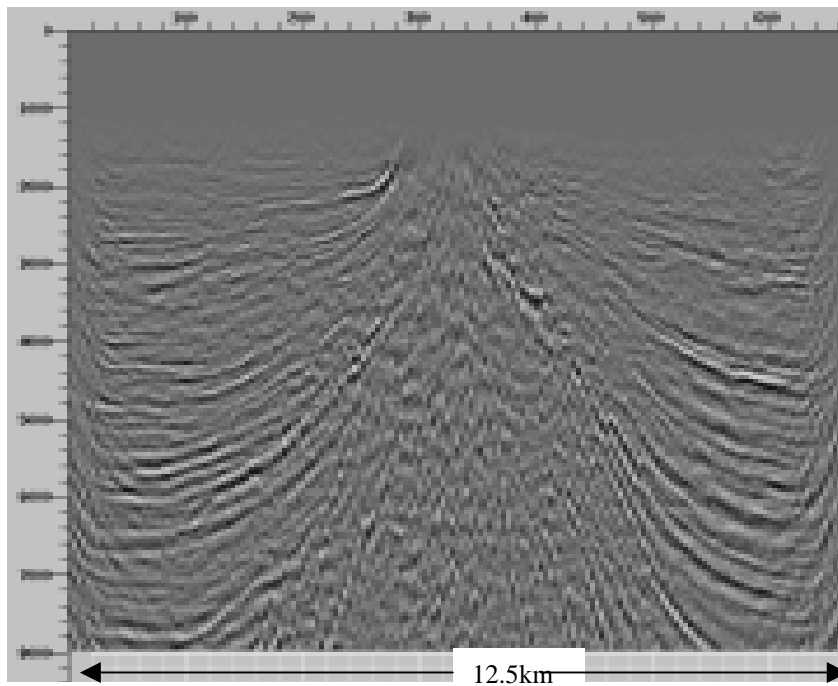


Figure 45. PSDM section of more aggressively pre-migration processed data with first breaks muted.

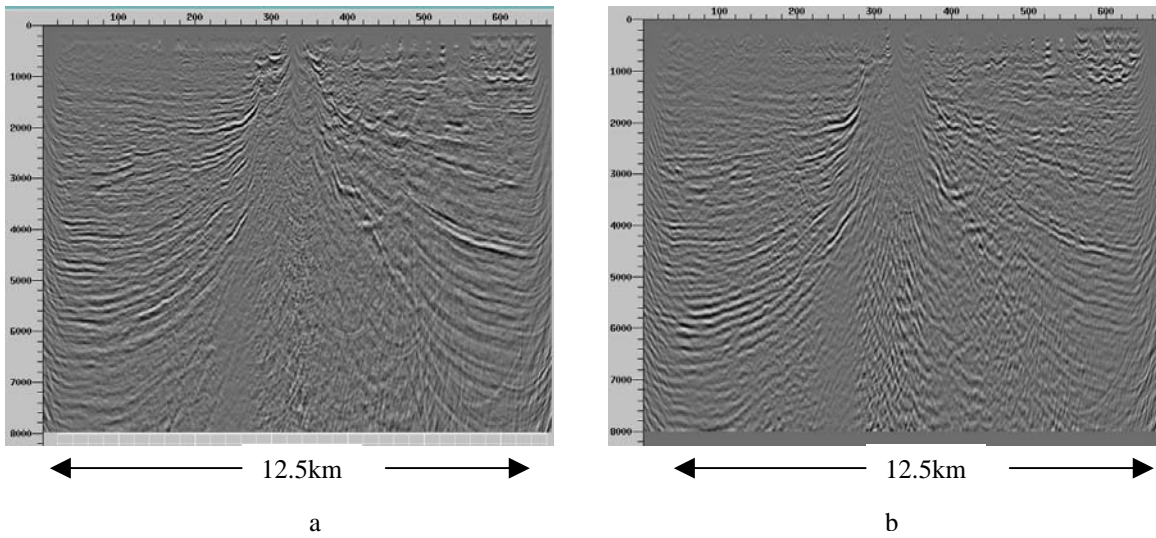


Figure 46. Sections comparing the processing flows with minimal processing Table 1(a) and more aggressive processing as described in Table 2 (b).

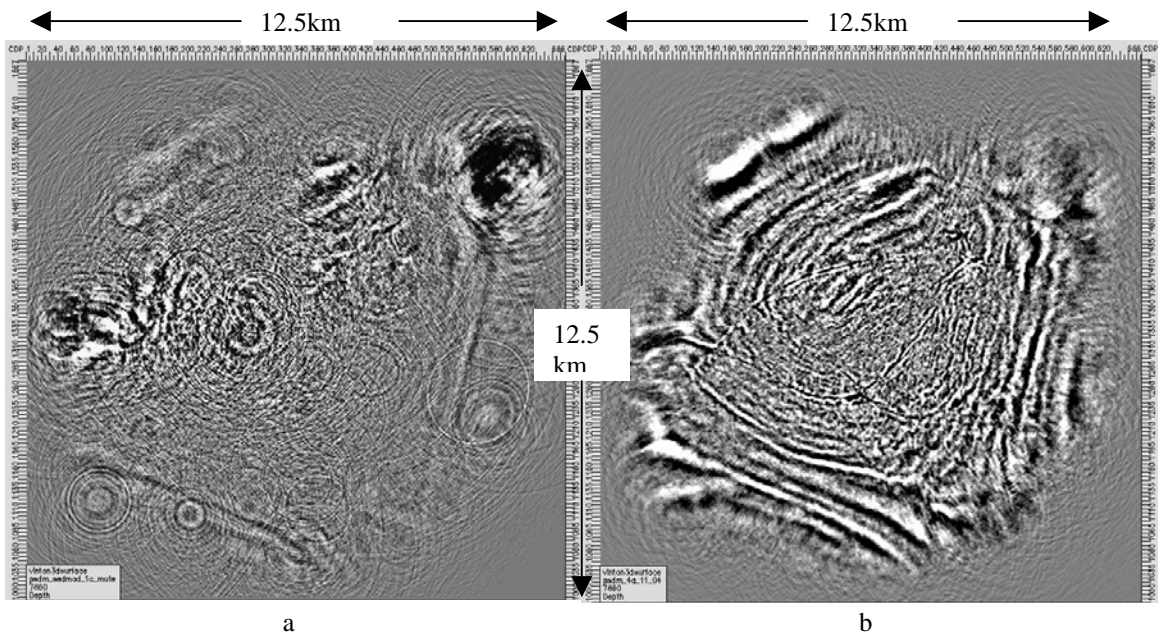


Figure 47. Depth slices used for comparing the processing flows with minimal processing (a) and as described in Table 2 (b).

Chapter 4

Velocity Modeling and PreStack Depth Migration (PSDM)

4.1 Introduction

Pre-stack depth migration (PSDM) has been widely used for large, 3-D seismic marine surveys. As a result the methods used to develop velocity models for the PSDM have been primarily based on marine data. Many of the same problems observed and mitigated in marine seismic data using PSDM exist in 3-D land surveys, but differences in 3-D marine data and 3-D land data warrant a reevaluation of methods used to generate velocity models for land data. Reexamining the methods for deriving velocity models for land PSDM has the potential for establishing a different paradigm for velocity modeling of 3-D land seismic data.

Problems resolved by PSDM in marine seismic data are observed in the pre-stack time migrated (PSTM) data in the 3-D Vinton Dome seismic survey. Misplaced salt, poor well ties and the inability to image small fault blocks are problems resulting from low fidelity of the Vinton Dome PSTM seismic data. Two primary reasons for these problems are strong lateral velocity variations caused by salt, and the related structures in the sediment section related to salt movement, and anisotropy mainly occurring in the shale bodies. PSDM using an accurate interval velocity model can generate high fidelity subsurface images in the presence of lateral velocity variations. Therefore, estimation of an accurate interval velocity model is key to improving the fidelity of the subsurface image at Vinton Dome (Fagin, 1999).

PSDM is the best current method for addressing strong lateral variations in velocity (Judson *et al.*, 1980). Greater accuracy in the velocity model relates directly to enhanced fidelity so that development of an accurate velocity model is essential in subsurface imaging (Fliedner *et al.*, 2002, Liu *et al.*, 2002, Popovici *et al.*, 2003, Schultz, 1999). I built a sediment velocity model using sonic logs, a well-based model, and compared it to the current practice of building the initial sediment model using seismic migration velocities. I will refer to the velocity model derived from the sonic logs as the well-based model, and I will refer to the velocity model derived from the seismic data as the prestack time migrated velocity model.

There were two reasons why I used the well-based approach. One is that the seismic data used to derive a prestack time migrated velocity model is prone to be noisy, especially with land data. Sources of noise in land data range from variable receiver coupling, cultural noise, static problems and a variety of other issues that are not as profound in marine data. Much of the noise that is inherent to land data is coherent and difficult to eliminate so it can have an adverse impact on velocity analysis, which in turn causes the PSDM to produce lower fidelity subsurface images. Another reason for using sonic logs to build the initial velocity model is the minimal manipulation of the velocity data. Sonic logs record velocities as depth interval velocities; and depth interval velocities are what I used for the PSDM velocity model. Seismic velocities are RMS time velocities. It is a two-step process to convert RMS time velocities to depth, once to an interval velocity and then to a depth interval velocity. Differences between land data and marine data

quality motivated a reassessment of methodologies for velocity modeling and the transformation of seismic velocities to depth interval velocities motivated the use of sonic log velocities.

4.2 Current Practices

There are two basic approaches in velocity model building, a grid-based approach and a layer-based approach (Guo and Fagin, 2002a). The grid-based approach uses seismic data to model the velocity field and velocity modeling using geologic information such as geologic horizons and structures characterizes layer-based approach. Layer-based velocity modeling uses seismic data and requires *a priori* knowledge of the subsurface. In some situations especially where there is little geologic information, a grid approach is the only applicable tool. I review both approaches before presenting my proposed improvements.

4.3 Background

Prestack depth migration (PSDM) is not a new technique; however, prestack time migration (PSTM) is more common. In general, depth migrations are appropriate only in areas with strong lateral velocity changes (Judson *et al.*, 1980). A salt dome such as Vinton Dome certainly exhibits strong lateral velocity variations. Traditionally, the limited application of PSDM was due to the large computational expense that was required to run them and the difficulty in estimating accurate velocity models. Advances in computing have reduced the computational time required to perform the imaging

procedure making the application of PSDM more common. Improved computing provides motivation for a reevaluation of the most critical phase of the process, the velocity modeling. Accurately estimating an interval velocity model from a 3-D land survey was essential to improving the fidelity of the subsurface image at Vinton Dome. In the next section I will begin by reviewing the two most common velocity modeling approaches, then I will discuss the well-based velocity modeling approach that I applied to the Vinton Dome 3-D surface seismic survey. I designed the method to make use of the sonic logs and extensive well log database.

4.4 Velocity Model Building

4.4.1 Grid-Based and Layer-Based Velocity Modeling

Grid-based velocity modeling begins by converting RMS velocities to time interval velocities. Converting RMS velocities to time interval velocities requires an x, y location, often referred to as a velocity location. The velocity location is typically associated with a reference horizon that serves to identify the interval. Using a flat horizon that is spaced evenly and increases with depth is one approach to designating the reference horizon. Interpreting a surface such as a water bottom in a marine survey that is spaced evenly at increasing intervals with depth is another common approach to identify the reference horizon. Interpreting seismic horizons is a third method to select the intervals used to determine the time interval velocity. Once the time interval velocity has been determined, application of the Dix formula (Dix, 1955) converts it to a depth interval velocity for use in the migration.

The layer-based approach is much more tedious. Identifying the shallowest layer, usually from an interval between two geologic horizons is the first step. Differing from the grid-based approach, where conversion of time RMS velocities to depth interval velocities is through the entire seismic volume, conversion of the seismic RMS velocities to depth interval velocities in the layer-based approach is only in the layer. Restricting the velocity model to a single layer allows modeling of detailed velocities by incorporating *a priori* geologic knowledge, often from well logs, into the model. A detailed velocity model will potentially enhance the fidelity of the subsurface image. Another important aspect to this approach is that it is critical to provide as much detail to the shallow layers to minimize the impact of spurious data that will propagate through the seismic volume. After migration in the shallowest layer, the next iteration follows using the same method to the next layer. This continues, identifying geologic layers, deriving a detailed velocity model, and migrating one layer at a time until completion of a velocity model to the targeted depth and applying a full PSDM to the entire survey (Guo and Fagin, 2002b).

4.4.2 Velocity Modeling of Vinton Dome

My motivation was to design a detailed velocity model like a layer-based model, and as efficient to build as a grid-based model. Velocity models for a PSDM must be accurate so using seismic velocities to build an initial sediment velocity model requires that the seismic data are accurate. PSDM is more common with marine data than land data so the methodologies for building velocity models are primarily for marine data. Differences between marine data and land data are in the superior quality of 3-D seismic marine data

because of the higher signal-to-noise ratio in marine data. This is a reason why marine data are better candidates for PSDM as well as for building an initial sediment velocity model.

Typically, in areas containing salt such as the upper Gulf of Mexico Basin, the focus of the velocity modeling is to image the shape of the salt. The first step in this iterative process begins with an initial sediment velocity model. With this model, data are PSDM and used to update the model by picking a top of salt horizon. Salt velocities are flooded beneath the salt and the data are re-migrated. Using the new PSDM volume allows for focusing details in the salt by iteratively updating and detailing the velocity model. The iterative nature of this process requires that the initial sediment velocity model be as accurate as possible. Removing errors that propagate throughout the process from the beginning often require starting over. Starting with high signal-to-noise ratio data and smoothing the velocity model reduces the spurious data in marine 3-D seismic surveys. I explored an approach to minimize the lower signal-to-noise ratio typically found in land data and to insure an accurate initial sediment velocity model.

I began deriving an initial sediment velocity model for a PSDM of 3-D surface seismic land data by addressing the differences in data quality between 3-D marine data and land data. Recognizing that land data has differences from the marine data that limit the strength of the signal, I devised an approach to velocity modeling that did not use the seismic velocities. I used sonic logs to build the initial sediment velocity model instead

of seismically derived velocities. Vinton Dome has a long production history resulting in an abundance of well control. Well data are often used to update a velocity model by providing information regarding well ties because they provide values for vertical velocities and as such are suitable for depth conversion (Schultz, 1999) but are regarded by some as inappropriate for a velocity model. Issues of velocity differences between well logs and seismic velocities typically preclude their exclusive use to build an initial velocity model. In this survey I used eighteen sonic logs to build an initial sediment velocity model. None of the wells were deviated and any borehole drift that may have occurred was not great enough to be detected with the lower resolution seismic data. Positioning of most of these wells was close to the flanks of the dome where the majority of production is located.

I plotted wells to determine their spatial relationship to each other and to the salt. Smoothing the log curves reduced the spurious effects of outliers caused by well bore conditions such as washout. I generated a 1-D, V_z , velocity gradient from the sonic logs biasing the farthest log from the salt to derive the gradient. I weighted this log because I regarded the velocities from it as reflecting the regional velocity trend (Figure 48).

I picked seven geologic horizons on PSTM data. To fill gaps created by the throw of faults and to bridge the gap created by the salt I interpolated and smoothed the horizons. Smoothing the horizons in this manner allowed me to create a reference that had a basis

in geology and depth, but more importantly, I maintained the relative position and spacing of each horizon to one another (Figure 49).

Using the V_z velocity gradient, I converted the horizons to depth. With the seven geologic horizons in depth, I plotted the wells with respect to the horizons to determine where the logs intersected the horizons. Logs extend to different depths so not all logs penetrated the same horizons. With points of known depth from the sonic logs, I flexed the horizons to fit the logs. I adjusted horizons I interpreted from the seismic data to match the sonic logs keeping the relative spacing between horizons. I applied the sonic log velocities at the point of intersection between the horizon and the log. Then I calculated a sloped interval velocity between horizons by using the velocity at the intersection from the top horizon to the next horizon down. By extrapolating velocities from the wells, I built the velocity cube (Figure 50). Variations in layer thickness resulted in a nonlinear extrapolation.

My initial QC of the model by comparison with known structures helped validate the model. Smoothing and extrapolation initially removed all structure from the horizons I used to build the model; yet, in the velocity cube there are faults as can be seen in Figure 51. By comparing the velocity model and the PSTM seismic volume, I confirmed that the structures were real. Even with sparse sampling of well logs, this technique was sensitive enough to include structure into the initial sediment velocity model.

To test differences between seismically derived velocity models and the method I developed in this study using velocities derived from well logs a prestack time migrated velocity model was built and the data were PSDM using it. I converted stacking velocities to depth interval velocities with the same horizons used to create the well log velocity model. Building the prestack time migrated velocity model followed an industry standard workflow using commercial software. I linearly extrapolated velocities to fill empty cells resulting in a blocky velocity model (Figure 52) that I smoothed (Figure 53). Surface seismic data were PSDM with the prestack time migrated velocity model smoothed and I compared it to the PSDM volume generated with the velocity model derived from well logs.

I compared the two methods using common image gathers (CIGs) from various locations (Figure 54). My conclusion is that differences in the two indicate the sonic log model is the more accurate of the two based on the flatness and coherence of the sonic log CIGs (Figures 55-58).

4.3 Migration

I used a Kirchhoff PSDM to migrate the surface seismic data with commercial software. Analysis of the acquisition, using software from the vendor, is what I used to determine processing parameters. Setup parameters were limited to what was available as options on the graphic users interface (GUI) (Figure 59). I determined the migration aperture parameters from the acquisition and generated two histograms showing offset in the

inline direction and crossline direction (Figure 60). From these histograms, I determined the parameters for migration. Output parameters were also set based on acquisition, a 0 - 180° radius was set because of the radial acquisition. The software vendor provided me with suggestions to improved efficiency.

4.4 Migration Results

I compared the results from the initial sediment model migration to the PSTM seismic volume. Improved resolution was apparent in the PSDM especially in imaging the salt flanks (Figure 61). I imaged the salt flanks with more detail, and coherent events were maintained deeper into the survey (Figure 62). One of the benchmarks I used to assess the value of this method was the ability to image small compartmentalized reservoirs. In the PSTM volume fault compartments that had been interpreted using log data were not imaged, but in the initial PSDM faults are more focused and smaller faults can be interpreted that were not imaged in the PSTM volume. Differences in the two volumes are apparent in the portion of the survey where small, compartmentalized fault blocks were interpreted using well logs but not imaged in the PSTM (Figure 63). I was able to interpret fault blocks in this portion of the survey, identified by the missing section in the Anahuac picks on the well logs, with the well-based PSDM (Figure 64).

Comparing the well-based and prestack time migrated velocity model PSDM I can identify several differences. The same events are at different depths, the prestack time migrated velocity model PSDM data places events at about 200 feet shallower, indicating a slower model, or a faster well-based model. Fault planes are more coherent in the well-

based data, indicating higher fidelity because seismic events are in their proper x, y, and z space. A section perpendicular to the traverse in Figure 65 also images fault planes that are more coherent in the well-based section. Another interesting observation is the event that intersects the Anahuac well pick when followed eastward merges into an event that is salt on the PSTM (Figure 65). Observing the depth sections of both velocity models also provides differences in the data set for comparison (Figure 66). Imaging of faults and the salt are more coherent in the depth slice from the well-based PSDM than from that of the prestack time migrated velocity model PSDM.

Another illustration of the improved fidelity provided by the PSDM is from the drilling of a bright spot interpreted with the PSTM (Figure 67) near the salt flank. A comparison of the PSDM from both the well-based velocity model and the prestack time migrated velocity model show that there is no bright spot. Analysis of the PSDM shows that there is salt at that location, although the impedance contrast is not as great as it is shallower (Figure 68). There are two issues in the differences of the PSTM and the PSDM that further demonstrate the improvements in imaging provided by the well-based PSDM. The first is the bright spot that appears in the PSTM but is not in the PSDM. An explanation for this is that incorrect modeling of velocities close to the salt flank resulted in constructive interference of noise. This explanation is appealing because of the close proximity to the salt and the inherent difficulty of imaging salt flanks with PSTM. Both of the PSDM seismic volumes do not image a bright spot demonstrating the ability of PSDM to image in areas of strong lateral velocity changes. The second issue is the

decreased impedance contrast of the salt flank in the PSDM. To investigate this I cross-plotted impedance with depth. I calculated the impedance of the sediments from sonic and density logs. Using a velocity of 15,000 ft/sec and a density of 2.2 gm/cm³ I calculated the salt impedance to be 33,000 and because the velocity and density of salt remain constant, the impedance does also. Using the cross-plot (Figure 69) and extrapolating the trend line shows that the sediments in the Vinton Dome survey begin to approach the same impedance as salt at about 7000 feet, the same as where the salt impedance contrast begins to diminish.

I interpreted compartmentalized faults on a traverse that was not along a dip line to the faults. To further investigate and compare the fidelity of the different migrations, I compared the dip lines through the fault blocks (Figure 70). Interestingly, what these indicate is that the well-based PSDM is higher frequency and images the faults and salt flanks better, but the PSTM has imaged the shallower faults almost as well. This further demonstrates the power of the PSDM is in areas of strong lateral velocity changes.

A final test was to compare synthetic seismic derived from well logs and compared to the data. Typically, synthetics are stretched and squeezed to fit the data but for this test I choose not to adjust the synthetics. By not adjusting the synthetics to match the seismic data, I could evaluate which most closely matched the synthetic. In some areas the differences were very compelling and in most the well-based PSDM most closely matched the synthetics (Figure 71)

4.5 Conclusions and Discussion

I compared 3-D surface seismic data from the Vinton Dome survey that were migrated using a well log velocity model to data generated using the seismic or prestack time migrated velocity model. I have identified improvements in both migrated sections compared to the PSTM based on the fidelity and detail of the images. To determine which of the two provided a better image, I used two criteria: comparison of CIGs and analysis of the migrated sections using well ties.

Analysis of CIGs was uniform throughout the survey. Near traces were close to the same in gathers from both models. Differences were primarily in the far offsets (Figures 55-58). In most all of the CIGs far offsets in the prestack time migrated velocity model were slightly to considerably less flat than those of the well-based model. An additional criterion used to justify the accuracy of the well-based migrated data was the coherence of the CIGs demonstrating that traces are correctly positioned from near to far offset in the well-based data.

I also used well ties to determine which of the two methods provided higher fidelity.

An area know to have small compartmentalized faults was used for comparison.

Identification of these faults in the PSTM volume was from well data because the PSTM does not image them. Both PSDM volumes image faults in the area that the well logs indicated. I based a fault interpretation from the well logs by the thinning of the Anahuac

between two closely spaced well bores. The well-based model on two perpendicular traverses imaged the faults more sharply than did the prestack time migrated velocity model PSDM. Differences in the depth of events indicate that the well-based model is faster. The question is which is correct or has the higher fidelity. On the prestack time migrated velocity model PSDM, the Anahuac horizon pick leads into what is likely salt, and was interpreted as such on the PSTM. Another example of improved fidelity is in the higher resolution of the well-based PSDM in the depth slice. Comparing depth slices both faults and the salt have greater fidelity in the well-based PSDM based on the events being better focused resulting in coherent events in the well-based volume. Generating synthetic seismic was another method of tying the wells to the seismic. In these examples the closest match of the synthetic was to the well-based velocity modeled PSDM seismic.

Differences in the quality of the migrated volumes can be due to several reasons. Generating velocities from time migrated common mid-point (CMP) gathers with velocities that were not as accurate is one way to explain the differences in quality. This is a reasonable explanation why the bright spot did not exist. Reduced accuracy of velocities can result from problems that are inherent with 3-D land surveys such as poor receiver coupling, background noise from cultural sources such as traffic and power lines, and a variety of other known sources of noise. Affecting data quality may be differences in the modeling. Transforming velocities from RMS to time interval velocities and then to depth interval velocities is necessary with a prestack time migrated velocity model.

By using sonic logs the velocities are already depth interval velocities. Based on the well ties, the consistency of the horizon picks, and the continuity of the data, the conclusion is that the well-based velocity model more accurately traces the seismic rays resulting in higher fidelity.

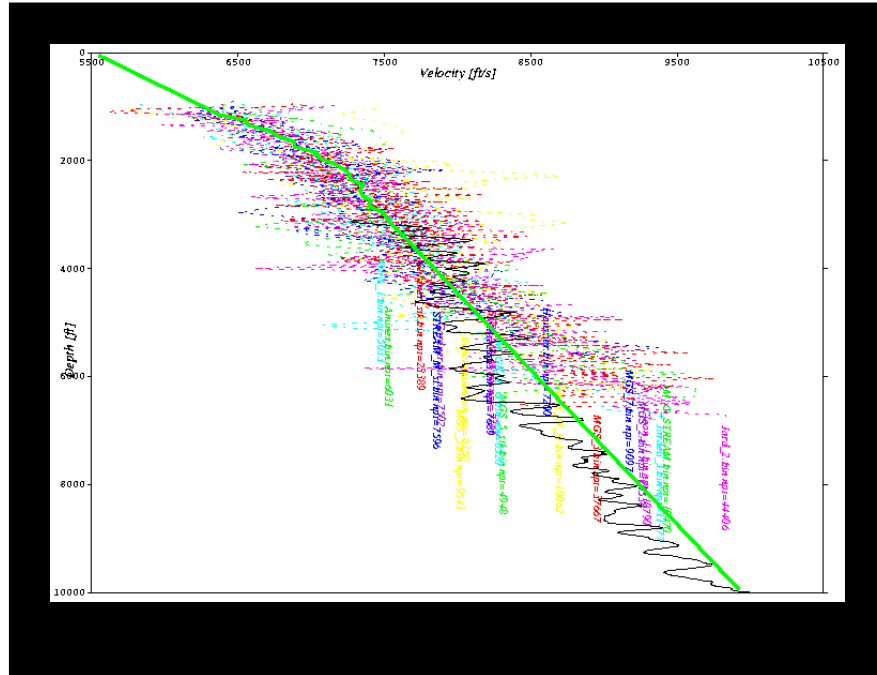


Figure 48. Depth interval velocities from sonic logs, velocity gradient derived from logs green represented by the green line.

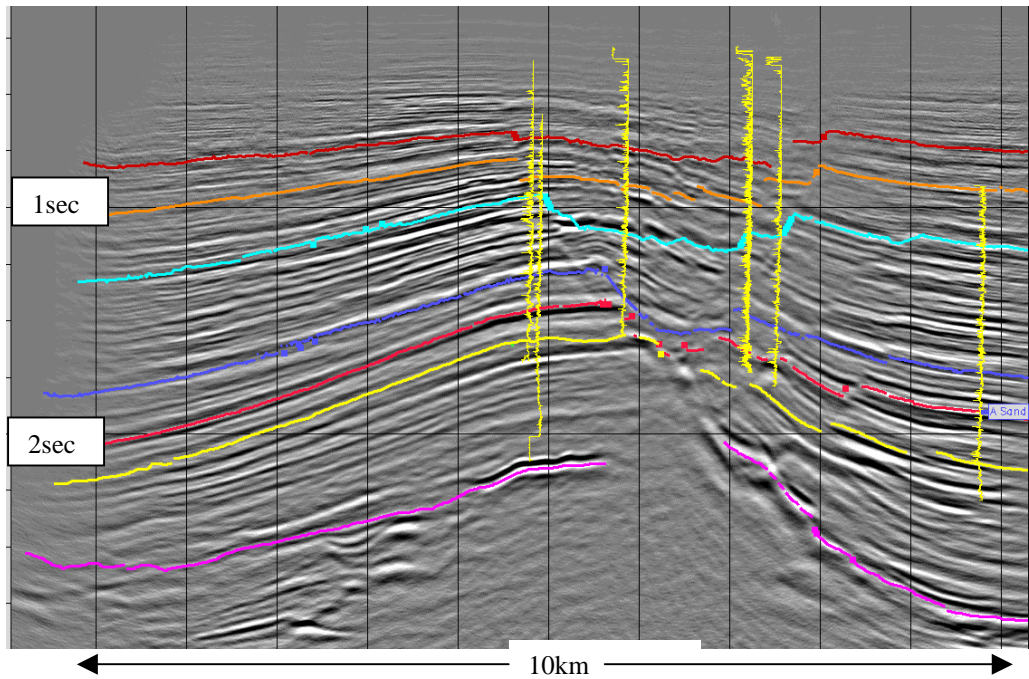


Figure 49. Horizons used to define intervals in the velocity model.

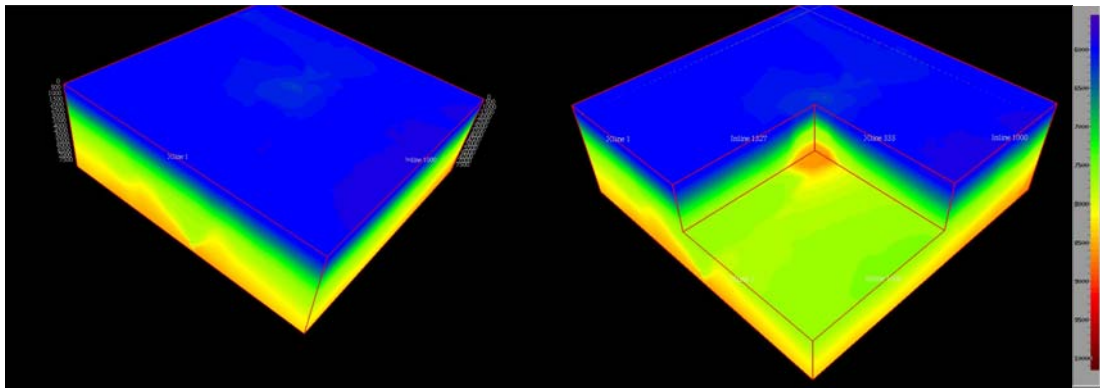
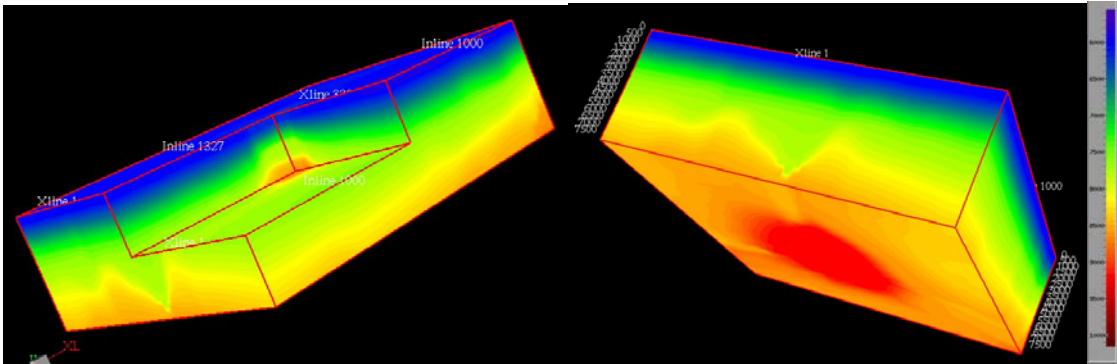


Figure 50. Velocity cube of the sediment velocity model derived from sonic logs.

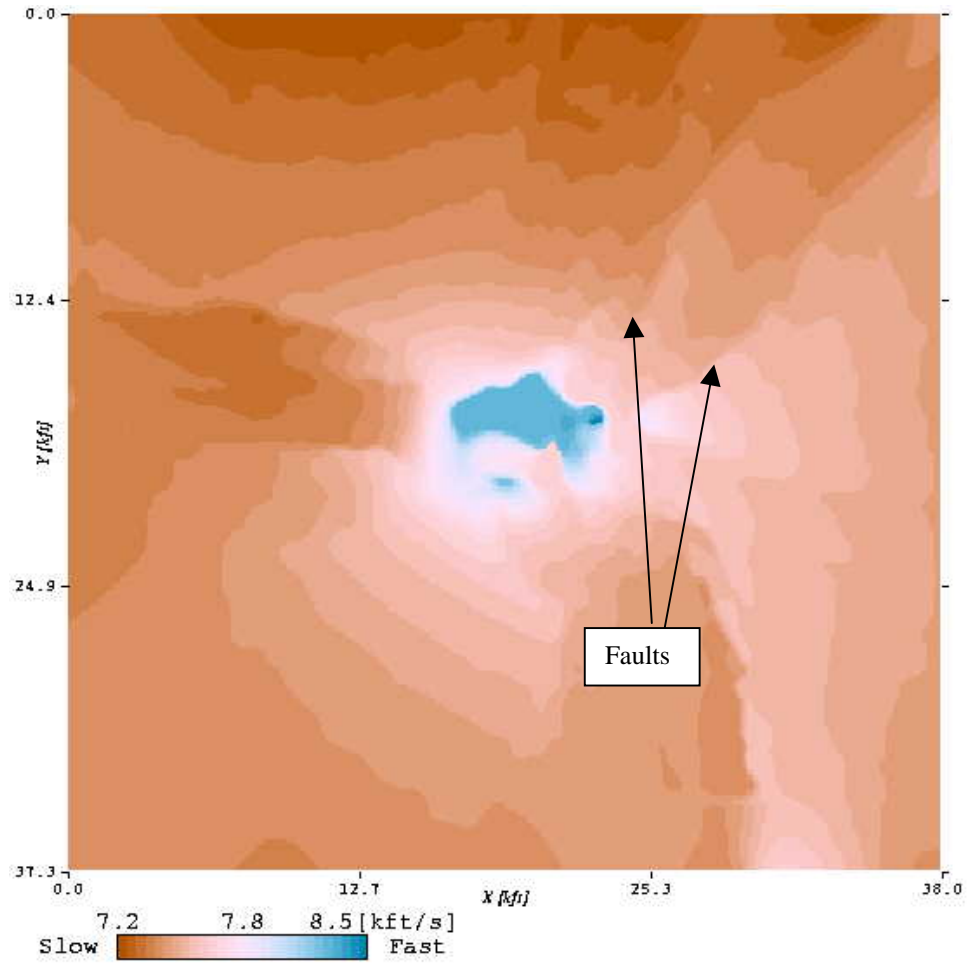


Figure 51. Depth slice from velocity model showing details such as faults appear in the sediment velocity model.

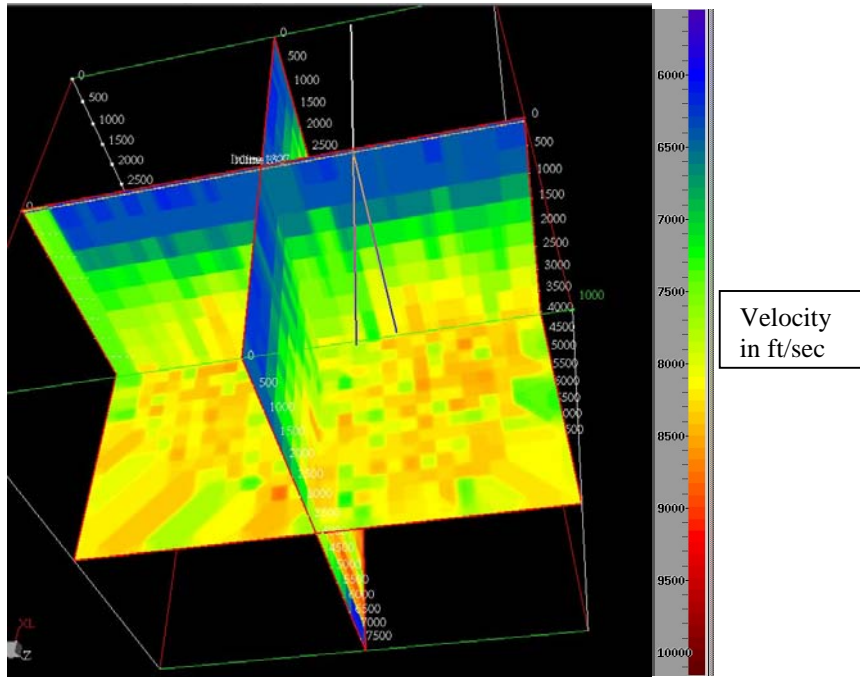


Figure 52. Prestack time migrated velocity cube of linearly extrapolated seismic velocities.

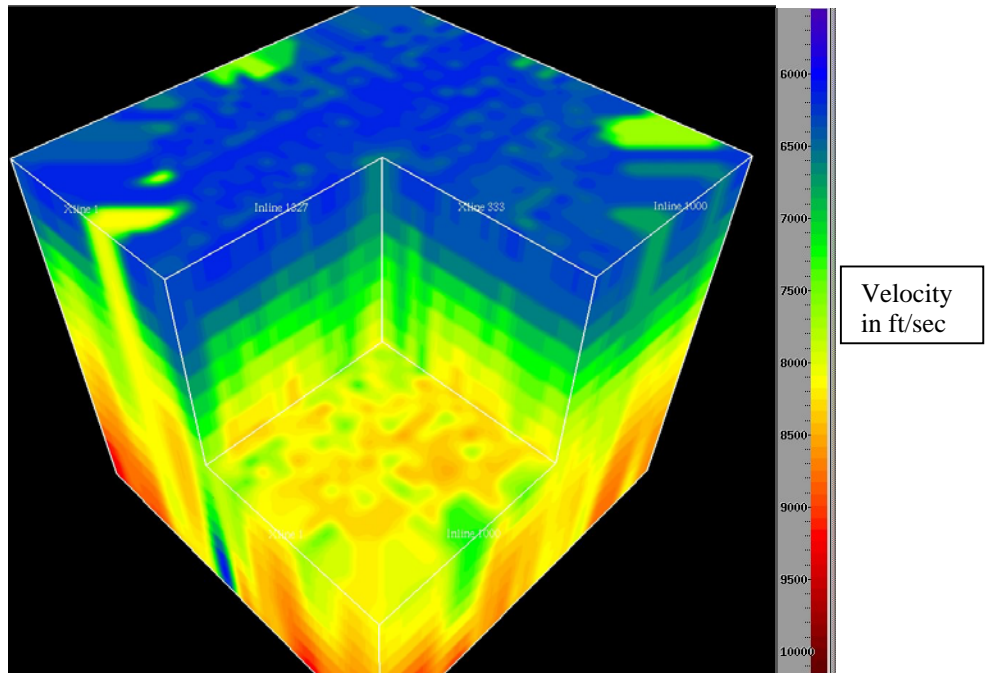


Figure 53. Smoothed prestack time migrated velocity cube used to PSDM data for comparison with PSDM from the well-based velocity model.

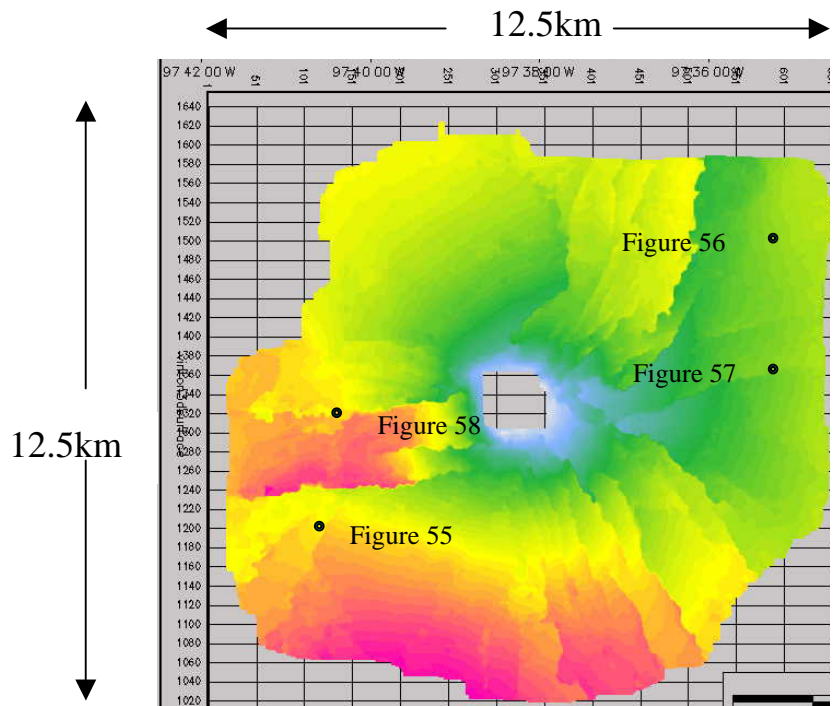


Figure 54. Map indicating locations of common image gathers used to compare the prestack time migration velocity model to the well-based velocity model.

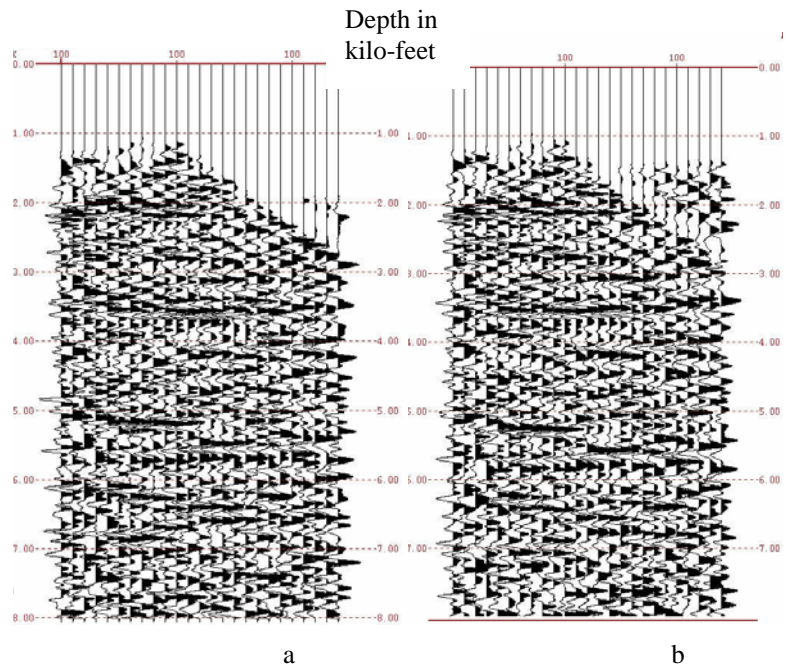


Figure 55. CIG line 1100 crossline 100 from well-based model (a) and prestack time migrated model (b) illustrating flatter and more coherent gathers in the well-based model.

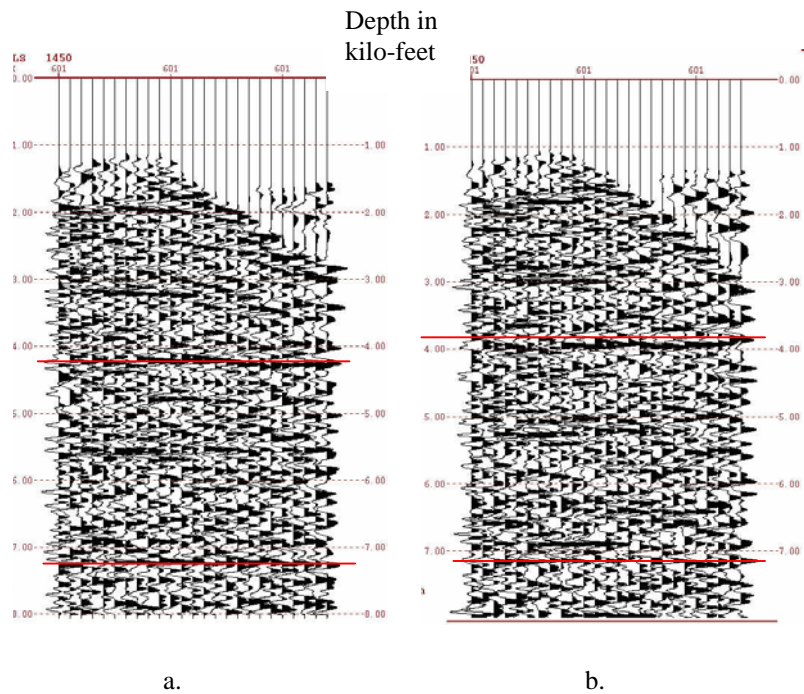


Figure 56. CIG line 1450 crossline 601 from well-based model (a) and prestack time migrated model (b) illustrating flatter and more coherent gathers in the well-based model.

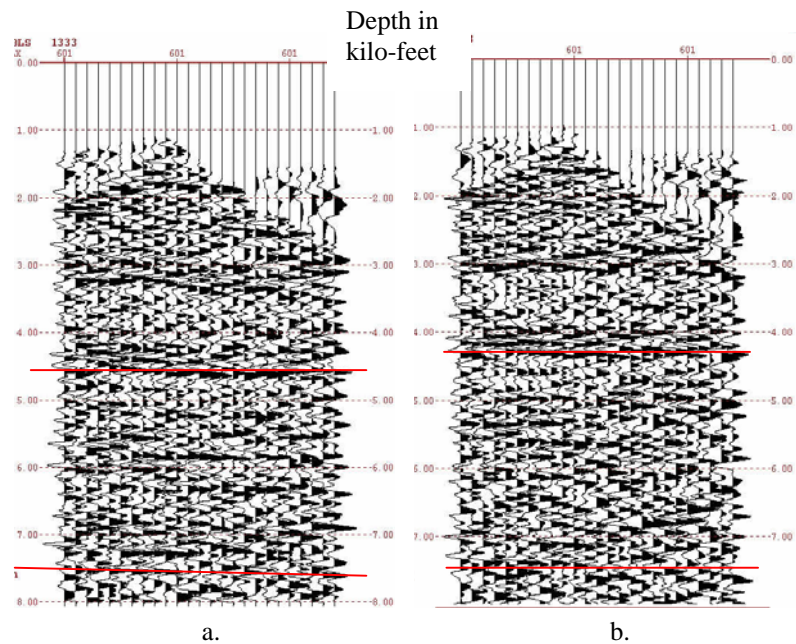


Figure 57. CIG line 1333 crossline 601 from well-based model (a) and prestack time migrated model (b) illustrating flatter and more coherent gathers in the well-based model.

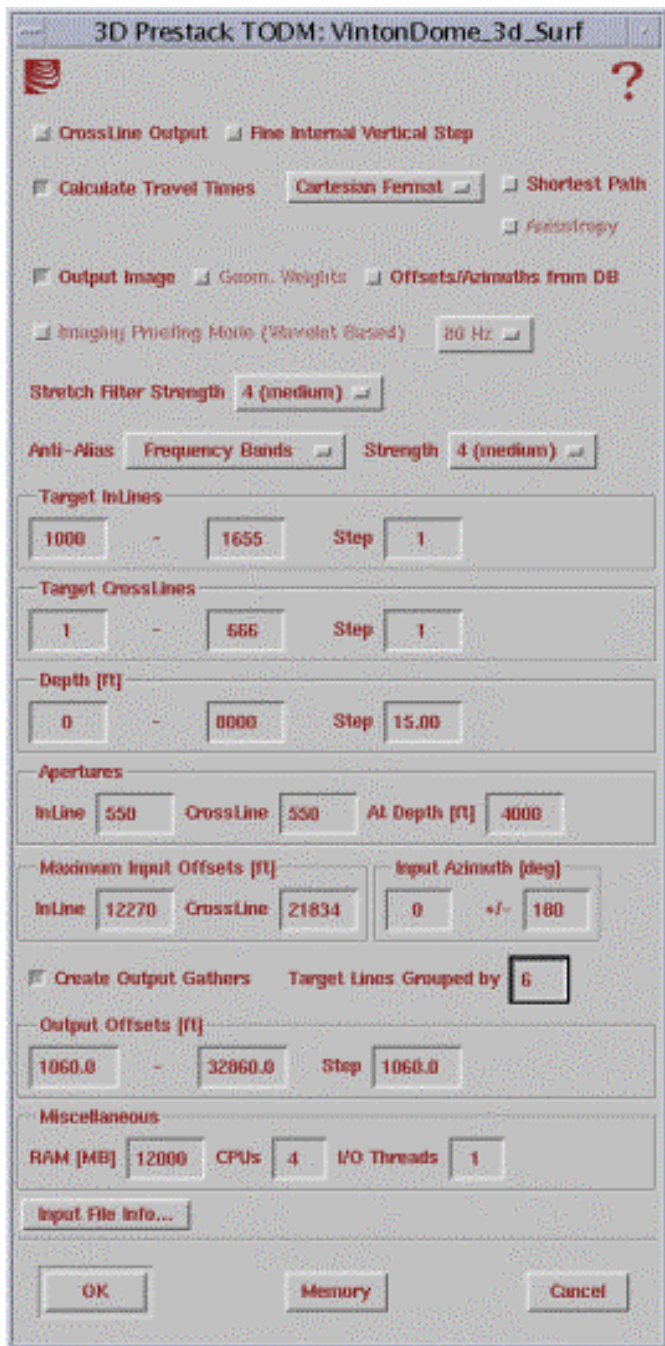


Figure 59. Graphic user interface showing setup parameters used for the PSDM.

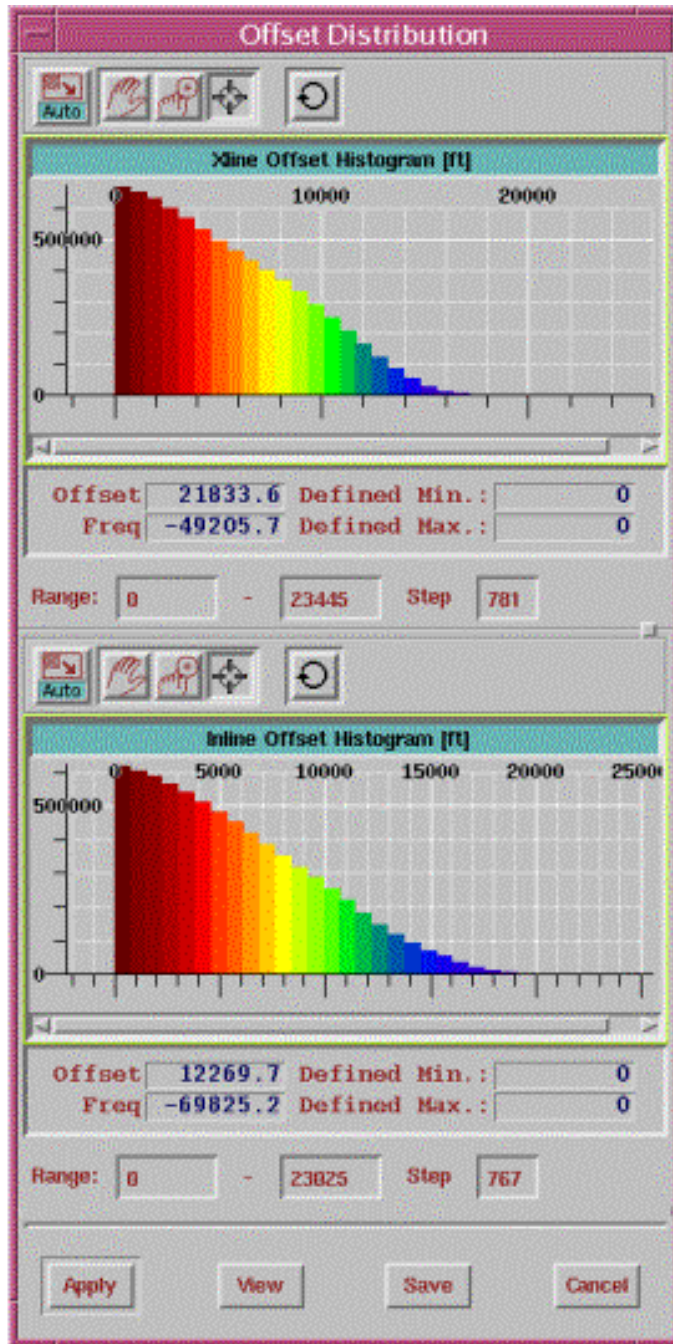


Figure 60. Histograms used to determine offset parameters for the PSDM.

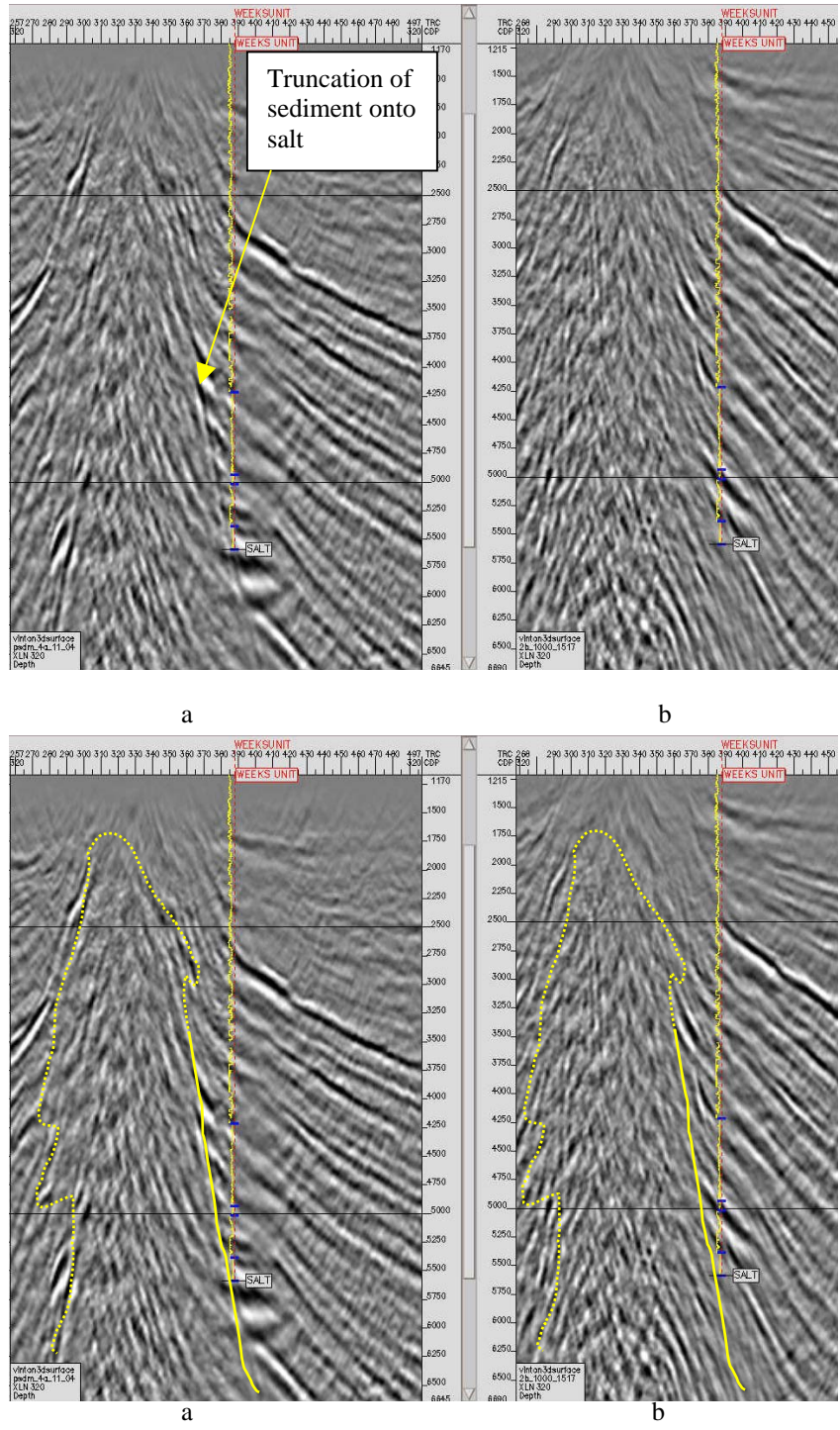
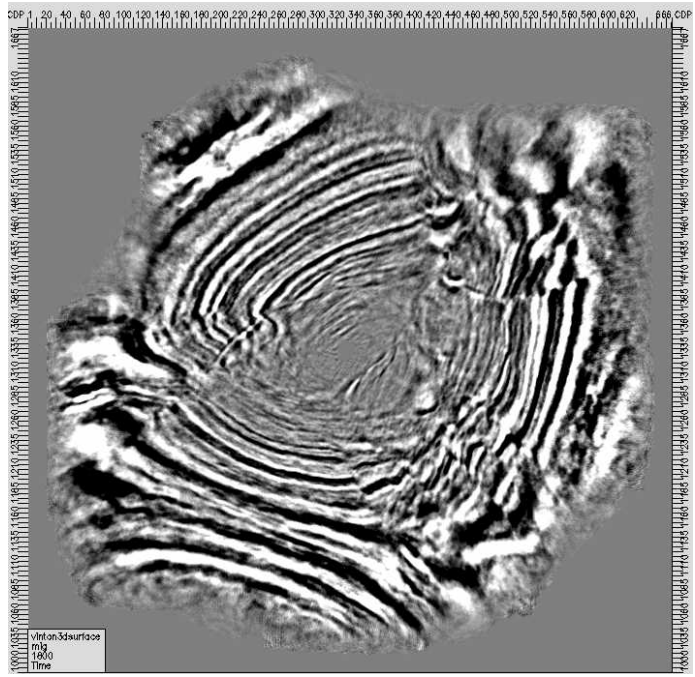
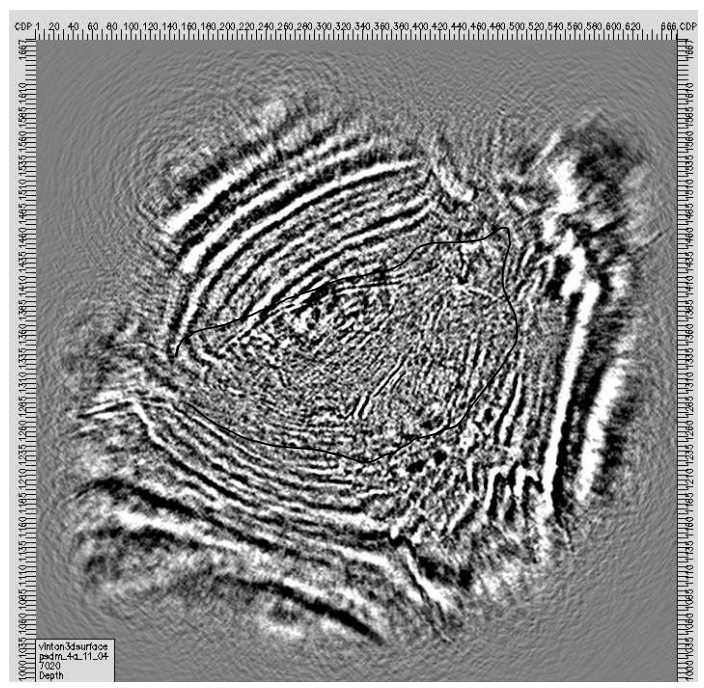


Figure 61. Seismic section (xline 320) from the well-based velocity model PSDM (a) and from the prestack time migrated model PSDM (b) used to compare the resolution of salt flank. Interpretation based on well tie and truncation of sediments.

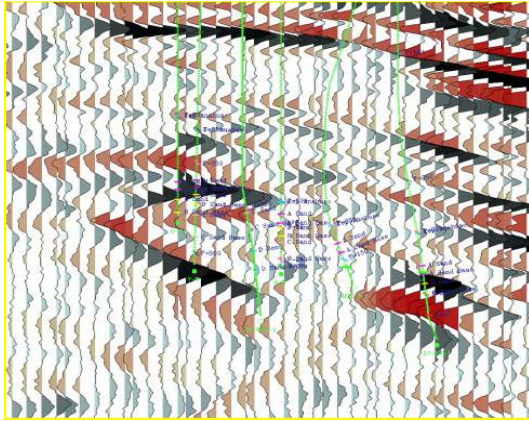


a

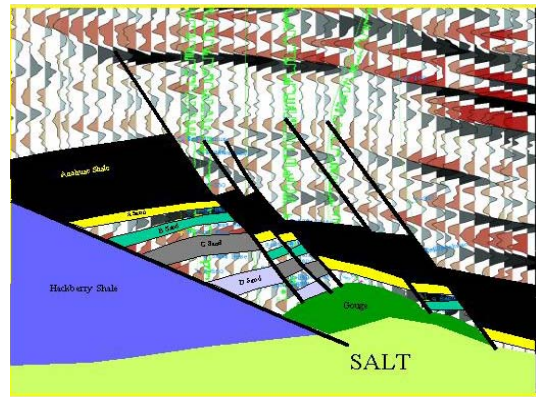


b

Figure 62. Time slice at 1.8 seconds used to compare the PSTM (a) to the PSDM using the well-based velocity model stretched back to time (b).

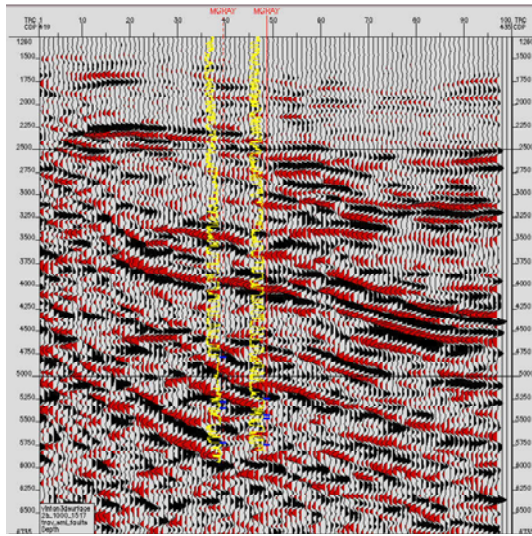


a

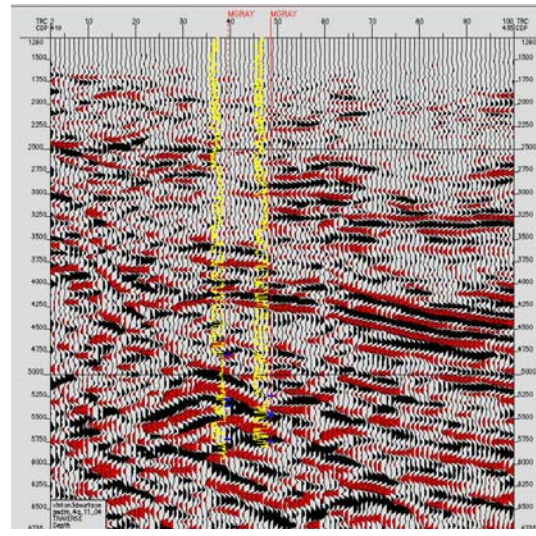


b

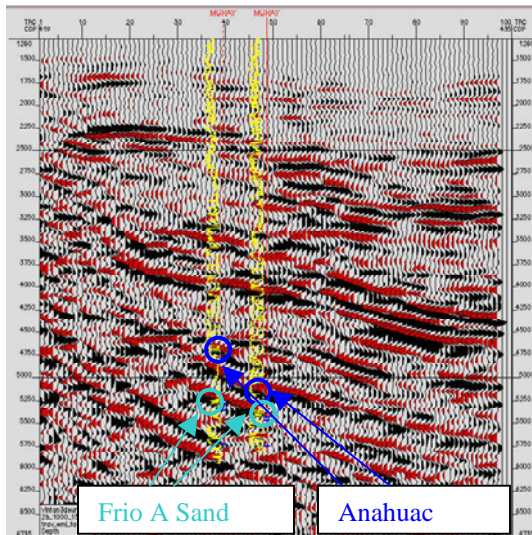
Figure 63. PSTM section in area with compartmentalized faults (a) that used well logs for the interpretation (b).



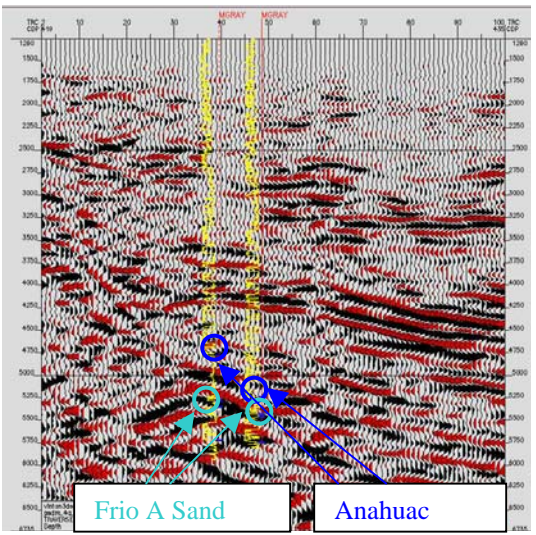
Prestack time migrated velocity model PSDM traverse through fault block.



Well-based PSDM traverse through fault blocks.

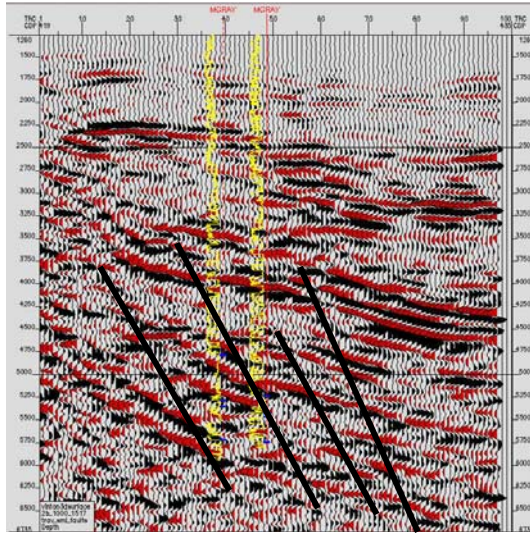


Prestack time migrated velocity model PSDM traverse through fault blocks illustrating the narrowing of the Anahuac possibly by faulting.

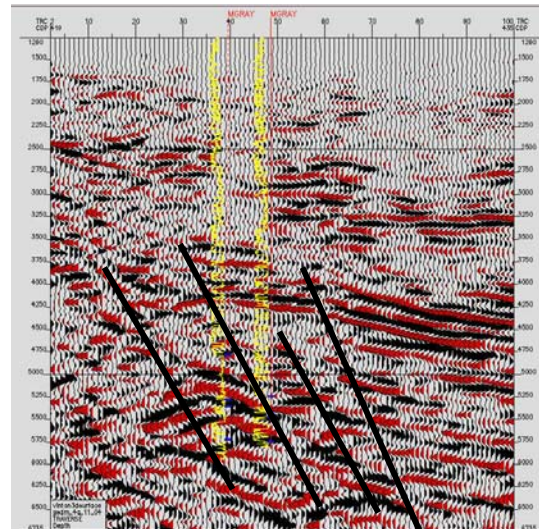


Well-based velocity model PSDM traverse through fault blocks illustrating narrowing of the Anahuac possibly by faulting.

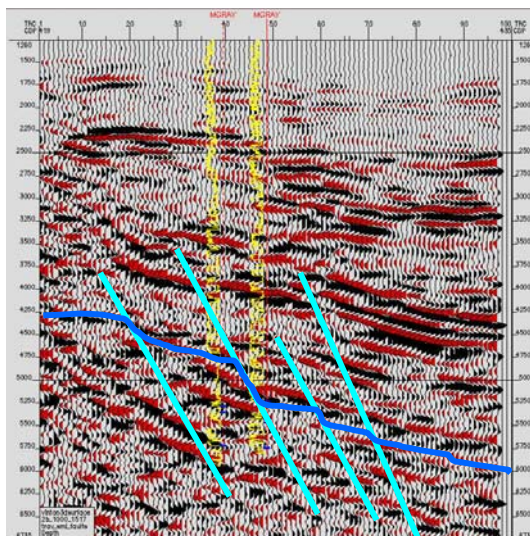
Figure 64 (continued)



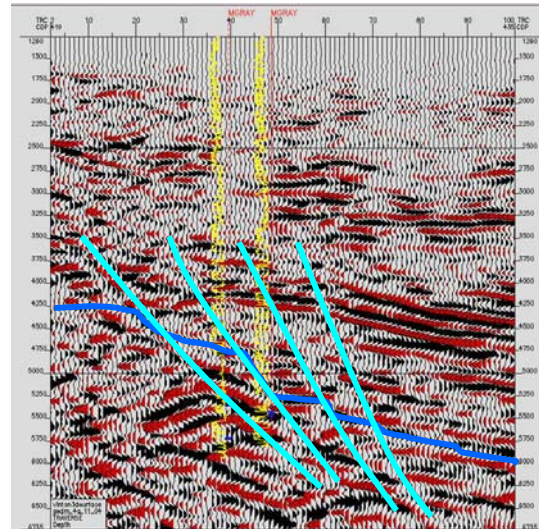
Prestack time migrated velocity model PSDM traverse through fault blocks with fault interpretation.



Well-based velocity model PSDM traverse through fault blocks interpreted on PSDM with fault interpretation.

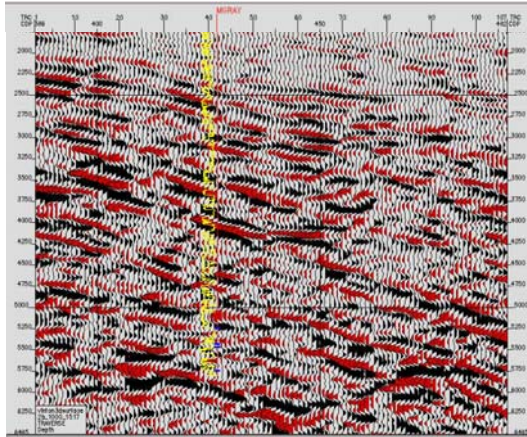


Prestack time migrated velocity model PSDM traverse through fault blocks with fault and Anahuac horizon interpretations.

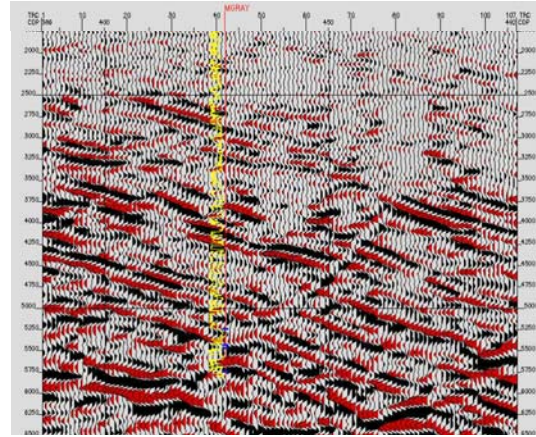


Well-based velocity model PSDM through fault blocks with fault and Anahuac horizon interpretations.

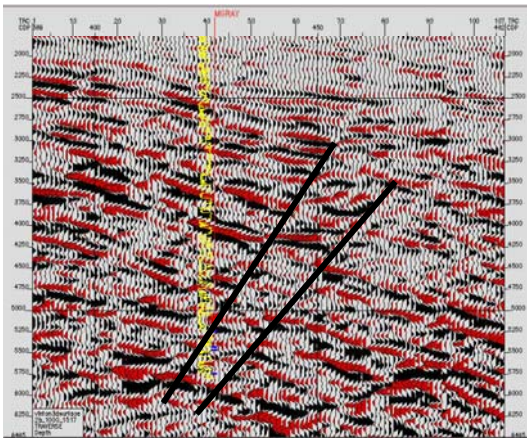
Figure 64. Traverse through the compartmentalized faults interpreted using well logs on the PSDM. Differences in the section thickness of the Anahuac indicate the presence of a fault. Prestack time migrated PSDM images events appear to be about 200 feet shallower than the well-based PSDM



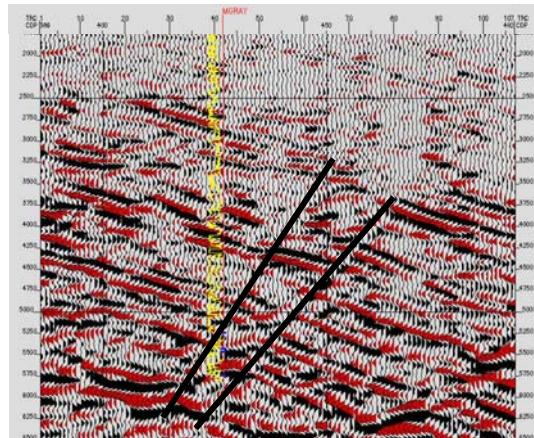
Prestack time migrated velocity model PSDM perpendicular to the traverse through fault blocks.



Well-based PSDM perpendicular traverse through fault blocks.

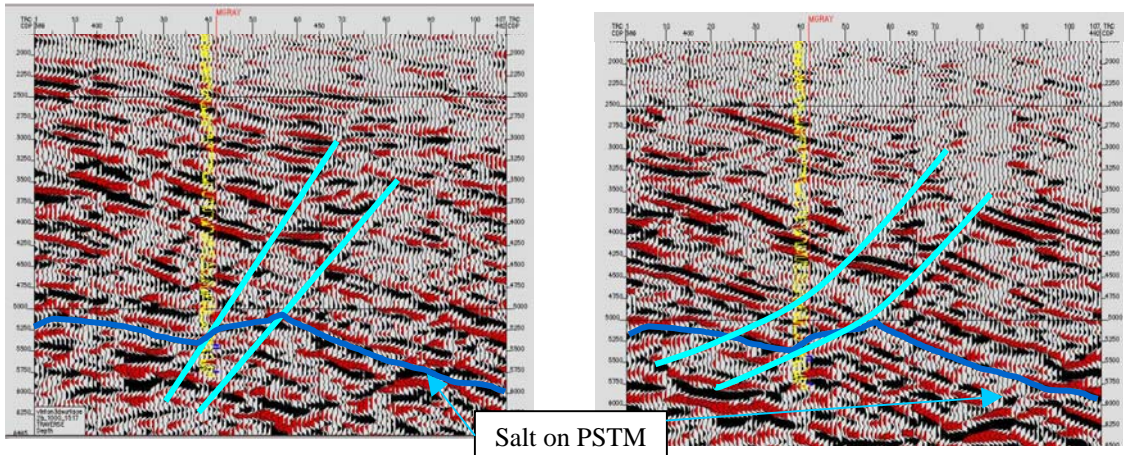


Prestack time migrated velocity model PSDM perpendicular to the traverse through fault blocks with fault interpretation.



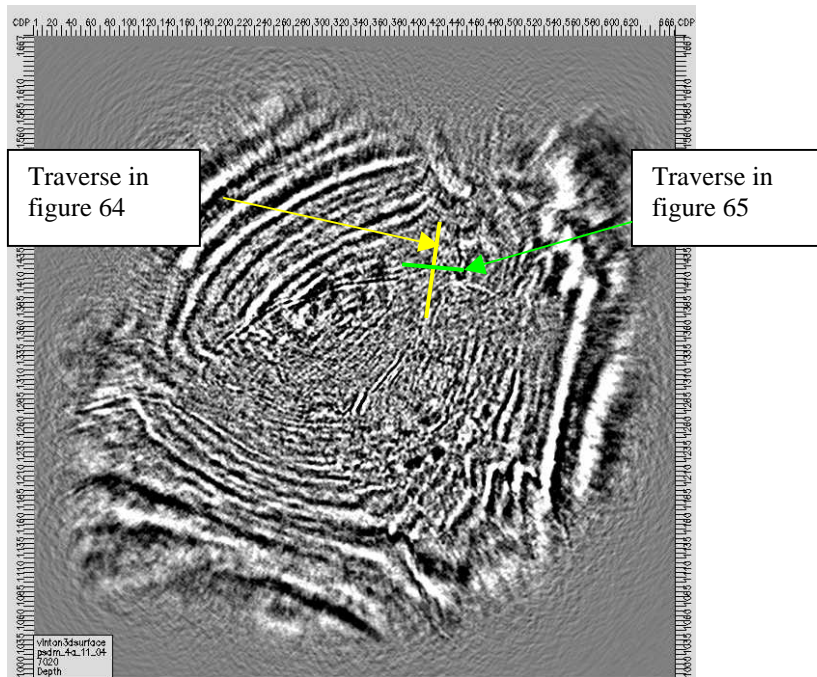
Well-based PSDM perpendicular traverse through fault blocks with fault interpretation.

Figure 65 (continued)



Prestack time migrated velocity model PSDM perpendicular to the traverse through fault blocks with fault and Anahuac horizon interpretation.

Well-based PSDM perpendicular traverse through fault blocks with fault and Anahuac horizon interpretation.



Depth slice showing locations of traverses.

Figure 65. Perpendicular traverse through the compartmentalized faults interpreted using well logs on the PSTM. The prestack time migrated velocity model PSDM interpretation of the Anahuac merges onto what was interpreted as salt on the PSTM indicating a misplaced event based on well logs. Depth slice showing locations of traverses.

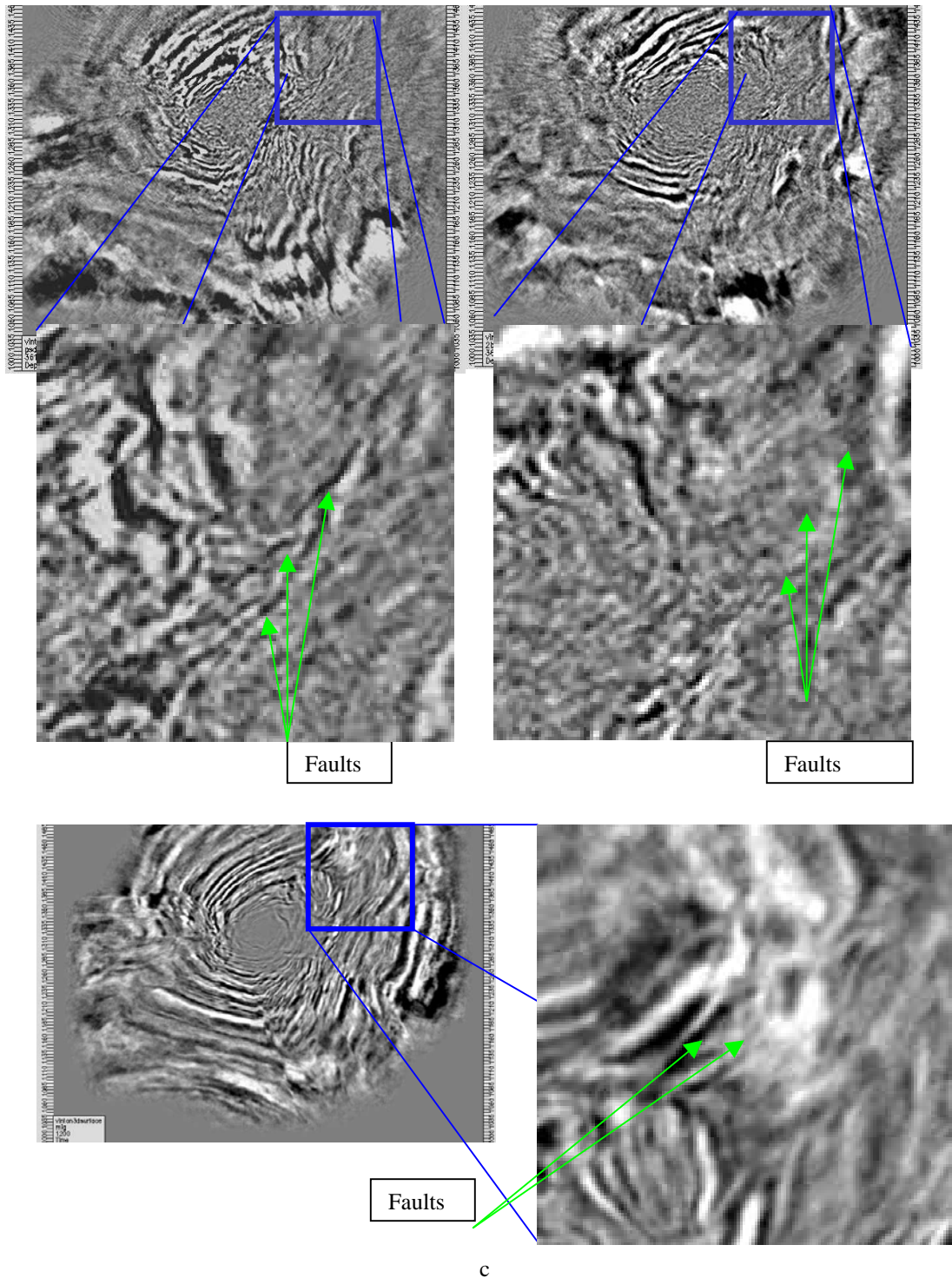


Figure 66. Depth slices of well-based PSDM (a) prestack time migrated velocity model PSDM (b) and time slice of PSTM (c) area of compartmentalized faults as interpreted from well logs in figure 54 outlined.

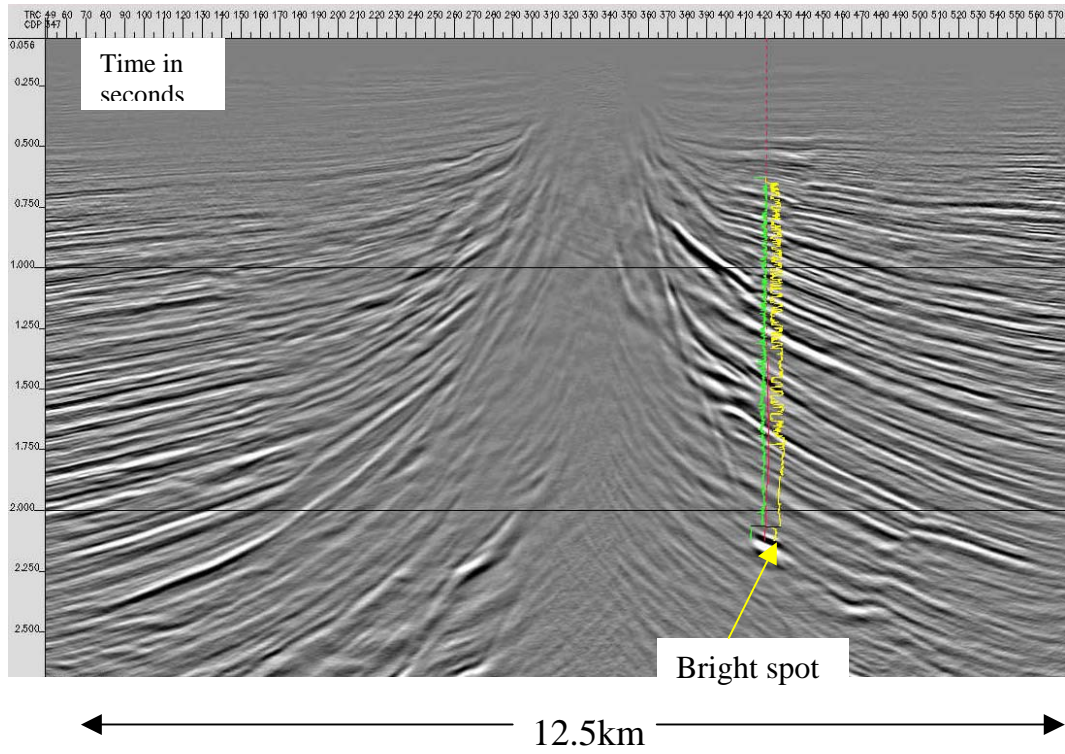


Figure 67 PSTM section showing bright spot that was drilled and turned out to be salt.

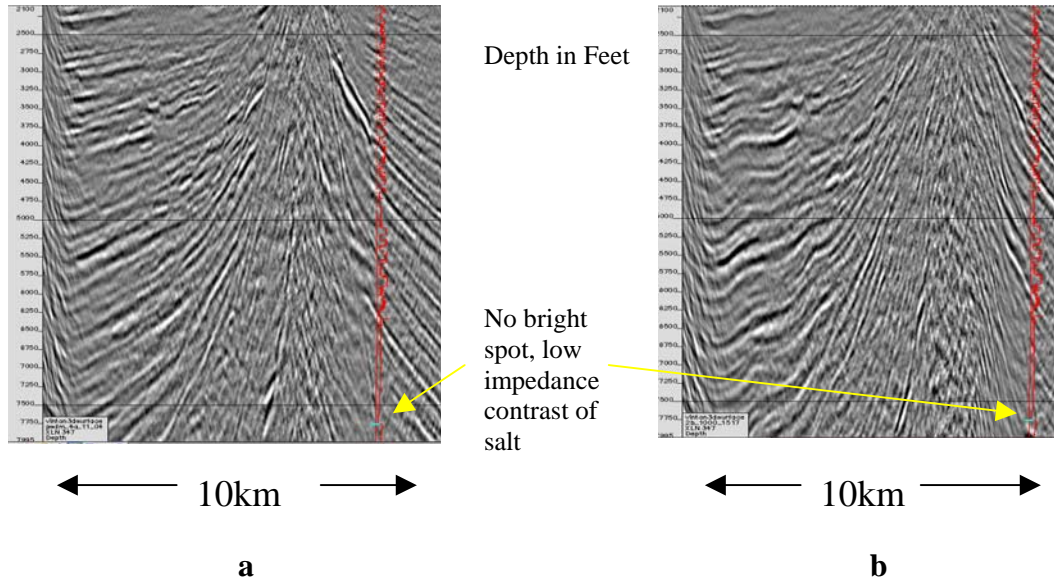


Figure 68 Well-based velocity model PSDM (a) and prestack time migrated velocity model PSDM (b), neither have a bright spot and both have a low impedance contrast for salt

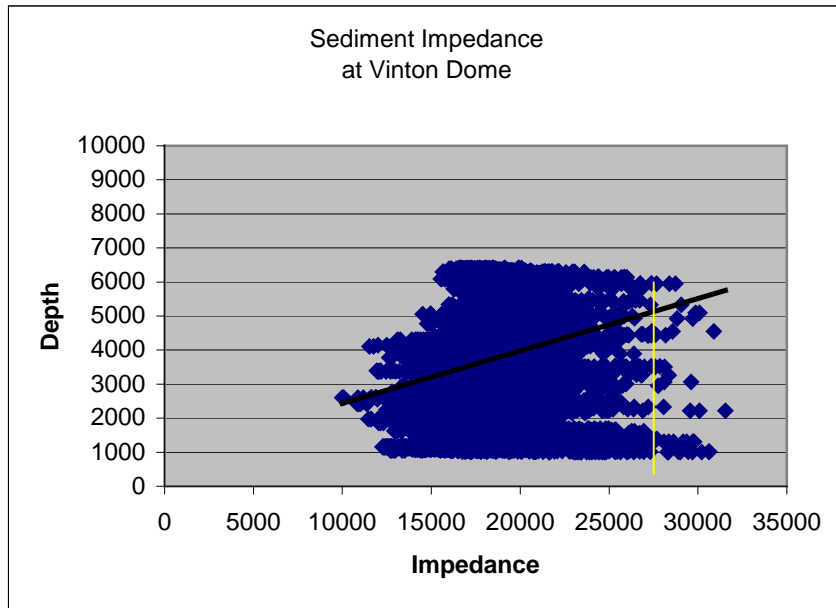


Figure 69 Cross-plot of sediment impedance and depth with the yellow line indicating where the salt impedance crosses that of the sediments at about 6000 feet.

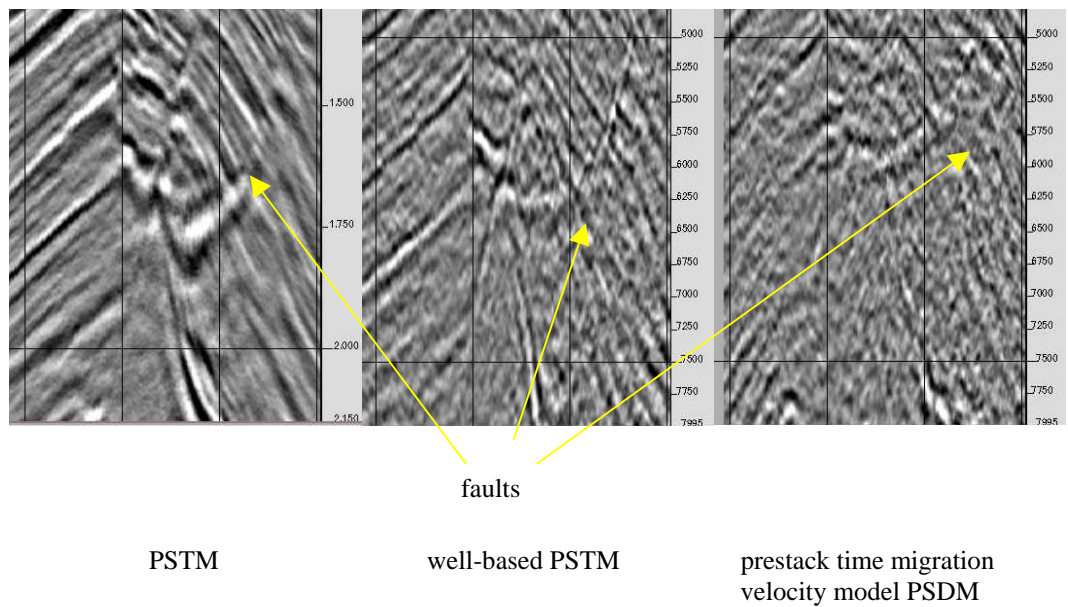
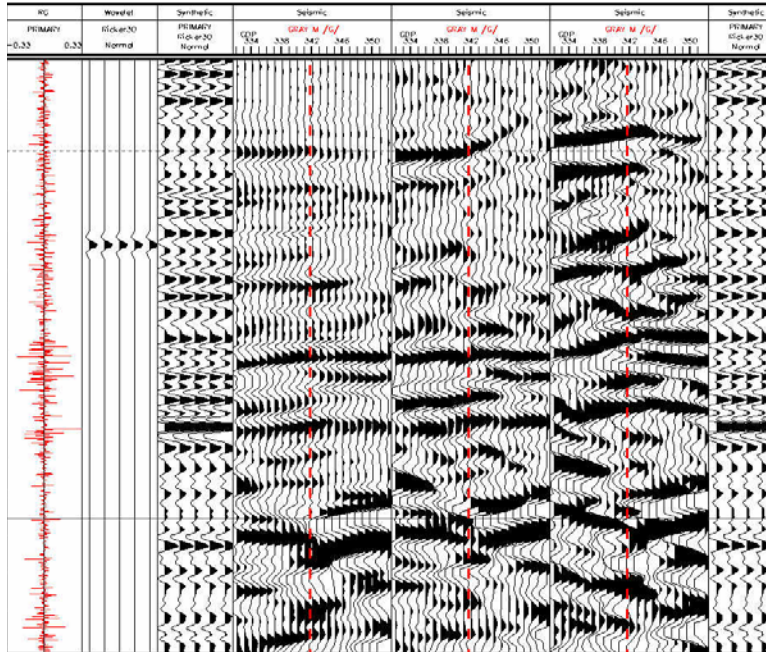
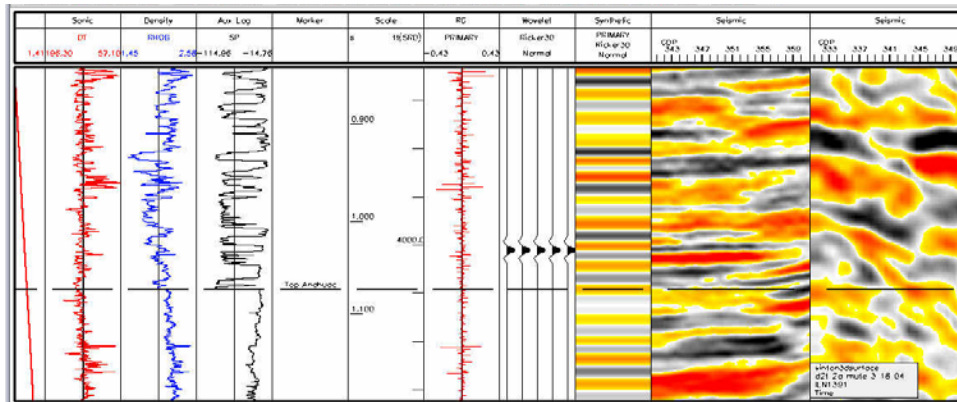


Figure 70 Dip lines through compartmentalized faults showing highest fidelity to image the faults in the well-based PSDM



PSTM prestack time well-based
 migrated velocity model
 velocity model PSDM
 PSDM



well-based prestack time
 velocity model migrated
 PSDM velocity model
 PSDM

Figure 71. Synthetics demonstrating closer ties to the seismic with the well-based PSDM than with either the PSTM or the prestack time migrated velocity model PSDM.

Chapter 5

Impact of Prestack Depth Migration on Seismic Attribute Analysis

5.1 Introduction

Improving the seismic fidelity of the Vinton Dome survey was the primary goal of this study. One of the techniques I used to achieve this was to use coherence for both interpretation and to QC data. Poor fidelity of the PSTM data volume presented a problem. Poor fidelity was manifested in low seismic resolution that reduced and eliminated interpretation of structures and stratigraphic features to include imaging of the salt flanks. Imaging these features was necessary to gain a better understanding of the geology of the area. Data were migrated using the robustness of the PSDM to image the features obscured by low fidelity. To take advantage of the power of the PSDM I used two different approaches to velocity modeling and tested the results using attributes as a QC tool.

Using attributes as a means to compare migration is a recognized technique (Rietveld, *et al.*, 1999). Coherence was the attribute used to compare two different velocity models used to PSDM and to compare the PSTM to the PSDM volumes. Coherence I applied to the data was enhanced using edge-preserving filtering. Edge-preserving filtering improves attributes (Duncan and Marfurt, 2003). I used improved attributes to interpret details that were not imaged in the seismic data volume.

Attributes provided both a means to qualitatively demonstrate the enhancements PSDM provided over PSTM and serve as a QC for the velocity models. Improved seismic

attributes also provided me with an interpretation tool that allowed for a more detailed interpretation. I demonstrated improvements in interpretation by imaging fine structural and stratigraphic details and the salt flank.

5.2 Background

Removing the seismic wavelet from data provides a perspective that allows identification of subtle features in the seismic data. Imaging subtle features that are often masked in the seismic data is a reason to generate coherence cubes from seismic data in order to image discontinuities such as stratigraphic features and faults. Coherence mathematically measures similarities. When used in the context of seismic data, coherence measures the continuity between measured traces. These measurements can reveal stratigraphic features and faults by scaling the measurements to between zero and one quantifying the continuity of traces. With this convention, one represents identical traces and high seismic continuity with a value close to one. Less than one represents a reduction in continuity between seismic traces. In terms of conventional display, shades of gray are the displayed values. Darker shades of gray represent low coherence while lighter shades of gray represent high coherence. Light shades of gray map coherent strata and dark shades of grays map discontinuities such as faults (Gersztenkorn and Marfurt, 1999).

I used this contrast between coherent seismic traces and those that lack coherence to demonstrate the effectiveness of attributes for interpretation (Bahorich and Farmer, 1995). I identified stratigraphic features such as channels and structural features such as

faults where there was enough change in lateral acoustic impedance. The degree of coherence is a measurement I used to interpret lateral variations in structure and stratigraphy caused by a wide range of geologic reasons to include lithology and porosity. The degree of accuracy in mapping geologic events using coherence depends on the accuracy of the input seismic data. Representing fault boundaries are sharp discontinuities in properly migrated data and conversely, fault edge diffractions that have been poorly migrated become coherent events. Normally poor imaging of coherent events such as horizons is due to backscattered noise mapped as low coherent events (Marfurt, *et al.*, 1998).

5.3 Methods

I used coherence attributes for interpretation and as a QC tool. Two attributes that I used were principle component coherency and edge detection. Rietveld *et al.* (1999) demonstrated the use of edge detection to improve interpretation of minor faults in PSDM. Duncan and Marfurt (2003) demonstrated that the resolution of attributes degrades at depth resulting from poor migrations. I exploited these two aspects to use attributes for interpretation and as a QC tool.

Based alternatively on edge detection and differences in waveform similarity are changes in dip/azimuth and lateral changes in amplitude. Advances in edge preserving smoothing are superior to other methods such as fx-decon and can be used to image faults on coherence data as well as the seismic data (Marfurt and Duncan, 2002). There are several

types of coherence. The first type developed by Bahorich and Farmer (1995) cross correlates each trace with neighboring inline and crossline, normalizes the energy and combines the results. Developed to improve the robustness of the technique developed by Bahorich and Farmer is a second generation of coherence Marfurt *et al.* (1998) that uses a multitrace semblance measure. The coherence I used in this study is a third generation method that also uses a multitrace coherence measure. What makes this different from the previous generation is that it uses eigenvalues from the covariance matrix formed from traces in the analysis cube (Gersztenkorn, 1996; Gersztenkorn and Marfurt, 1996a, b; Gersztenkorn *et al.*, 1999). To improve results I used filters and interpolations in this method. Eigenstructure measures projections only onto the signal subspace using a covariance matrix to partition signal and noise subspaces (Gersztenkorn and Marfurt, 1999).

I made comparisons between the well-based velocity model PSDM, prestack time migrated velocity model PSDM, and the PSTM attributes. The setup parameters were similar to insure that comparisons were of the same events. Specifically the dip window height for the time migration was set at 2ms and the dip window height for the depth migrated data was set at 75 feet.

5.4 Attributes for QC

Rietveld *et al.* (1999) used coherence to compare results from prestack and post stack depth migrations. I used the same premise justified using attributes to compare the

PSTM and the PSDM volumes in this study. I derived coherence from the PSTM volume and analysis of the coherency revealed problems with the migration. After about one second the migration began to fall apart. Before one second, faults and channels were low coherency events and the continuous strata were high coherence events (Figure 72). After one second the faults are imaged as more coherent and the coherent strata as less coherent and began producing a "wormy" pattern due to poor migration (Figure 73).

Degradation in the coherency cube from a poor PSTM motivated me to use PSDM. I used the application of attributes as a QC tool in two aspects of the study. The first to determine the need for PSDM and the second was to QC two separate approaches to velocity modeling. Velocity modeling is a critical step in the PSDM process. The two approaches I used in this study, using a velocity model derived from well logs and using a velocity model derived from seismic data, are different and required a method of QC to determine which method produced a higher fidelity image.

After the migrations of each of the initial sediment velocity models, I applied two passes of edge preserving smoothing to the data and coherence volumes were output. Since problems were apparent in the PSTM volume at about one second two way travel time, only 8000 feet of data were migrated in the PSDM primarily to save time. I compared depth slices from both PSDM (Figure 74) in the area of compartmentalized faults used in Chapter 4. Since the two volumes were migrated with different velocities, there is a difference of about 200 feet in the positioning of events. I examined both direct

comparisons, those at the same depth, and comparisons of differences of 200 feet. In the shallower section, around 4500 ft and 4305 feet there was not a noticeable difference between the two PSDM volumes. I used the well-based PSDM for the final interpretation because it imaged faults and salt more clearly at 6000 ft and 5805 feet.

5.5 Attributes for Interpretation

Coherence has been recognized and used as an interpretation tool. In this study coherence, especially with edge preserving smoothing provided a robust interpretation tool. Integrated with the seismic data coherence allowed interpretation of several structural and stratigraphic features that otherwise would have been missed. Imaged from the coherence cube were several faults and channels not easily detected in the seismic data alone (Figure 75). Figure 75 also illustrates how the well-based model improved the fidelity over the prestack time migrated velocity model PSDM and the PSTM, especially deeper in the section. Another significant improvement was the ability to accurately image the salt flanks (Figure 76). Using coherence as an interpretation tool, contrasts between the faults and channels allowed me to interpret them (Figure 77). Interpreting geologic features using coherence that were not imaged with seismic alone demonstrated the robustness of coherence with edge preserving smoothing.

I also generated curvature and gradient attributes to see if they too could be used for interpretation. To determine the degree of folding in areas of folded strata is where the curvature attribute is most useful. I calculated the curvature attribute for the Vinton

Dome data to determine if any of the fault blocks had rotated. Gradient data is a derivative designed to sharpen the resolution based on amplitude variations to delineate sub-seismic resolution for imaging faults and channels. I used an area with both channels and faults as a test-bed for these attributes in the southern half of the Vinton Dome survey.

Curvature data did not reveal evidence to support rotation of the fault blocks. The curvature attribute was generated for both the well-based and the prestack time migrated velocity model PSDM. Slices of data in the shallower sections are very similar but like the coherence, the resolution begins to degrade with depth for the prestack time migrated velocity model data (Figure 78). The gradient data, both inline and crossline, did show sharpening of faults and enhanced imaging of channels in both the well-based and prestack time migrated velocity model PSDM, but the well-based PSDM appears to have sharper resolution at all depths. Like the other attributes, resolution was degraded more noticeably in the prestack time migrated velocity model data than in the well-based PSDM (Figure 79).

5.6 Conclusions and Discussion

I used an innovative approach to coherence by using it as a QC tool. I was able to reveal fidelity issues in the PSTM data volume using coherence resulting from failure of the migration to accurately place events resulting in reduced data quality. With seismic alone this is not readily apparent, but with the coherence I identified the degradation.

Identifying reduced fidelity in the PSTM using coherence was a justification I used for PSDM. By testing the fidelity of the PSDM using coherence, I demonstrated significant improvement in the PSDM over the PSTM. After demonstrating improvements in PSDM over PSTM, I used coherence to compare two velocity models for the PSDM. Results from the coherence comparison were independent of a more traditional method of comparison, comparing CIGs, and lead to the same conclusion that the well-based velocity model was more accurate and provided higher fidelity of the seismic data.

Details in seismic data that are imaged with high frequencies are often difficult to distinguish from noise presenting a problem when QCing the data. I demonstrated an appropriate QC of the migrated data in the comparison of two separate methods of modeling sediment velocities. A new tool to qualitatively assess and compare data was necessary to identify the best approach to model sediment velocities for an initial PSDM. With subtle features, like those present in the Vinton Dome survey, traditional QC methods such as comparison of CIG gathers are not robust enough to identify the highest fidelity data and this can easily translate into an inferior interpretation. In this study I used the power of edge preserving smoothed coherence to qualitatively identify the highest resolution data.

I applied two other attributes, curvature and gradients to the Vinton Dome data.

Interpretation of the curvature showed little rotation has occurred in the fault blocks and indicated a decrease in fidelity at deeper depths in the prestack time migrated velocity

model PSDM. Inline and crossline gradients sharpened the imaging of both channels and faults and indicated degradation in the fidelity of the prestack time migrated velocity model PSDM.

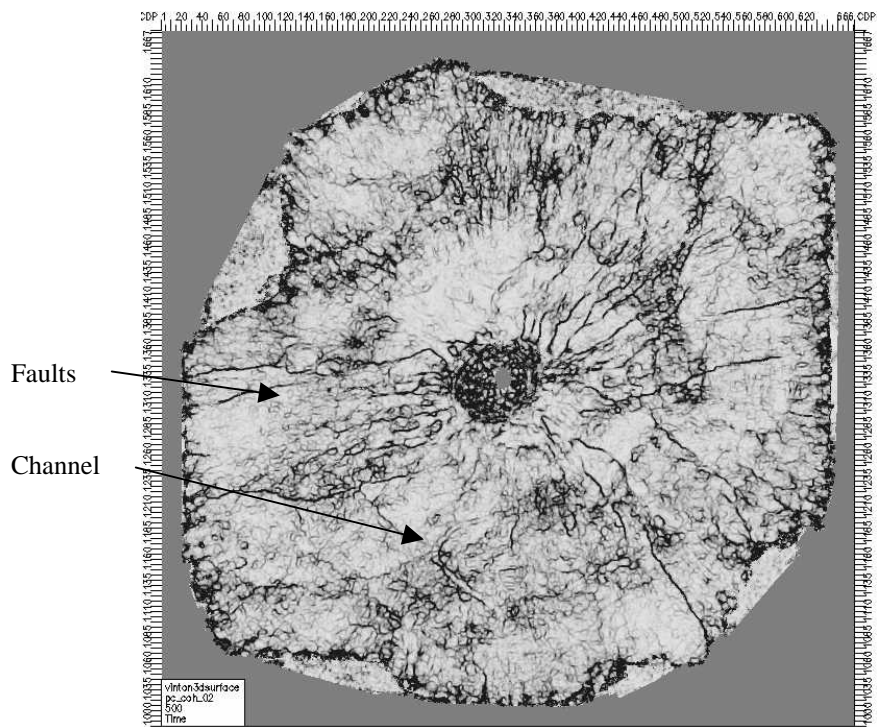
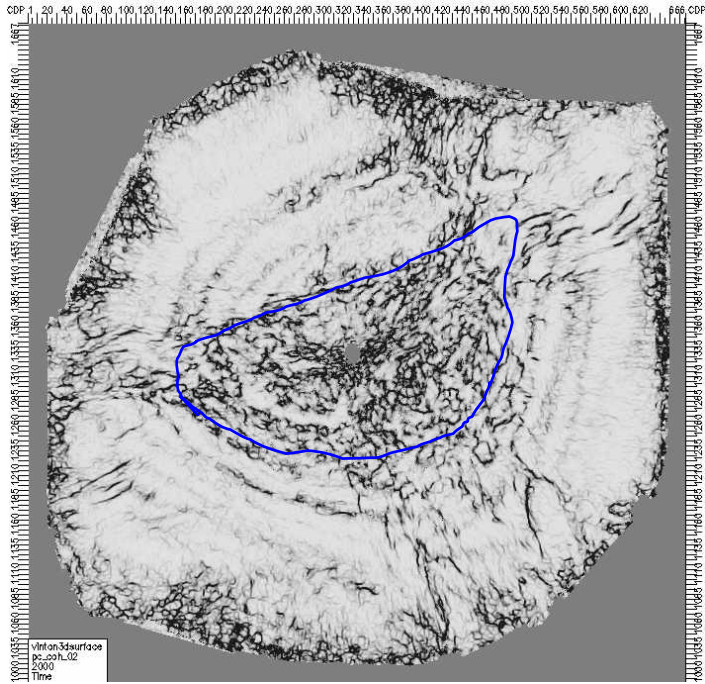
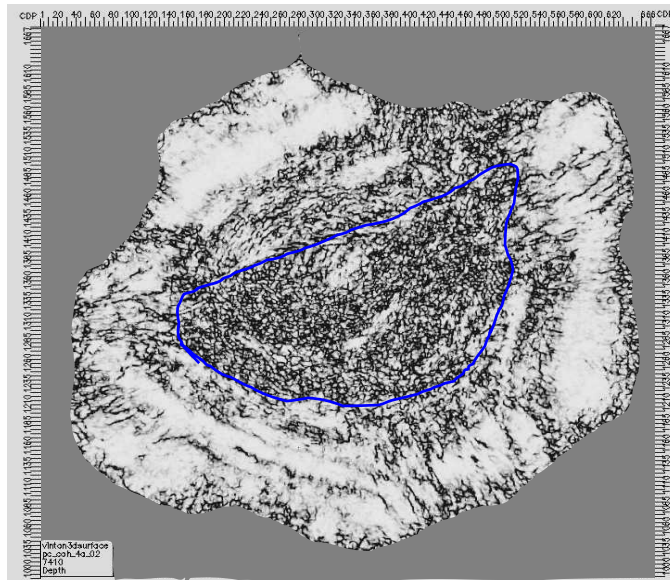


Figure 72. PSTM coherence data at 500 milliseconds. Coherence images channels and structures.

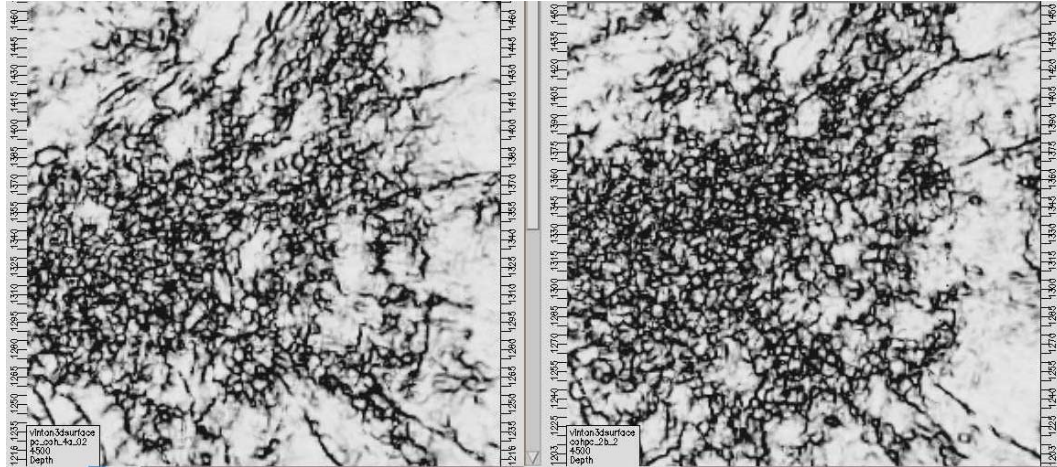


a



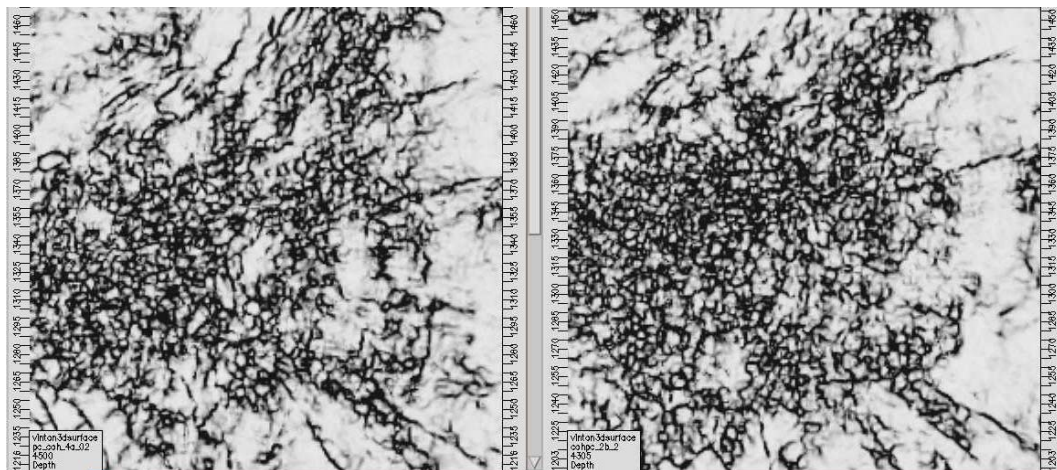
b

Figure 73. PSTM coherence data at 2 seconds (a), data begin to loose resolution especially near the salt, the PSDM equivalent depth slice as the time slice (b) shows more detail in the salt flank (blue) indicating higher fidelity.



Depth slice of coherence cube from
4500 feet of well-based PSDM

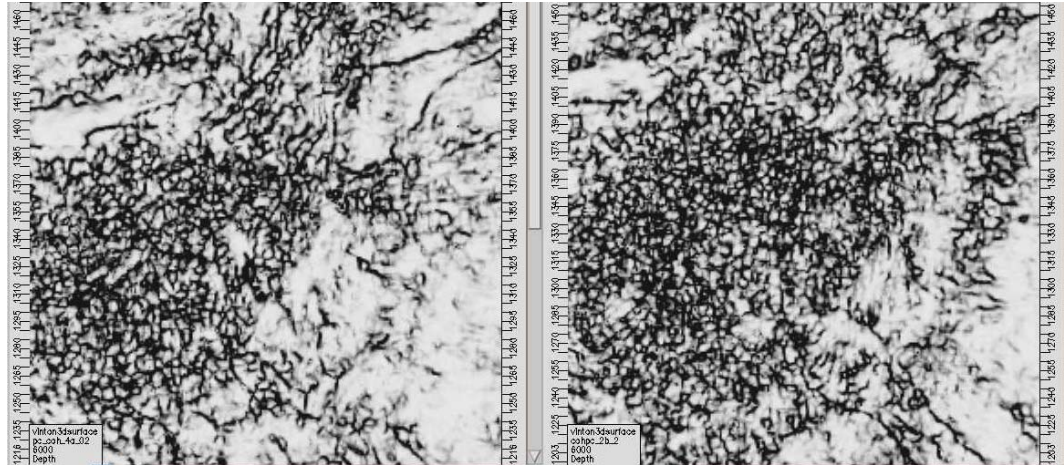
Depth slice of coherence cube from
4500 feet of prestack time migrated velocity model PSDM



Depth slice of coherence cube from
4500 feet of well-based PSDM

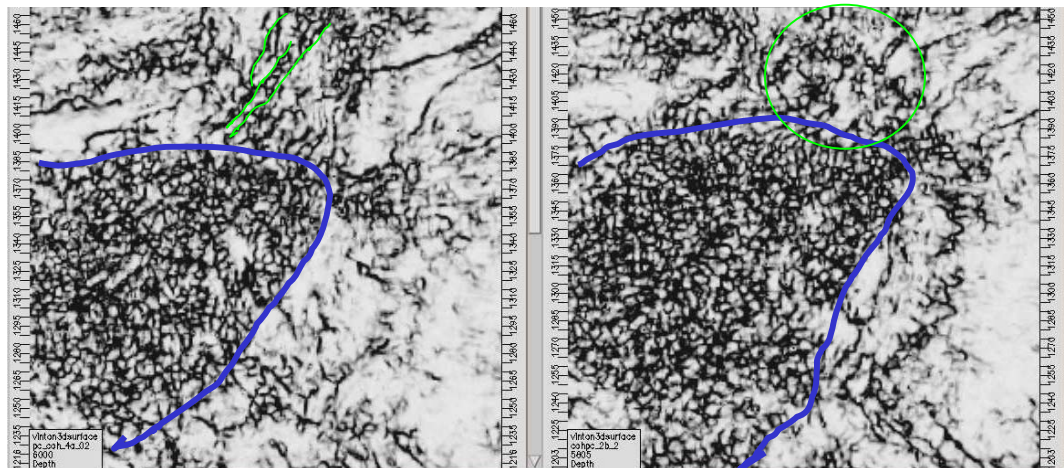
Depth slice of coherence cube from
4305 feet of prestack time migrated
velocity model PSDM

Figure 74 (continued)



Depth slice of coherence cube from 6000 feet of well-based PSDM

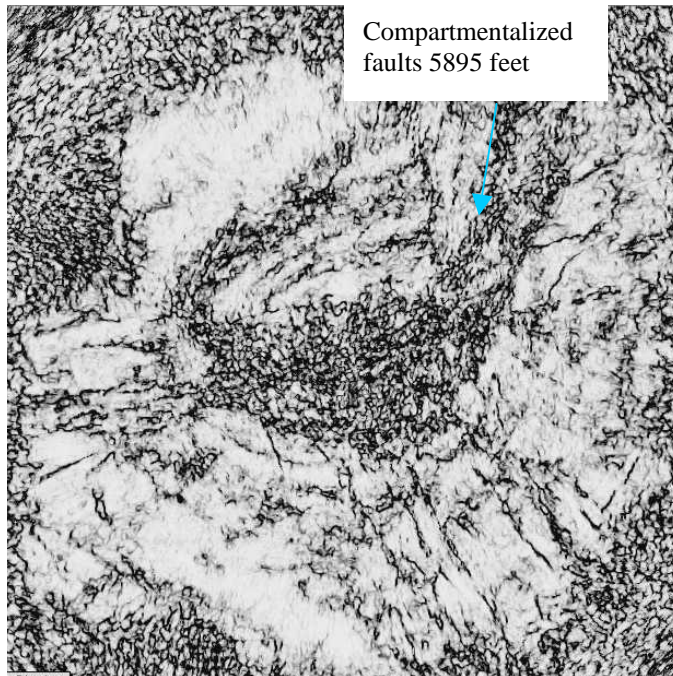
Depth slice of coherence cube from 6000 feet of prestack time migrated velocity model PSDM



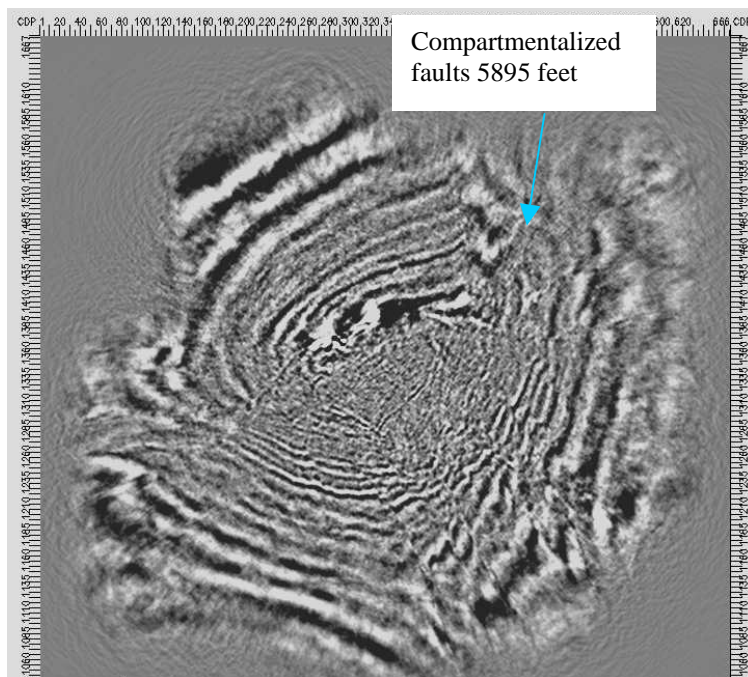
Depth slice of coherence cube from 6000 feet of well-based PSDM

Depth slice of coherence cube from 5805 feet of prestack time migrated velocity model PSDM

Figure 74. Comparison of depth slices of coherence between the well-based model and the semblance based model. Faults and salt used to illustrated higher fidelity in the previous chapter (Chapter 4) Figure 64 were also used in this example. Because the same events are imaged at different depths, the prestack time migrated velocity model velocity being slower and about 200 feet shallower, comparisons are made at the same depth, compensating for the difference. At shallower depths there is not much difference. As depth increases faults interpreted in the seismic and seen on the coherence are imaged with the well-based PSDM data, but not with the prestack time migrated velocity model PSDM. The salt also appears to be more sharply imaged in the well-based PSDM data.

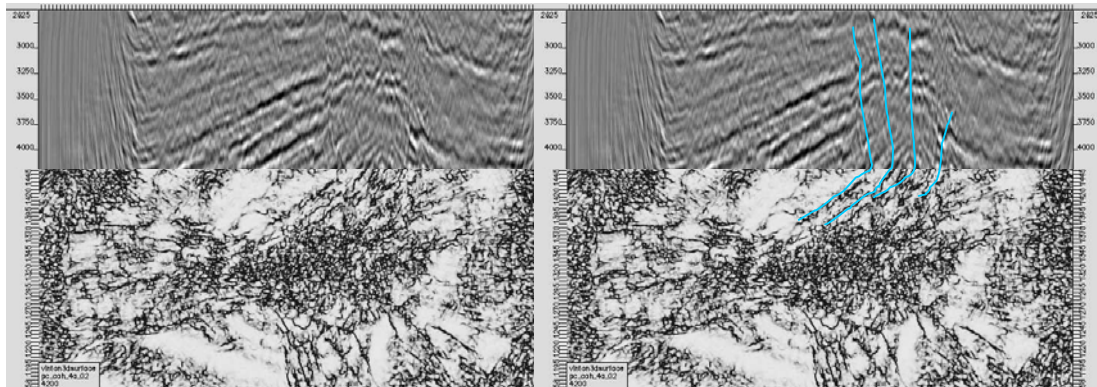


a



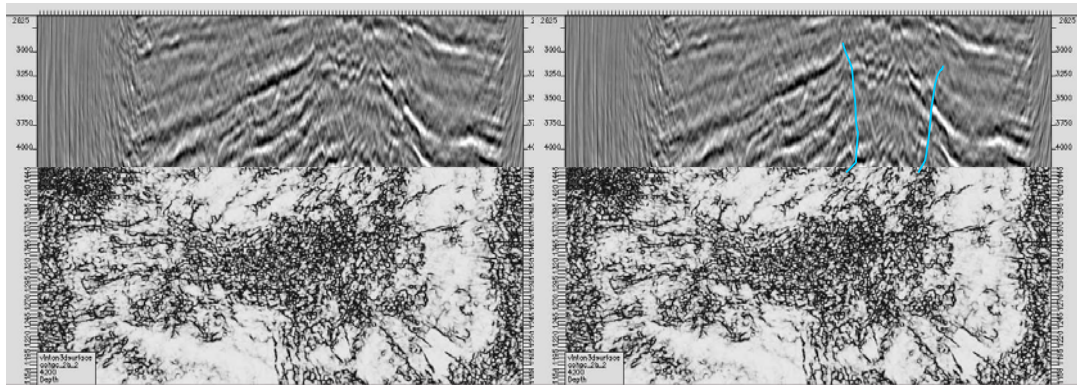
b.

Figure 75 (continued)



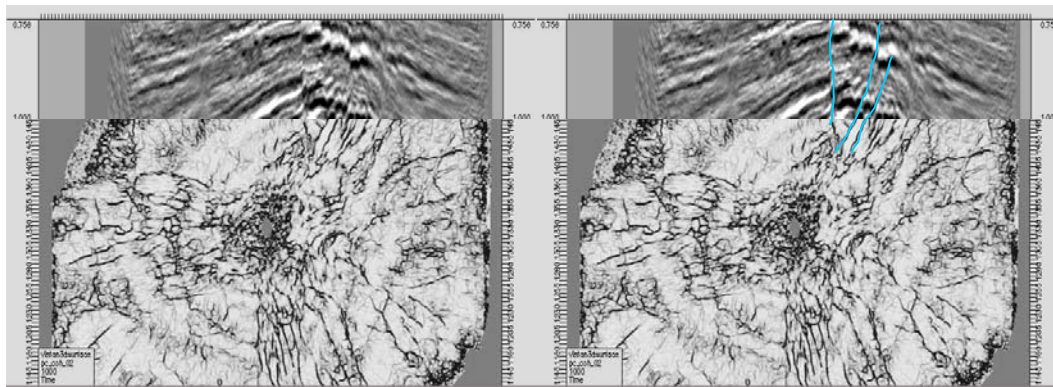
Well-based PSDM – faults can be traced from the seismic section on to the coherence depth slice at 3000 feet

c



prestack time migrated PSDM cannot be traced from the seismic section on to the coherence depth slice at 3000 feet

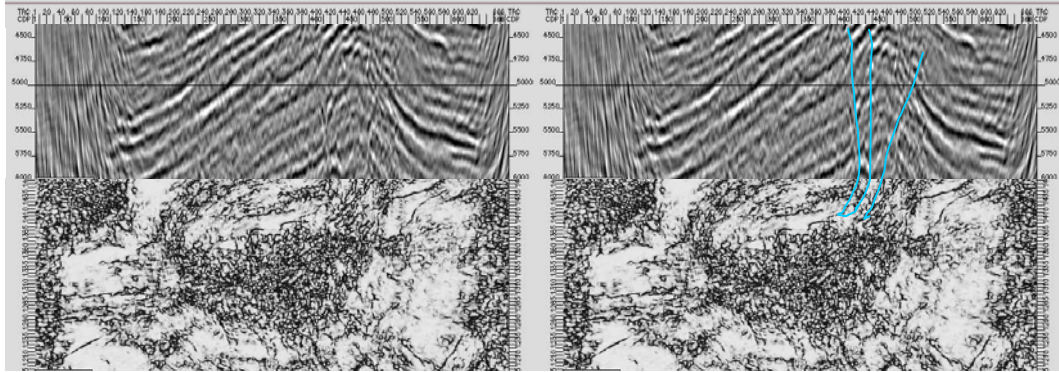
d



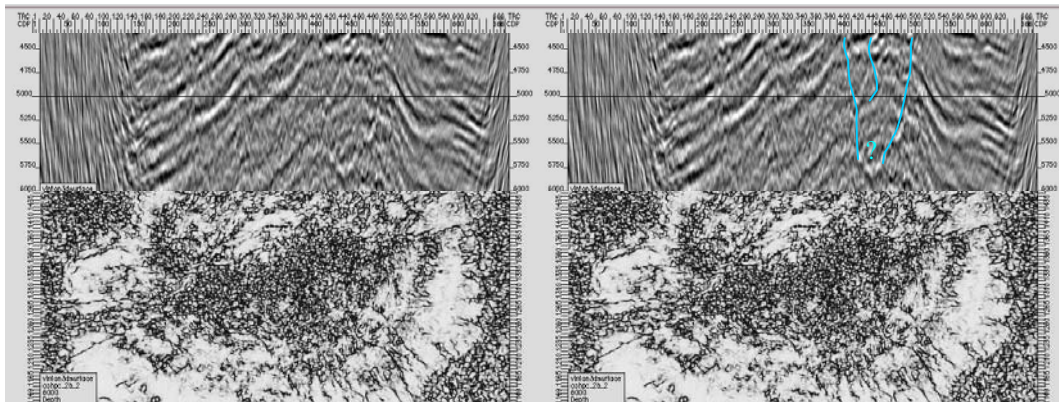
PSTM – some faults traced from the seismic section on to the coherence time slice at 1 second

e

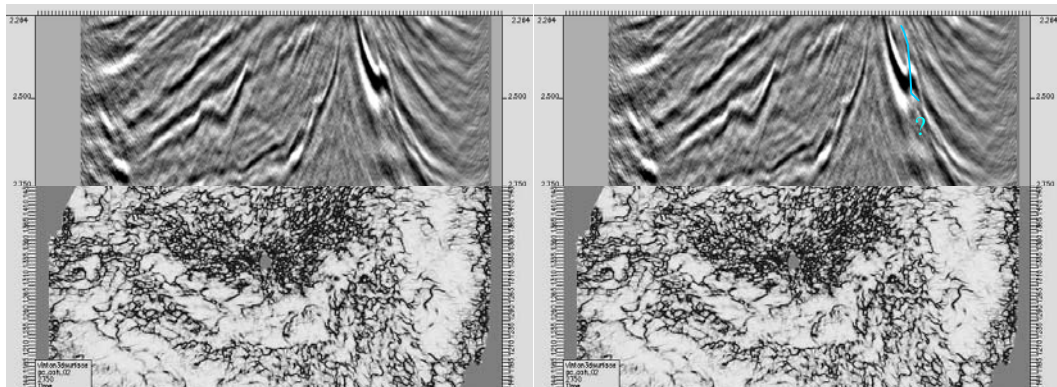
Figure 75 (continued)



Well-based PSDM – faults traced from the seismic section on to the coherence depth slice at 6000 feet
c

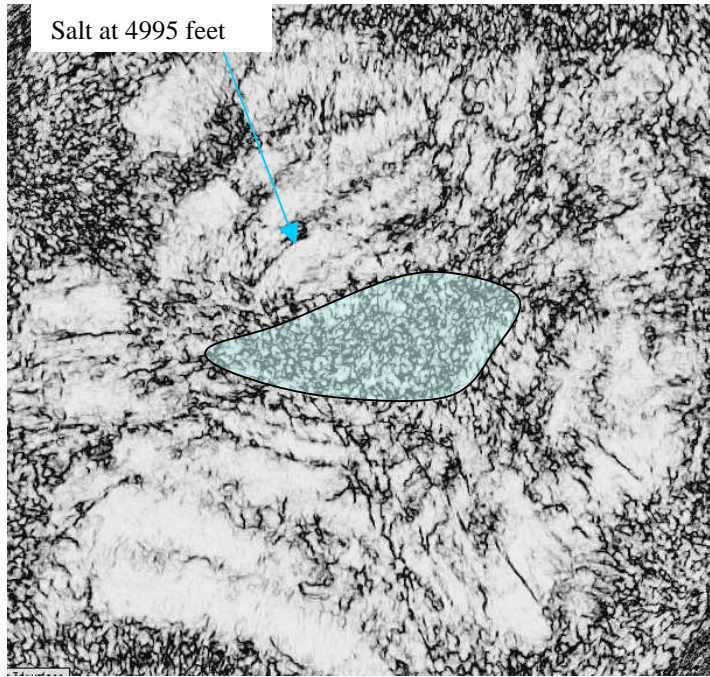


prestack time migrated PSDM cannot be traced from the seismic section on to the coherence depth slice at 6000 feet
d

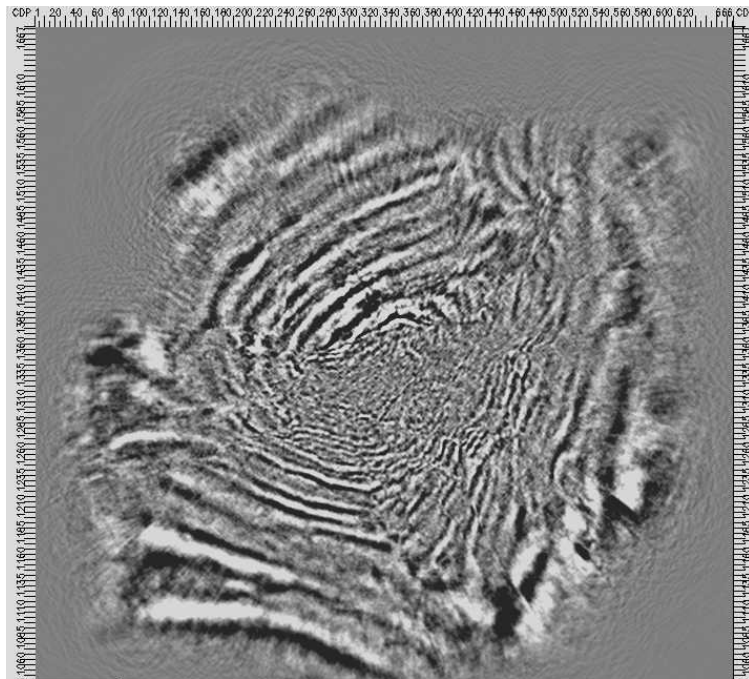


PSTM – faults cannot be traced from the seismic section on to the coherence time slice at 1.5 second
e

Figure 75. Comparison of depth sections from the PSDM coherence data (a) to the PSDM seismic data (b) to demonstrate the improvement coherence provided for structural interpretation. Comparison of well- based interpretation at 3000 feet (c) to prestack time migrated PSDM interpretation at 3000 (d) to PSTM at 1 second (e). Comparison of well-based interpretation at 6000 feet (f) to prestack time migrated PSDM interpretation at 6000 feet (g) to PSTM at 1.5 seconds (h)



a



b

Figure 76. Comparison of depth sections from the PSDM coherence data(a) to the PSDM seismic data (b) to demonstrate the improvement coherence provided for salt interpretation.

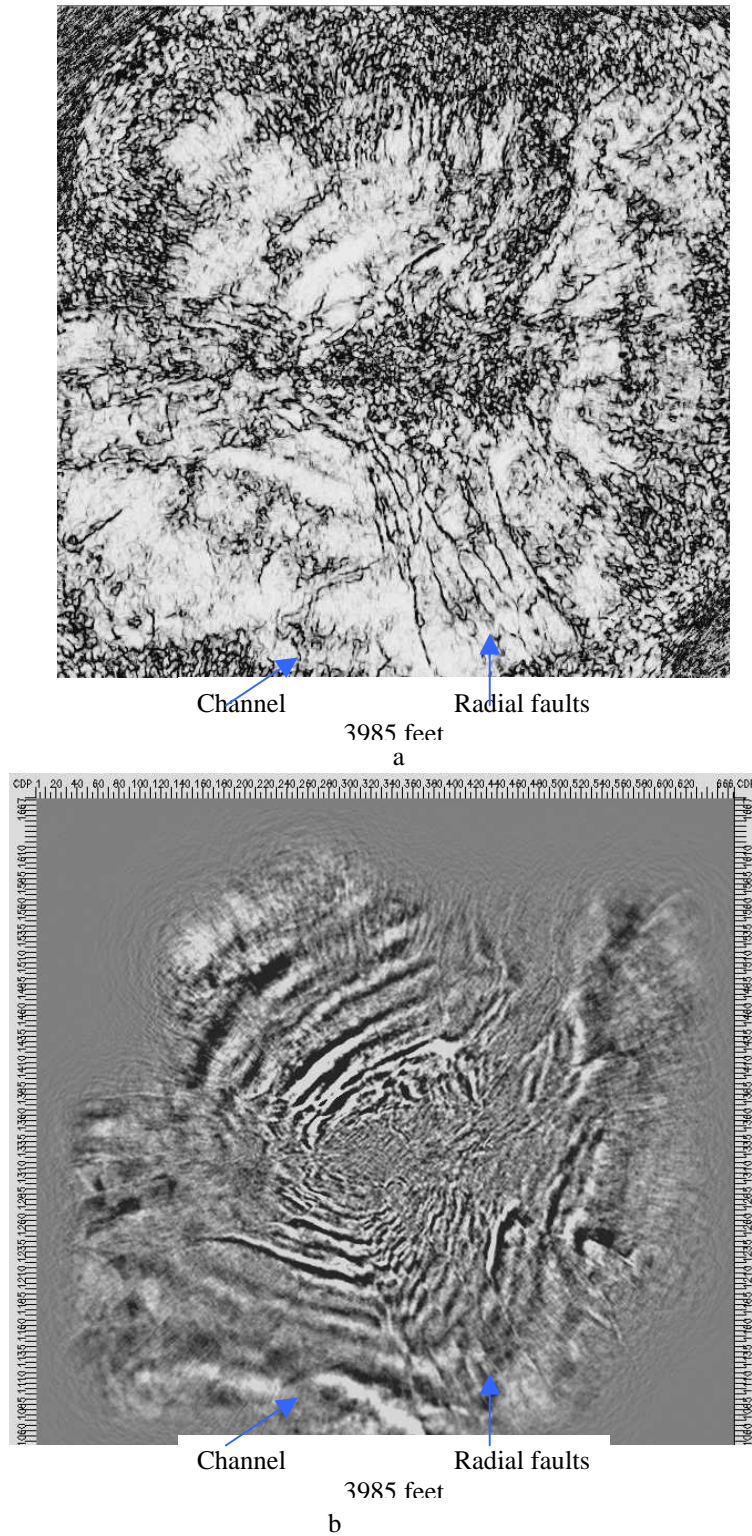
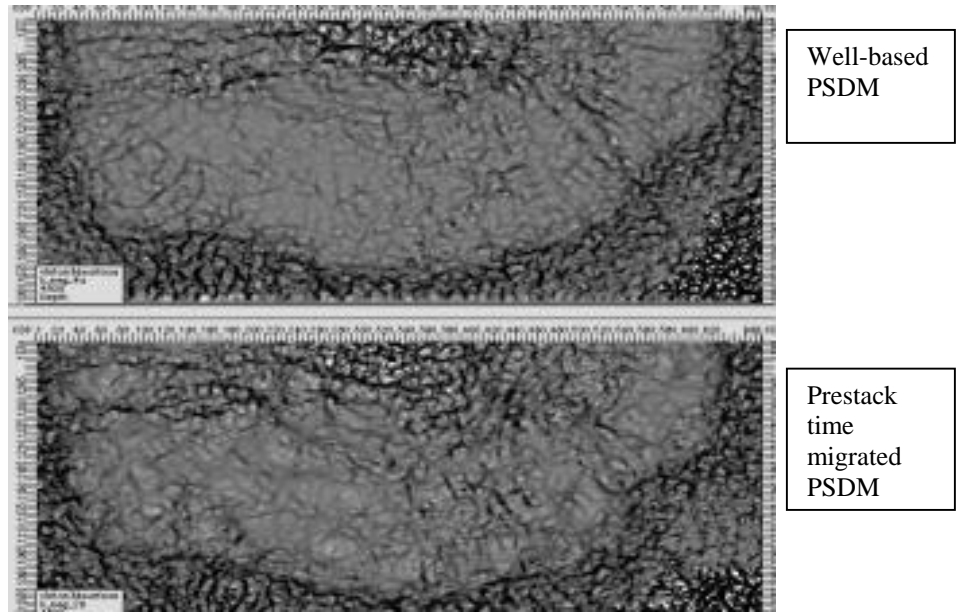
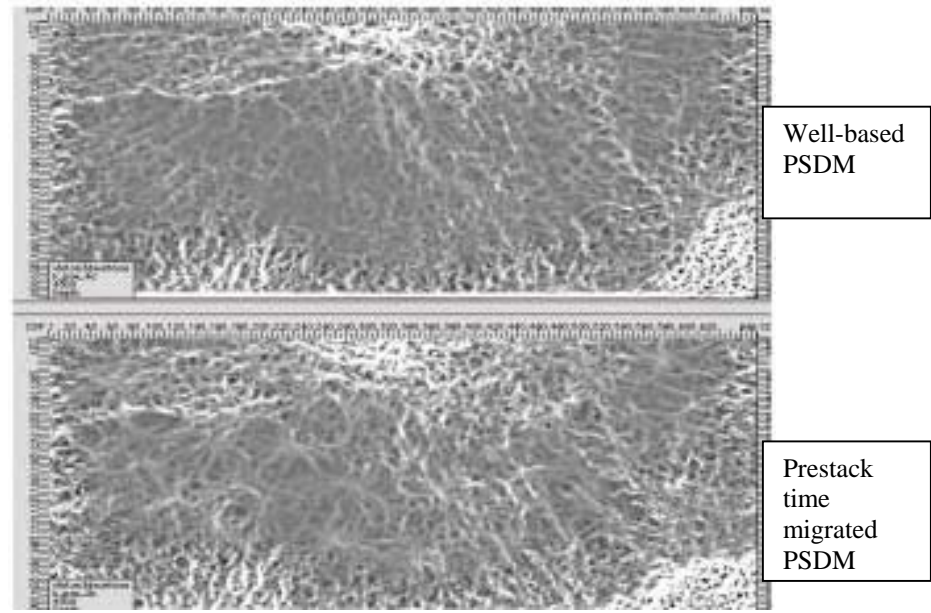


Figure 77. Comparison of depth sections from the PSDM coherence data (a) to the PSDM seismic data (b) to demonstrate the improvement coherence provided for interpretation of both faults and channels.

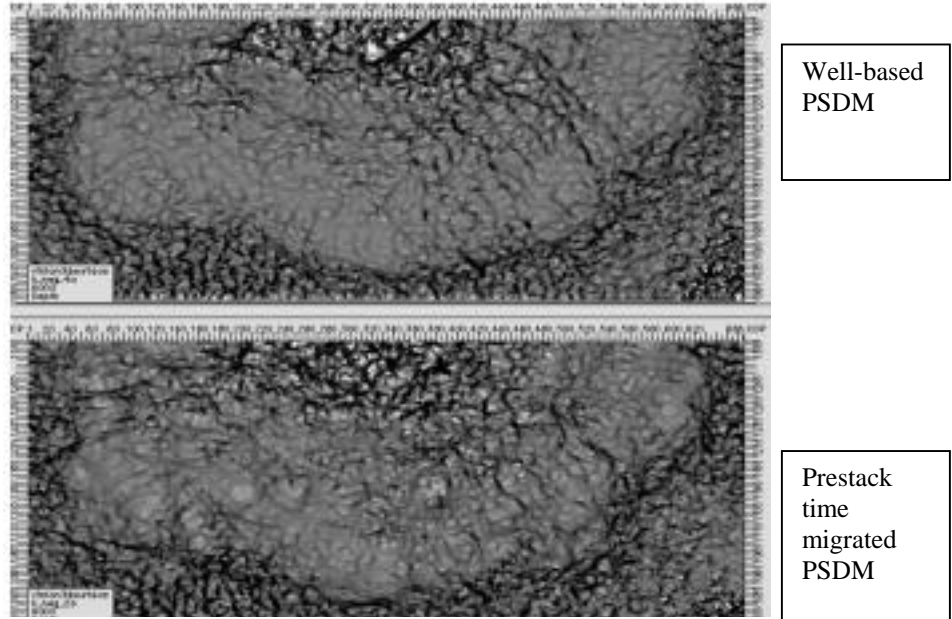


a

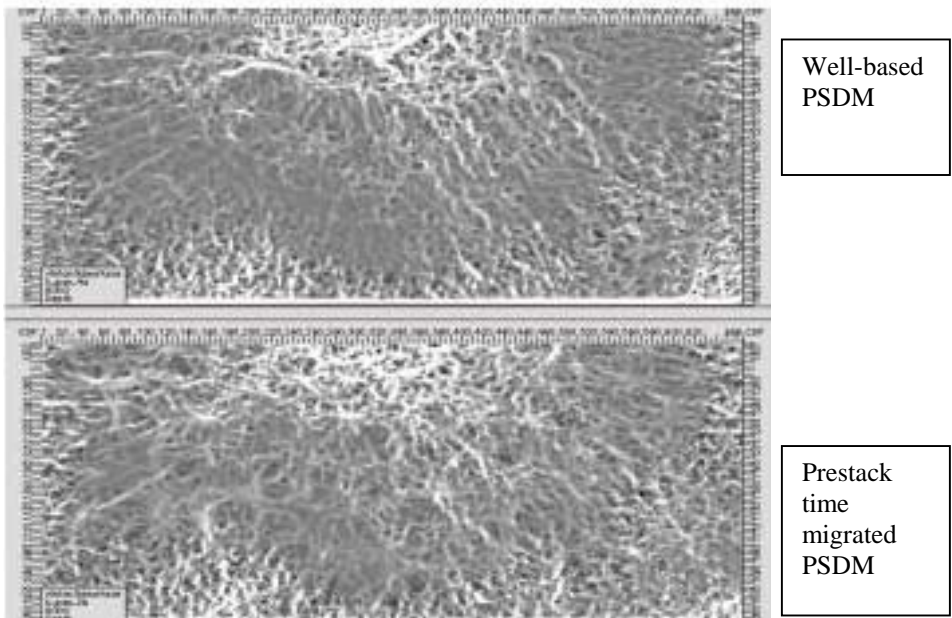


b

Figure 78 (continued)



c



d

Figure 78. Most positive and most negative curvature of both the well-based and prestack time migrated velocity model PSDM. Little difference at shallower depth (a) positive curvature, (b) negative curvature, well-based has sharper resolution on the southeast sector at a deeper depth for both positive curvature (c) and negative curvature (d).

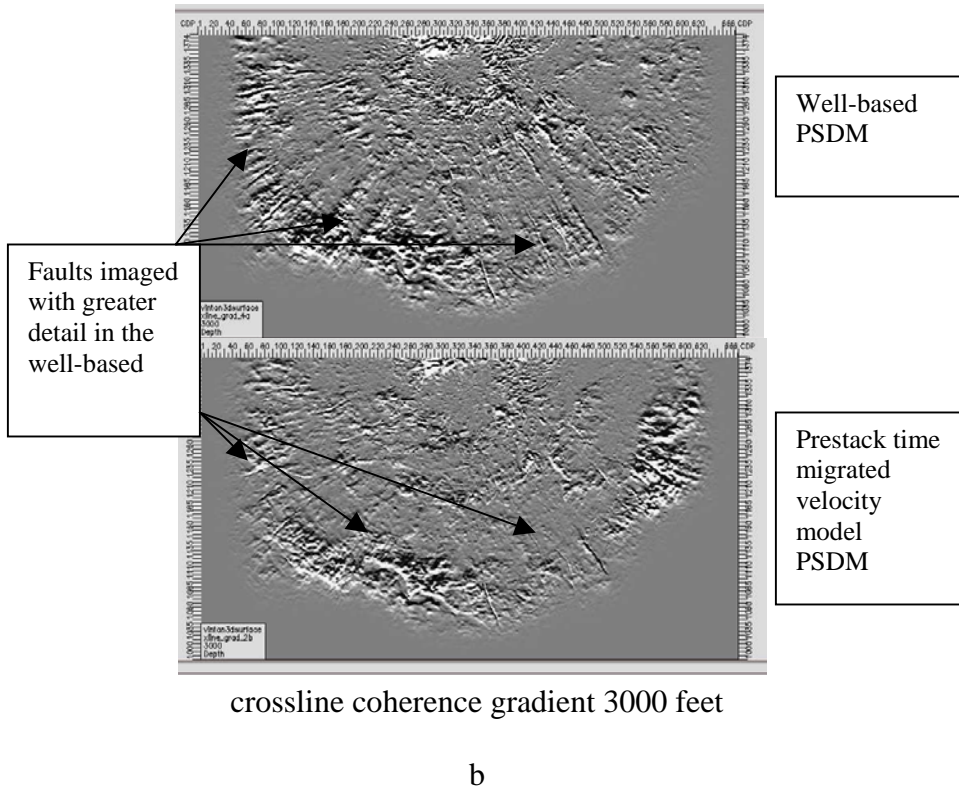
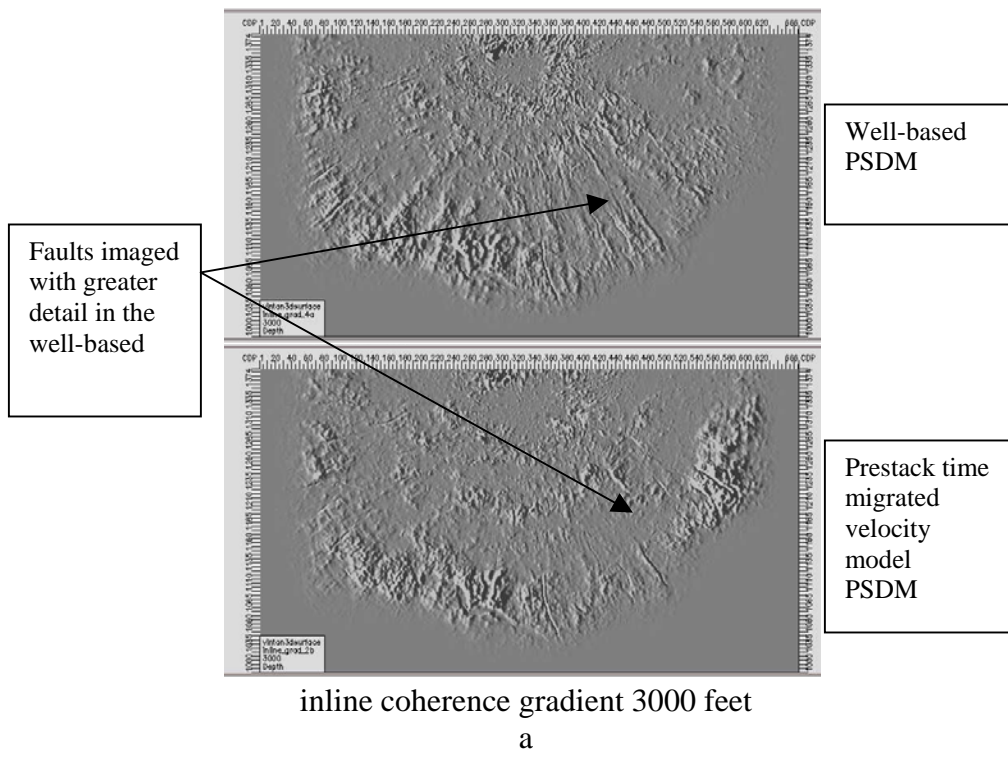


Figure 79 (continued)

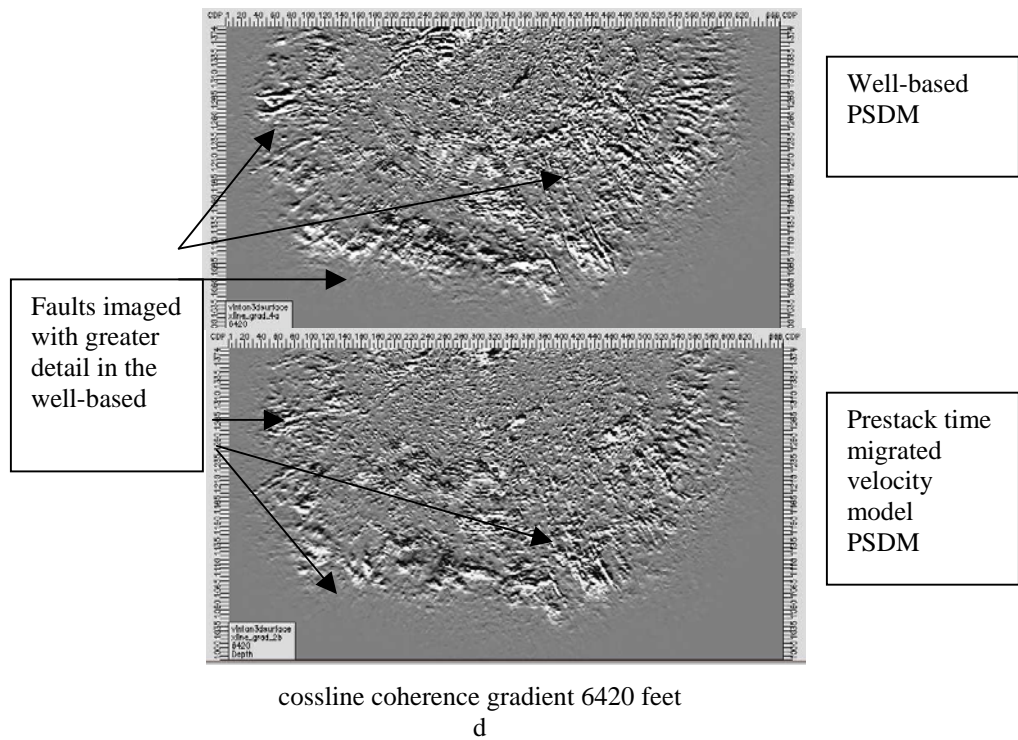
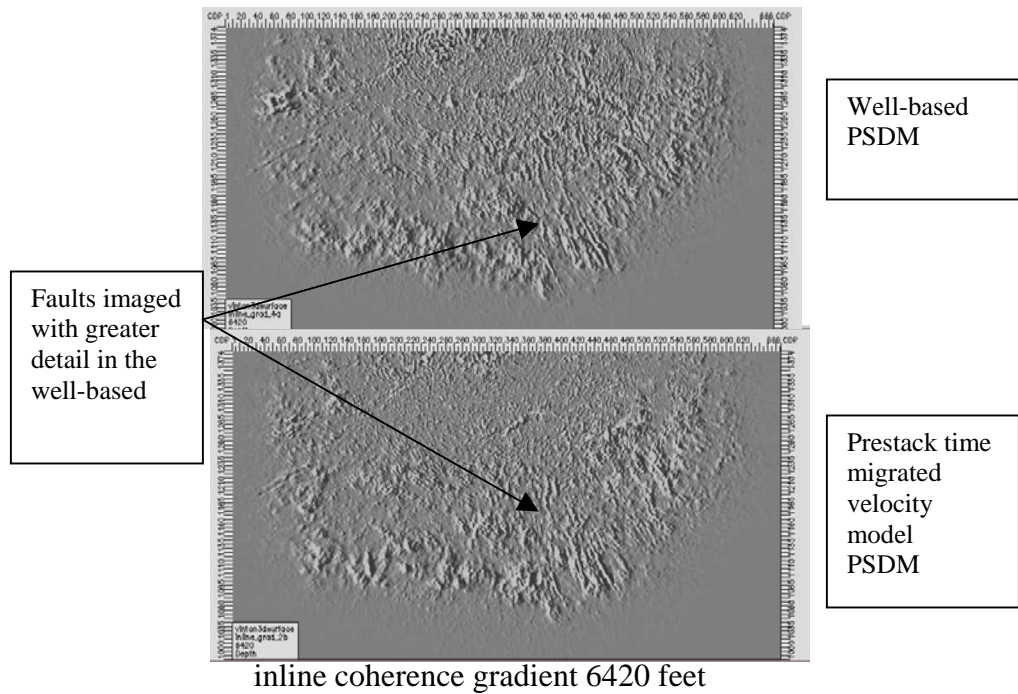


Figure 79. Inline and crossline coherent energy gradient of both the well-based and prestack time migration velocity model PSDM. Well-based gradients in both inline shallow depth (a) and crossline shallow depth (b) and inline deeper depth (c) and crossline deeper depth (d) shows sharper faults and channels.

Chapter 6 Interpretation

6.1 Introduction

Improvements I made to enhance the seismic image positively impacted data in several ways. One of the more significant improvements was providing information that permitted a higher degree of interpretation accuracy. As a final measure to assess an increase in fidelity I interpreted the data to determine if more geologic information could be gleaned. I used coherence to demonstrate an improved migration over the PSTM, data that were also valuable as an interpretation tool. I compared common image gathers (CIGs), the fidelity of the seismic sections, and well ties to the seismic for QC. Using all of the various criteria for improvement I determined that the data generated using well velocities were better suited for interpretation than those from semblance velocities.

Objectives for the interpretation were to further verify improved fidelity by providing a more detailed interpretation and to gain new insights into the geologic processes associated with Vinton Dome. I used two benchmarks to evaluate improvements in interpretation. One was imaging near the flanks of the dome assessed by higher accuracy in identifying the truncation of sediments on the flanks of the salt dome. Identification of small faults was the second benchmark I used in evaluation and well ties were used as a guide in interpretation.

A more general objective was to gain insights into the geology surrounding Vinton Dome. Three areas of interest were investigated, salt tectonics, stratigraphy, and

structure and they must complement each other in the final analysis. I designed a preliminary assessment of the geology to identify perturbations in the salt geometry along the flanks of the salt dome and I could use these to identify different stages in salt dome development. Objectives in the structural interpretation were to identify the structures and to determine the dip of the major fault controlling salt development. Stratigraphic objectives were to identify channels to determine the environment of deposition.

6.2 Methods

I interpreted the seismic and attribute data on a workstation using commercial interpretation software. Data used on the workstation were the PSDM volume, coherence data, and over 500 log curves. After I established that the seismic data I had processed and PSDM were more detailed because of higher fidelity, I used the improved image to interpret the geology.

I used information provided by the operator as a guide for identification of small, compartmentalized fault blocks. An interpretation based on well logs demonstrated the lack of resolution in the PSTM that prevented a seismic interpretation of these fault blocks (Figure 80). I used interpretation of the fault blocks from well logs as a template to identify details in the PSDM volume.

I initially based my stratigraphic interpretations on coherence data. Coherence allowed me to identify channels not imaged on the coherence derived from the PSTM. I began to

integrate stratigraphic interpretations into the geologic model to begin to piece together events related to salt tectonics.

6.3 Interpretation

6.3.1 Seismic

I was able to identify small, compartmentalized faults in the area identified by the operator on the well-based PSDM volume. A comparison of the well-based PSDM with the prestack time migrated velocity model PSDM data shows the higher resolution achieved with the well-based model (Figure 81). To determine which of the two is the proper placement I used electronic well logs to compare well ties. The well-based PSDM consistently placed the salt picked with well logs at the high acoustic impedance boundary on the surface seismic data while the prestack time migrated velocity model PSDM placed the salt pick from well logs below the high acoustic impedance boundary. Wells tie in the inline, crossline, and depth slices with the well-based data (Figure 82). Based on the correct placement of salt in the x, y, and z directions it is apparent that the prestack time migrated velocity model is too slow and the fidelity of the well-based PSDM is higher.

I was able to enhance resolution along the salt flanks with depth migration. Using sediment layers to determine where they truncate next to the salt flank, a complex geometry begins to emerge. Interpretations show the salt body is mainly a cylindrical shape with various protuberances, salt wedges, and overhangs (Figure 83).

Imaged poorly was a fault identified in the western half of the survey in the PSTM, but was focused with detail in the well-based data (Figure 84). The large fault is a normal fault clearly dipping to the north. Based on this interpretation a counter regional fault is the controlling fault for Vinton Dome.

6.3.2 Coherence

I used coherence data to identify several channels (Figure 85). These channels are at a depth that corresponds to the Miocene. To gain a better understanding of the depositional history around the dome needs further interpretation and integration of these data.

Details of the depositional history help to guide a better understanding of the sediment load that in turn impact the salt tectonics.

6.4 Conclusions and Discussion

To provide the detail needed to image structures and stratigraphy near Vinton Dome required PSDM, more precisely a PSDM migrated with a well-based sediment velocity model. Demonstration of the improved fidelity achieved through a well-based PSDM was in the details revealed in small faults and the details imaged in sediments near the salt dome. I interpreted three areas with a higher degree of accuracy than was previously available, the salt, stratigraphy, and structure.

From the interpretation of salt it appears that a transition from active diapirism to passive diapirism took place as the salt progresses upward through the section. I based my interpretation of the salt tectonics on the changes in salt geometry and the structural components associated with the salt. Improvements in the resolution provide detailed data to calculate a kinematic ratio of A/R and R/A of the salt. A kinematic ratio is a method used to determine the growth stage of the salt dome. I also used structural data such as radial faults to identify the growth stage of the salt dome.

My stratigraphic interpretations were also considerably more detailed with the PSDM volume. Of particular interest is the imaging of stream channels not imaged in the PSTM. These gave a more precise understanding of the stratigraphy and specifically the drainage systems around Vinton Dome in the Miocene. Improved resolution near the salt also provided the ability to see the influence of salt on the dip of the beds and potential areas of sand ponding.

Structural features such as the dips of beds can be significant in terms of petroleum exploration. With these data strata can be imaged beneath salt overhangs that previously were not imaged; these can be potential hydrocarbon traps. These features are also significant in understanding the salt tectonics. Other features relevant to salt tectonics are the large growth fault that controls the salt movement and the smaller radial faults that indicate passive or active diapirism. These data strongly indicate that the large controlling fault is a high angle, counter regional growth fault, further substantiating the

interpretation of the high angle growth fault in the presence of numerous radial faults on the southern side of the fault radiating from the salt dome. Radiating faults away from the salt dome on the footwall of a growth fault is typical of where active diapirism is taking place and further indicates the fault is counter regional.

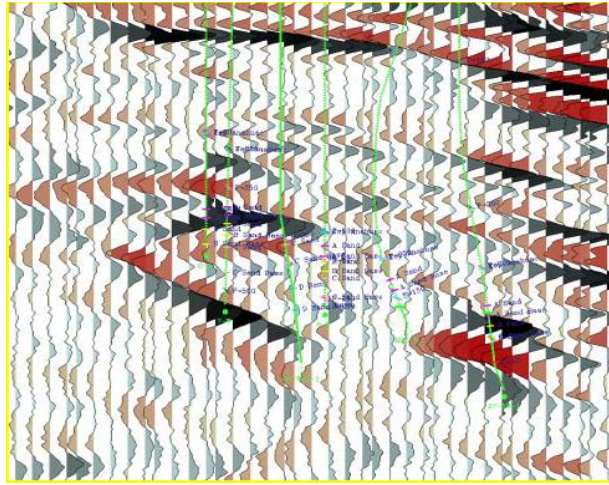


Figure 80. Interpretation based on well logs demonstrates the lack of resolution in the PSTM limiting a seismic interpretation of small fault blocks.

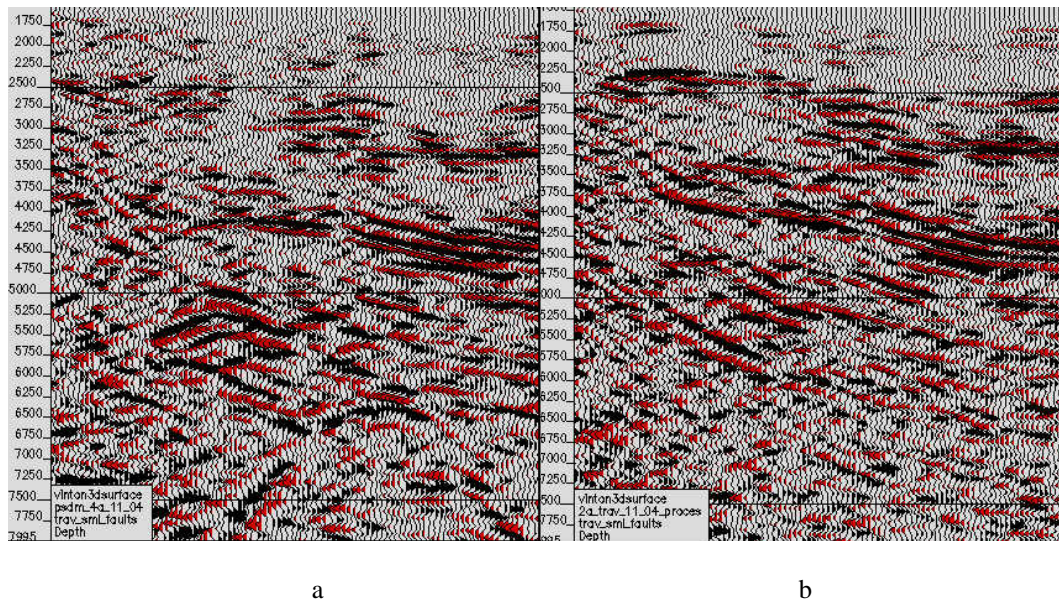
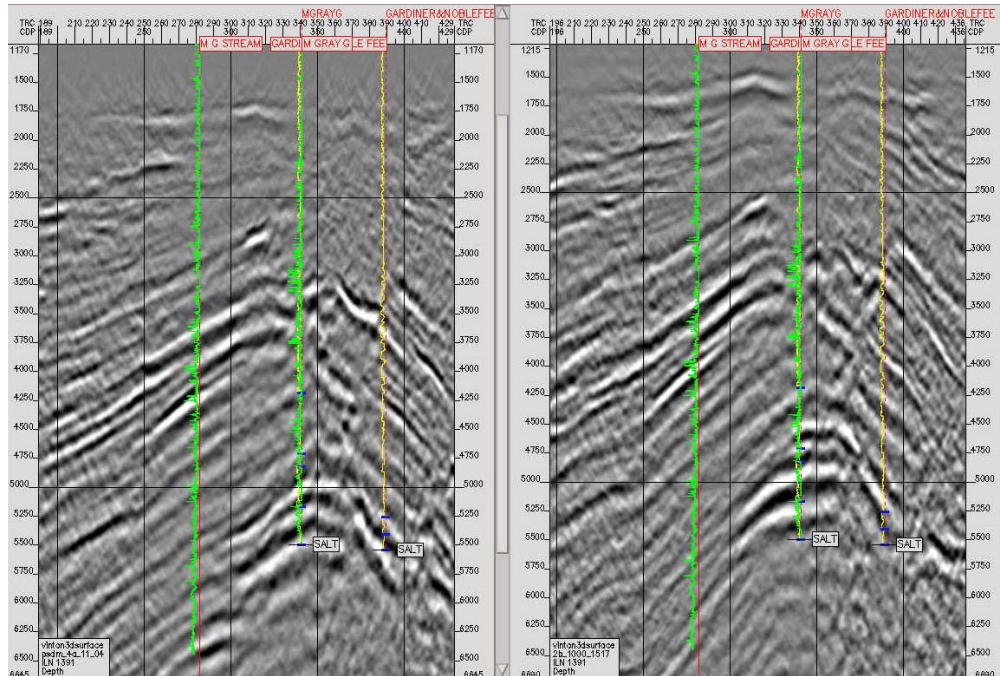
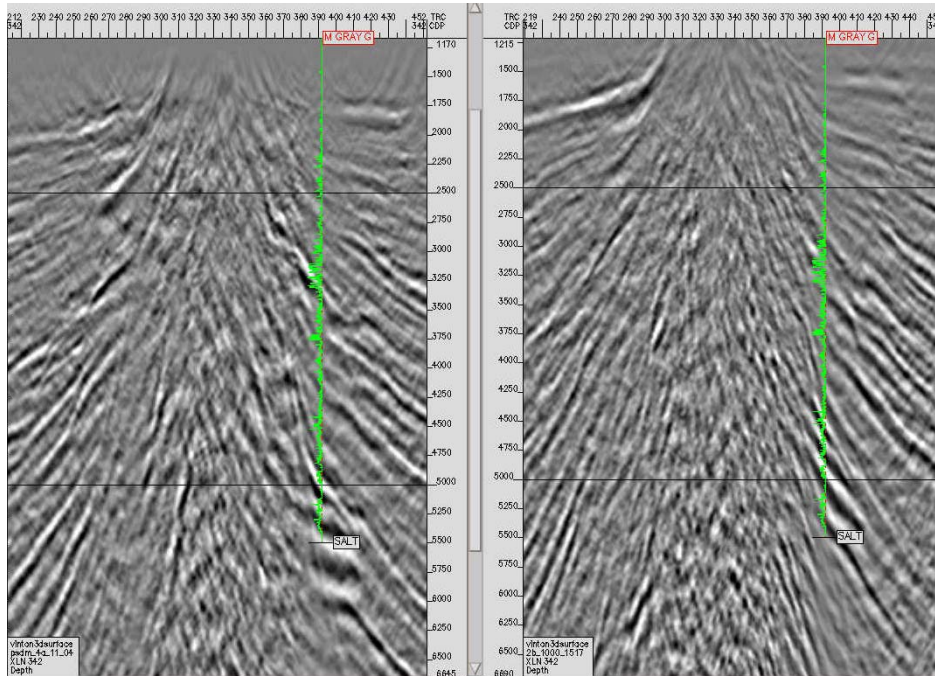


Figure 81. A comparison of well-based data (a) to the semblance-based data (b) showing the higher resolution achieved with the well-based model.



Inline 1391 well-based PSDM

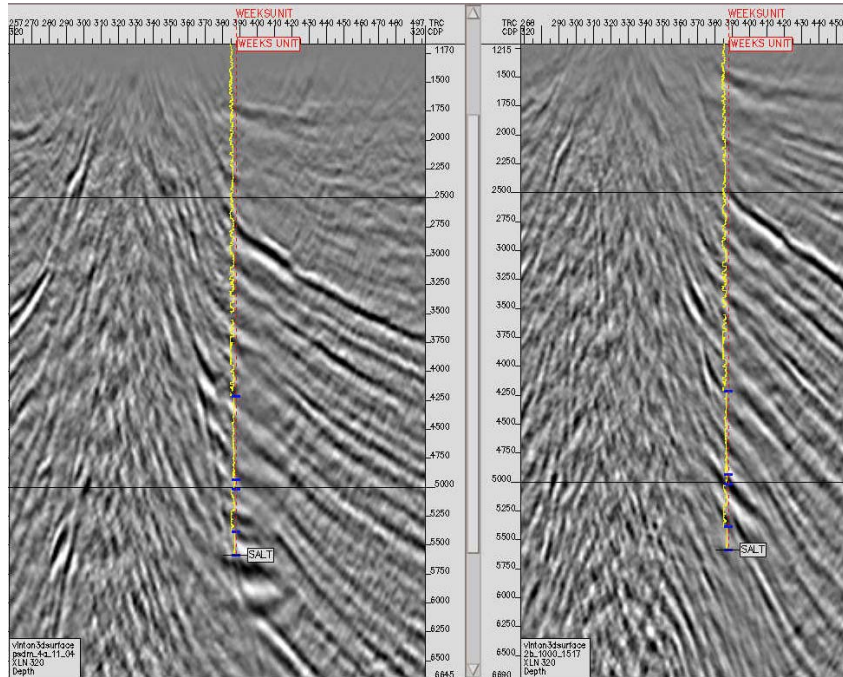
Inline 1391 prestack time migrated velocity model PSDM



Crossline 342 well-based PSDM

Crossline 342 prestack time migrated velocity model PSDM

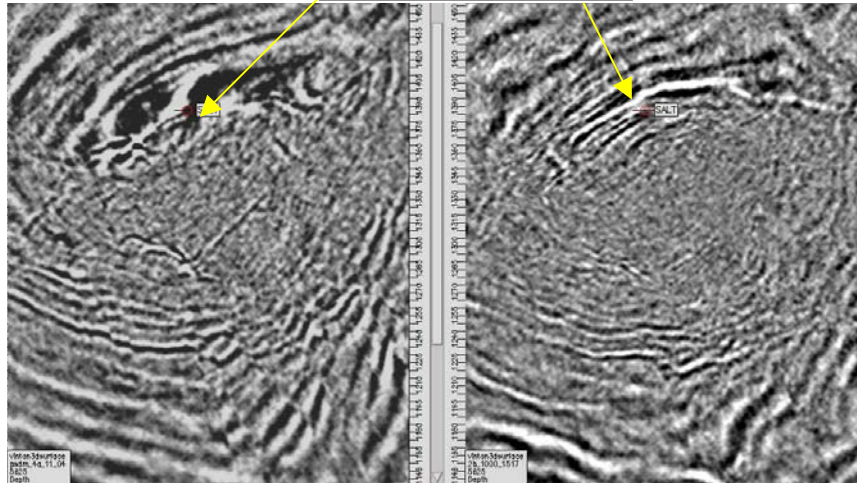
Figure 82 (continued)



Crossline 320 well-based PSDM

Crossline 320 prestack time migrated velocity model PSDM

Salt Pick from Well Log



Depth slice 5625 well-based PSDM

Depth slice 5626 prestack time migrated velocity model PSDM

Figure 82. Sections and depth slice illustrating the differences in fidelity. Well-based PSDM encounter salt at the high impedance contrast, where the prestack time migrated velocity model PSDM encounter salt below the high impedance, indicating the velocities are too slow. The depth slice illustrates that the salt is possibly an overhang from the well-based depth slice. The prestack time migrated velocity model depth slice appears to be sediment.

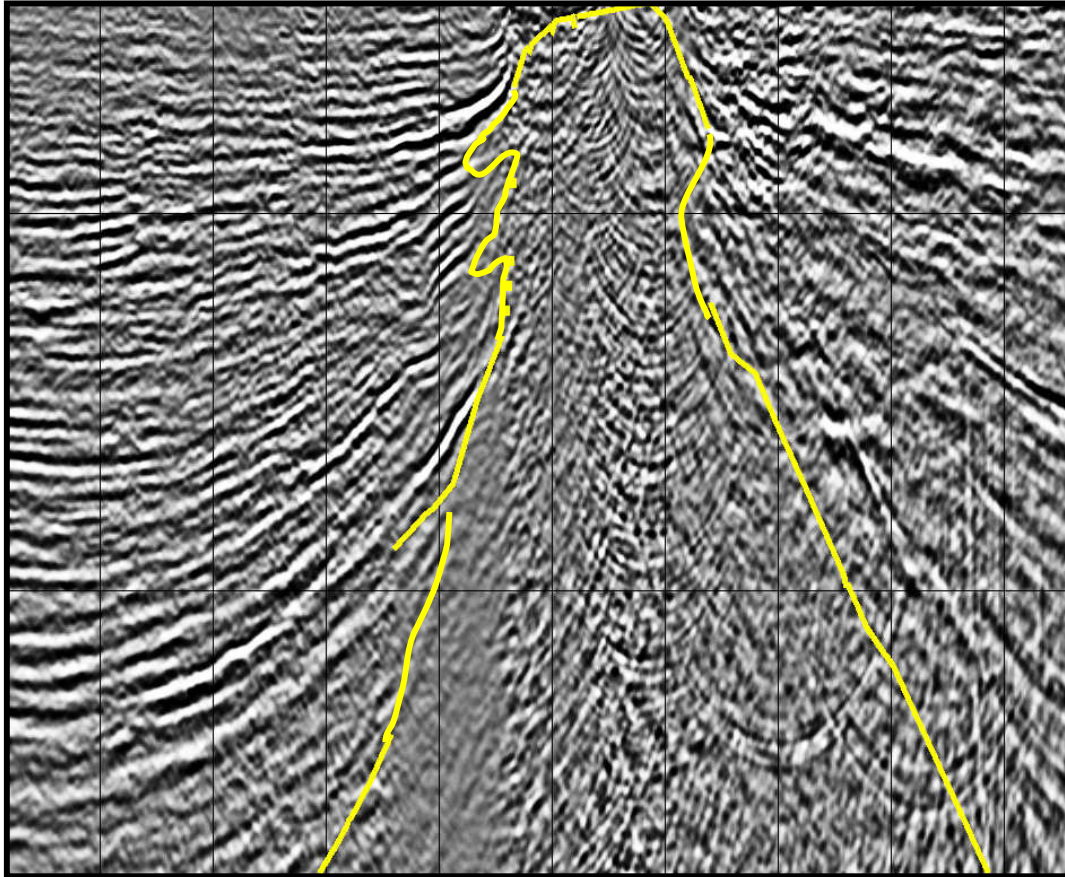
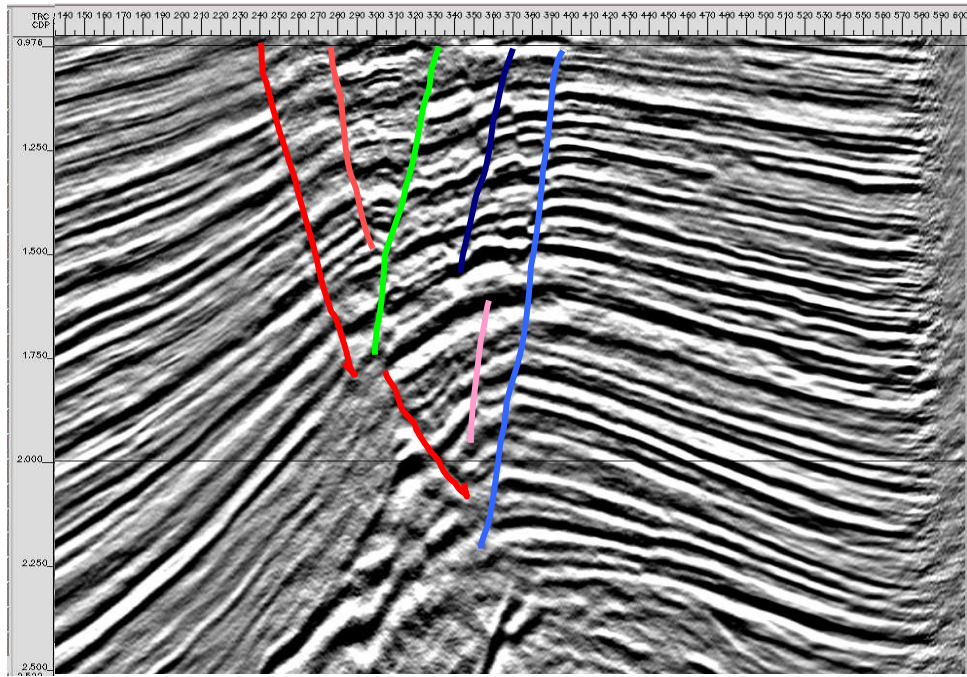
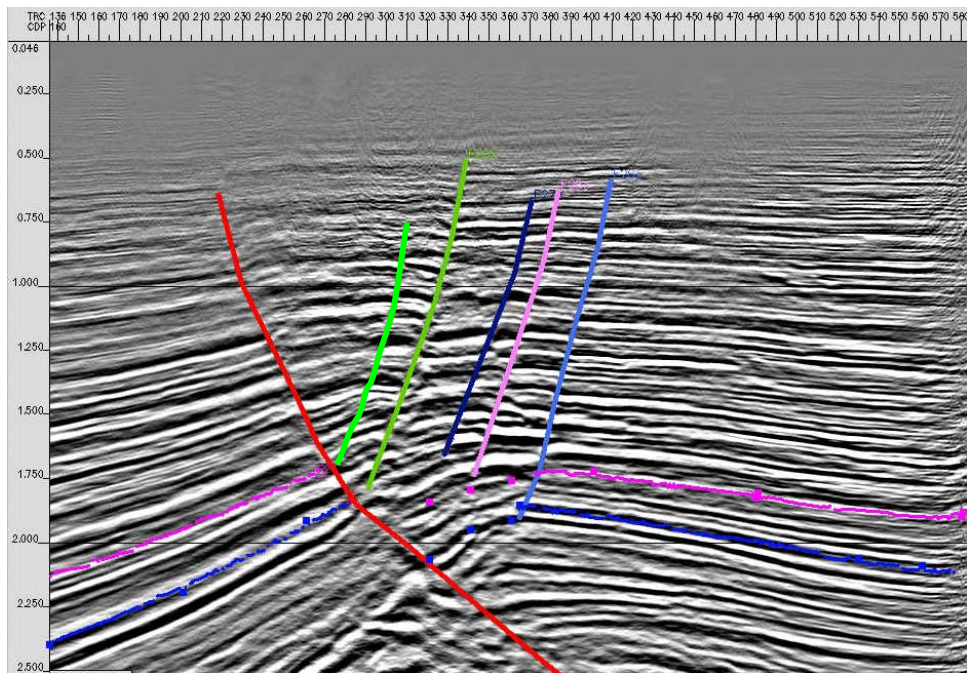


Figure 83. Interpretation showing the salt body is mainly a cylindrical shape with various protuberances, salt wedges and overhangs. Interpretation is based on various salt picks from well logs around the dome, impedance contrasts, and the truncation of sediments onto the salt.

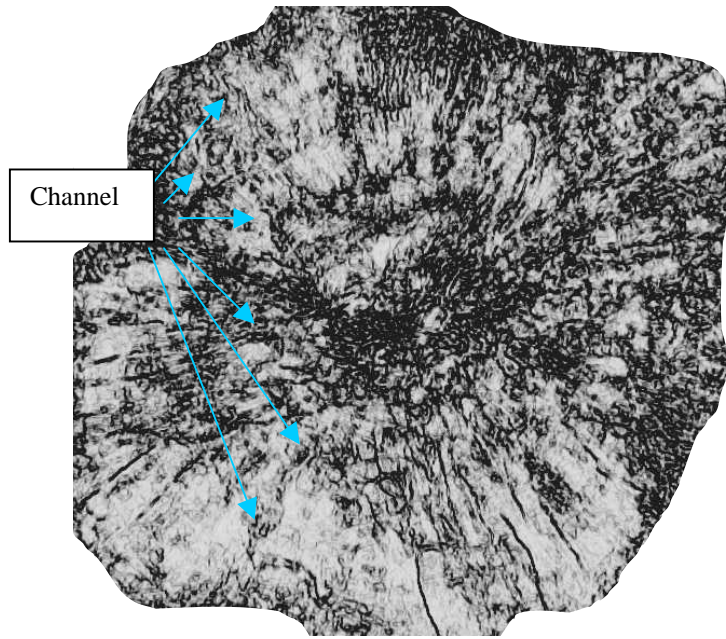


a

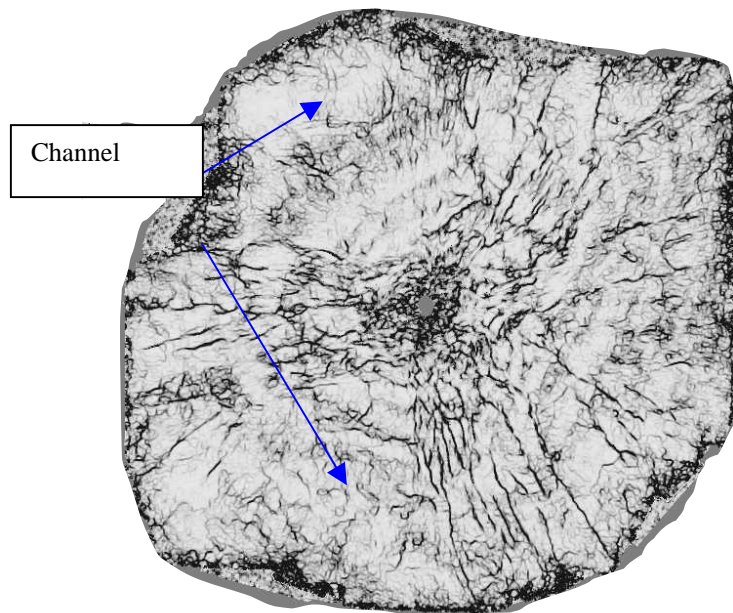


b

Figure 84. Counter regional fault in the southwest quadrant of the survey that is poorly imaged in the PSTM (a) and focus with greater detail in the well-based data (b).



a



b

Figure 85. Example of PSDM (a) coherence data used to identify one of several channels in the Miocene (2925 feet). PSTM (b) also shows channels but not with as high a resolution

Chapter 7

Conclusions and Discussion

7.1 Introduction

The goal of this study was to improve the spatial fidelity of seismic imaging through a deterministic evaluation of surface seismic data with velocity modeling and attribute analysis. To achieve the goal I modeled sediment velocities using sonic log velocities, a well-based model, and migrated using a Kirchhoff PSDM. I compared the well-based method of velocity modeling to a more traditional method of using residual migration velocities or prestack time migrated velocity model velocities to model sediment velocities for the migration. I evaluated the results through velocity analysis using CIGs, interpretation, and an innovative use of attributes as a QC tool. Using a velocity model derived from sonic logs improved the spatial fidelity of the land 3-D surface seismic data at Vinton Dome Louisiana and that coherence is an attribute for quantifying improvements is a conclusion I reached in this study.

7.2 Evaluation of Methods

7.2.1 Processing

Generally, 3-D surface seismic land data have a lower signal-to-noise ratio than 3-D marine surface seismic data because of noise sources and irregular acquisition and 3-D land surface seismic data require a higher degree of processing than do marine data. The lower signal-to-noise ratio is a reason why marine data are generally better candidates for PSDM. The goal of this study was to improve the spatial fidelity of seismic imaging using velocity modeling and attribute analysis. Field data were processed to reduce noise

yet there are several issues regarding processing of land data such as the Vinton Dome survey that are acquired in nontraditional patterns that were not addressed in this study.

The approach to processing that I took in this study was to pre-migration process the data so that they maintained a broadband and a high signal-to-noise ratio. I was able to increase the signal-to-noise ratio to a high level using a processing flow enhanced using AGC. Improving the data quality through pre-migration processing allowed the focus of the study to be on velocity modeling of the sediment velocities. There are processing issues that were beyond the scope of this study such as finding the least invasive means to remove surface waves.

Another significant issue is the need for development of an acquisition specific processing flow. Data acquisition of the 3-D surface seismic data was in a radial pattern at Vinton Dome. Processing is usually for a brick pattern 3-D seismic acquisition. The impact of a processing flow designed for brick pattern acquisition, applied to data acquired in a radial pattern is not fully understood and for the Vinton Dome survey this is an issue that should be addressed.

7.2.2 Velocity Modeling

Data migrated with a velocity model derived from sonic logs provided a superior image than PSTM data and PSDM that used a traditional prestack time migrated velocity model. Two issues that factored into this were vertical and horizontal velocities. In the seismic

domain, velocities typically travel faster in the horizontal direction than in the vertical. Factoring in the higher frequencies of sonic logs means that vertically sampled sonic logs will travel faster than vertical seismic velocities. Differences in velocities between the two domains means that in the vertical direction the sonic velocities should be faster because of higher frequencies, and in the horizontal direction seismic velocities will be faster (Stewart, 1982).

By using the faster vertical sonic velocities and extrapolating them horizontally achieved a balance between the two opposing velocity issues. I verified this three ways. One, wells did tie with the well-based velocity model seismic data, while they did not with prestack time migrated velocity modeling PSDM data. Second, far offsets in the CIGs were consistently flatter in the well-based gathers than in the prestack time migrated velocity model PSDM gathers. Three, data were migrated deeper in the well based model because of a faster overall velocity field than the prestack time migrated velocity model. Three different means of verification lead me to the conclusion that sonic logs are the optimum data for building velocity models in the Vinton Dome survey. Because Vinton Dome is typical in many regards to numerous other peircement type domes in the Upper Continental Margin of the Gulf of Mexico, it is reasonable to predict that these conclusions also apply to other areas.

7.2.3 Attributes

I used attributes to assess improvements in velocity modeling. Using attributes as a QC tool is significant because it is a nontraditional application of attributes, specifically coherence, to qualitatively evaluate velocity modeling. The standard method has been to use CIGs to update velocity models and serve as a QC of the velocity model. Completion of updating the velocity model is determined by evaluating the gathers. By using coherence as a QC tool I was able to compare different models and evaluate them based on the noise content revealed in the coherence. A coherence cube provides an evaluation of the entire survey, enables the interpreter to quickly assess the quality of the data, and isolate problem areas.

Using coherence for QC provides an efficient tool. Throughout the PSDM process the velocity model is updated and data are re-migrated. Errors incorporated into the initial sediment velocity model propagate throughout the entire process. Generating and assessing coherence quickly is a factor that makes it an attribute that is appropriate as a QC tool. A tool that is quick and efficient as coherence means that different models can be tested and evaluated. I demonstrated that attributes, specifically coherence, were used as an effective QC tool.

7.2.4 Geology

I based much of the body of research regarding the subsurface geology of the Upper Gulf of Mexico Basin on well log analysis and 2-D seismic lines. Another way to view this is

as 1-D well logs and 2-D seismic lines. 3-D data is best to build 3-D models and further expand the database. Interpretations from this study of Vinton Dome are preliminary and cursory but show both the accuracy and the shortcomings of known 3-D velocity modeling methods. An example of the accuracy is in the mapping of small, compartmentalized fault blocks using well logs. The interpretation in this study was very similar to that made with well logs. Several other such fault blocks may exist in the survey but the well control is not present to make those interpretations, but I demonstrated using the higher fidelity well-based PSDM seismic data would allow those interpretations.

Another area of interest was to begin unraveling the salt tectonics. Understanding detailed salt tectonics is not as likely using strictly well logs but I demonstrated the enhancements made with 3-D seismic. A method that holds promise is using the angle of the sediments at the salt/sediment interface to evaluate salt tectonics in the context of active vs. passive diapirism. 3-D data are essential for a complete study of this application. What I demonstrated in this study is that I can image in detail the sediment/salt interface to evaluate salt tectonics using a well-logs based velocity model to PSDM the data.

Well logs are limited to 1-D so it is difficult to use them to provide the regional details needed to interpret a 3-D geologic model. Not a single well in the Vinton Dome survey extends to the depth that I imaged with 3-D surface seismic data. 3-D PSTM surface

seismic data provided a more detailed geologic model of Vinton Dome but lacked the fidelity to image fine details. I was able to demonstrate that 3-D PSDM improves fidelity and the ability to accurately interpret the geology provided I use of the proper velocity model of sediments in the initial PSDM.

7.3 Future Work

Processing of 3-D surface seismic land data is an area where future research can be beneficial. One area that holds the potential for improvement is designing an acquisition specific workflow for processing. In the case of Vinton Dome, designing a processing workflow specifically for radial acquisition could improve the premigration processing results.

Another 3-D land surface seismic processing project is to determine the most efficient method to reduce ground roll while maintaining broadband bandwidth. There are several ways to approach this problem, but further research will determine the most appropriate method to reduce ground roll. Maybe the method I used was the best, so further research in this area needs to make comparisons with my results.

My primary emphasis in this study was to develop a robust initial sediment velocity model. As a case study it is appropriate to recognize that my results may be particular to Vinton Dome. What this study provides is a benchmark for future studies in the field of sediment velocity modeling for PSDM of 3-D surface seismic land data. Examining the

effects of geology such as the impact of the inclination of strata on the velocity model is one area of future work. An explanation for the success of using a well-based velocity model for the PSDM is that sonic log velocities in dipping strata sample the horizontal velocity.

My study has provided a benchmark for seismic data, especially land data acquired over piercement salt domes and provides an opportunity to use data from this study to further the understanding of the geology of Vinton Dome and the surrounding areas. Details regarding structure and salt tectonics integrated along with the stratigraphy will yield greater precision. Building on the initial improvements in the geologic model of Vinton Dome will lead to a fuller understanding of geology.

7.4 Conclusions and Discussion

PSDM are not common to 3-D land surface seismic data, there are several reasons for this some I have mentioned. A motivation for this study was to apply the current state-of-the-art technology to data over a mature oil field. The goal of this study was to improve the spatial fidelity of seismic imaging through a deterministic evaluation of surface seismic data with velocity modeling and attribute analysis. To achieve the goal and fulfill the motivations behind the study current methods had to be either modified or replaced. Identification of areas needing improvement required an assessment of current methods and testing. Testing allowed for data to be pre-migration processed in a manner that

reduced the noise in the field data and provided a high enough signal-to-noise ratio that made them suitable for PSDM.

3-D surface seismic land data contain noise that is not as common in 3-D marine data. 3-D surface seismic land data noise is one of the principle issues to address to accurately model sediment velocities for a PSDM. Errors incorporated into an initial, sediment velocity model will propagate throughout the iterative PSDM process resulting in spurious data. At best, non-unique solutions result from the resolution of noise issues through processing in 3-D surface seismic land data. Non-uniqueness was a motivation for using a non-seismic method, specifically sonic logs, to model initial sediment velocities. Comparing PSDM volumes generated from a well-log velocity model to a traditional seismically derived velocity model demonstrates the improvements that result from the well-log velocity modeling method. I based comparisons on analysis of CIGs and an innovative use of coherence attributes as a QC tool.

Steeply dipping beds tend to diminish the accuracy of a PSTM as demonstrated in this study. To overcome the effects of steeply dipping beds and lateral velocity changes induced by salt, data are PSDM. Using geologic horizons from the PSTM domain and integrating them with depth interval velocities from sonic logs the two domains are merged. Using an accurate velocity to convert time picked horizons to depth allows the horizons to be accurately spaced from each other. By extrapolating the velocities vertically between each horizon, I was able to insert a smooth and accurate velocity

between each horizon throughout the velocity model. Using well logs to generate the initial sediment velocity provides a novel approach to generating an accurate velocity model for PSDM resulting in higher fidelity for 3-D surface seismic land data.

I demonstrated how to derive an accurate initial sediment velocity model by using the depth interval velocities from sonic logs. Methods developed and used in the study resulted in a more accurate initial sediment velocity model than one derived from seismic data and the methods are more efficient than seismically derived initial sediment velocity models. What is not resolved is if these results are particular to this case study alone. The conclusion is that because 3-D surface seismic land data are prone to low signal-to-noise ratios for several reasons, an initial sediment velocity model derived from sonic logs will reduce the adverse effects of the noise. Further updates will not be prone to maintaining spurious data frequently introduced to the data that use traditional seismic or prestack time migrated velocity models for the PSDM. I found that by minimizing the effects of spurious data using the well-based velocity modeling approach for the initial sediment model it is appropriate to use a traditional flow to update the velocity model and re-migrate the data to further enhance the fidelity.

I investigated using attribute analysis, specifically using coherence as a QC tool in this study. Use of this method provides another tool for velocity modeling, especially for the critical initial sediment velocity model. Applying coherence as a QC tool was efficient and allowed a qualitative assessment of velocity models. There is a need for QC tools for

PSDM data to evaluate velocity modeling; the method developed for this study helps address the need.

Finally, the reason I needed to enhance the fidelity was to improve the geologic model of Vinton Dome. By imaging small, compartmentalized faults and determining the dips of faults a clearer structural picture of Vinton Dome has emerged. A more detailed understanding of depositional details is now possible by imaging channels and gaining a better understanding of sediment distribution. Results from my research provided data to further study how structure and deposition both interrelate with the salt tectonics and the timing of these three components. Based on my observations, active diapirism continued through the Frio and became passive through the Miocene. I also observed that the controlling fault through Vinton Dome is counter-regional, not regionally dipping as presented in the literature. This observation needs further study because the dip of the controlling fault has an impact on the salt tectonics.

References

- Al Husseini, M. I., Glover, J. B., and Barley, B. J., 1981, Disspersion patterns of the ground roll in eastern Saudi Arabia, *Geophysics*, **46**, 121-137.
- Alvarez, G., 1995, A comparison of moveout-based approaches to ground-roll and multiple suppression: M.Sc. Thesis, Colorado School of Mines.
- Bahorich, M. S., and Farmer, S. L., 1995, 3-D seismic discontinuity for faults and stratigraphic features: The Leading Edge, **14**, 1053-1058.
- Constance, P. E., Holland, M. B., Roche, S. L., Bicquart, P., Bryans, B., Gelinsky, S., Ralph, J. G., and Bloor, R.I., 1999, Simultaneous acquisition of 3-D surface Seismic data and 3-C, 3-D VSP data, 69th Ann. Internat. Mtg., Soc. Expl. Geophys., Expanded Abstracts, 104-107.
- Cox, M. J. G., 1999, Static corrections for seismic reflection surveys, *in*, Scherrer, E. F., and Chen, R. eds., *Geophysical Reference Series*, **9**, Society of Exploration Geophysicists.
- Curtis, D. M., 1970, Miocene deltaic sedimentation, Louisiana gulf coast: *in*, Morgan, J. p., ed., *Deltaic sedimentation, modern and ancient: Soc. Econ. Paleontologists and Mineralogists Special Pub. 15*, 293-308.
- D'Agosto, C., 2002, Modeling and removal of ground roll from horizontal component of c-waves: M.Sc. Thesis, University of Houston.
- Diegel, F. A., Karlo, J. F., Schuster, D. C., Shoup, R. C., and Tauvers, P. R., 1995, Cenozoic structura; evolution and tectonostratigraphic framework of the Northern Gulf Coast continental margin, *in* Jackson, M. P. A., Roberts, D. G., and Snelson, S., eds., *Salt tectonics a global perspective: AAPG Memoir 65*, 109-151
- Dix, C. H., 1955, Seismic velocities from surface measurements, *Geophysics*, **20**, 68-86.
- Duncan, W. S., and Marfurt, K. J., 2003, Improved attributes for interpretation and QC of the Vinton Dome 3-D surface seismic, 73rd Ann. Internat. Mtg., Soc. Expl. Geophys., Expanded Abstracts, 2199-2202.
- Evans, B. J., 1997, A handbook for seismic data acquisition in exploration, *in* Fitterman, D. V., and Dagoet Jr., W. H., Eds., *Geophysical Monograph Series*, **7**, Society of Exploration Geophysicists.
- Fagin, S., 1999, Model-based depth imaging, *in* Young R. A., Ed., *Course Notes Series*,

10, Society of Exploration Geophysicists.

Fliedner, M., Crawley, M., Bevc, D., Popovici, A. M., and Biondi, B., 2002, Velocity model building by wavefield-continuation imaging in the deepwater Gulf of Mexico: The Leading Edge, **21**, 1232-1236.

Galloway, W. E., Hobday, D. K., and Magara, K., 1982, Frio formation of Texas gulf coastal plain: Depositional systems, structural framework and hydrocarbon distribution: Am Assn. Petr. Geol. Bull., v. 66, no. 6, 649-688.

Galloway, W. E., 1989, Genetic stratigraphic sequences in basin analysis II: application to northwest Gulf of Mexico Cenozoic basin: Am. Assn. Petr. Geol. Bull., **73**, 143-154.

Galloway, W. E., Ganey-Curry, P. E., Li, X., and Buffler, R. T., 2000, Cenozoic depositional history of the Gulf of Mexico basin: Am Assn. Petr. Geol. Bull., v. 84, no. 11, 1743-1774.

Gersztenkorn, A., and Marfurt, K. J., 1999, Eigenstructure-based coherence computations as an aid to 3-D structural and stratigraphic mapping: Geophysics, **64**, 1468-1479.

Gersztenkorn, A., and Marfurt, K. J., 1996a, Coherence computations with eigenstructures: 58th Conf. and Tech. Exhibition, Eur. Assn. Geosci. Eng., Expanded Abstracts, X031.

Gersztenkorn, A., and Marfurt, K. J., 1996b, Eigenstructure based coherence computations: 66th Ann. Internat. Mtg., Soc. Expl. Geophys., Expanded Abstracts, 328-331.

Gersztenkorn, A., Sharp, J., and Marfurt K., 1999, Delineation of tectonic features offshore Trinidad using 3-D seismic coherence: The Leading Edge, **18**, 1000-1008.

Gibson, R. L. and Tzimeas, C., 2002, Quantitative measures of image resolution for seismic survey design: Geophysics, **67**, 1844-1852.

Girdler, G. H., and Whitmarsh, R. B., 1974, Miocene evaporites in Red Sea cored, their relevance to the problem of the width and age of oceanic crust beneath the Red Sea: *in* Initial Reports of the DSDP, **23**: R. B. Whitmarsh, O.E. Weser, and D. A. Ross *et al.*, Eds., Washington D. C., U. S. Govt. Printing Office, 913-921.

Guo, N., and Fagin, S., 2002a, Becoming effective velocity-model builders and depth imagers, part1-the basics of prestack depth migration: The Leading Edge, **21**, 1250-1209.

Guo, N., and Fagin, S., 2002b, Becoming effective velocity-model builders and depth

imagers, part2-the basics of velocity-model building, examples and discussion: The Leading Edge, **21**, 1210-1216.

Hilterman, F. J., 2001, Seismic amplitude interpretation, *in*, 2001 Distinguished Instructor Short Course, Distinguished Instructor Series, **4**.

Humphris, C. C., Jr., 1978, Salt movement on continental slope, northern Gulf of Mexico, *in* Framework, Facies, and Oil-Trapping Characteristics of the Upper Continental Margin, Bouma, A. H., Moore, G. T., and Coleman, J. M., Eds., Studies in Geology no. **7**: Am. Assn. Petr. Geol., 69-85.

Jackson, M. P. A., and Talbot, C. J., 1986, External shapes, strain rates, and dynamics of salt structures, Geol. Soc. of Am. Bull., **97**, 305-323

Judson, D. R., Lin, J., Schultz, P.S., and Sherwood, J. W. C., 1980, Depth migration after stack: Geophysics, **45**, 376-393.

Laughton, A. S., 1970, A new bathymetric chart of the Red Sea: Royal Soc. London Phil. Trans., Series A, **269**, 21-22.

LeVie, D. S., 1986, Interdomal Sediment ponding: a new Lower Hackberry play?: Gulf Coast Association of Geological Societies Transactions, v. 35, 171-178.

Letouzey, J., Colletta, B., Vially, R., and Chermette, J. C., 1995, Evolution of salt-related structures in compressional settings, *in* Jackson, M. P. A., Roberts, D. G., and Snelson, S., eds., Salt tectonics a global perspective: AAPG Memoir 65, 41-60.

Liu, W., Popovici, A., Bevc, D., and Biondi, B., 2001, 3-D migration velocity analysis for common image gathers in reflection angle domain, 71st Ann. Internat. Mtg., Soc. of Expl. Geophys., Expanded Abstracts, 925-928.

Lowell, J. D., Genik, G. L., Nelson, T. H., and Tucker, P. M., 1975, Petroleum and plate tectonics of the southern Red Sea, *in* Petroleum and global tectonics, A. Fischer, L. Judson, Eds.: Princeton University Press, 129-153.

Lowrie, A., 1994, Seismic stratigraphy and hydrocarbon traps: Louisiana onshore and Offshore, *in* Domenico, S. N., ed., Course notes series, No. 5: Society of Exploration Geophysics.

Manning, E., 1990, The early Miocene Sabine River: Gulf Coast Association of Geological Societies Transactions, v.40, 531-549.

Marfurt, K. J., Duncan, W. S., Constance, P., 2002, Comparison of 3-D edge detection seismic attributes to Vinton Dome Louisiana: 73rd Ann. Internat. Mtg., Soc. Expl. Geophys., Expanded Abstracts, 577-580.

- Marfurt, K. J., Kirilin, R. L., Farmer, S. L., and Bahorich, M. S., 1998, 3-D seismic attributes using a semblance-based coherency algorithm: *Geophysics*, **63**, 1150-1165.
- Martin, R.G., 1978, Northern and eastern gulf: framework, *in* Framework, Facies, and Oil-Trapping Characteristics of the Upper Continental Margin, Bouma, A. H., Moore, G. T., and Coleman, J. M., Eds., *Studies in Geology* no. **7**: Am. Assn. Petr. Geol., 21-42.
- Nelson, T. H., 1991, Salt tectonics and listric-normal faulting, *in* Salvador A., ed., *The geology of North America. Vol. J, The Gulf of Mexico basin*, The Geol. Soc. of Am., 73-89.
- Paine, W. R., 1968, Stratigraphy and sedimentation of subsurface Hackberry wedge and associated beds of southwestern Louisiana: *Am Assn. Petr. Geol. Bull.*, v. **52**, 322-342.
- Peel, F. J., Travis, C. J., and Hossack, J. R., 1995, Genetic structural provinces and salt tectonics of the Cenozoic offshore U.S. Gulf of Mexico: a preliminary analysis , *in* Jackson, M. P. A., Roberts, D. G., and Snelson, S., eds., *Salt tectonics a global perspective: AAPG Memoir 65*, 153-175.
- Popovici, A. M., Fleider, M> M., Crawley, S., Ritchie, W., Stewart, K., Lau, A., and Yin, C., 2003, Building Gulf of Mexico piercement-type velocity models with wave-equation depth migration: 2003 Spring Symposium, Depth Imaging: Proceedings of the Geophysical Society of Houston.
- Rietveld, W. E., Kommedal, j. H., and Marfurt, K. J., 1999, The effect of prestack depth migration on 3-D seismic attributes: *Geophysics*, **64**, 1553-1561.
- Rowan, M. G., 1995, Structural styles and evolution of allochthonous salt, central Louisiana outer shelf and upper slope, *in* Jackson, M. P. A., Roberts, D. G., and Snelson, S., eds., *Salt tectonics a global perspective: AAPG Memoir 65*, 199-228.
- Salvador, A., 1987, Late Triassic-Jurassic Paleogeography and Origin of Gulf of Mexico Basin: *Am. Assn. Petr. Geol. Bull.*, **71**, 419-451.
- Schlager, W., 1981, The paradox of drowned reefs and carbonate platforms: *Geological Society of America Bull.*, v. **92**, 197-211.
- Schultz, P., 1999, The seismic velocity model as an interpretation asset, *Distinguished Instructor Series*, **2**, Society of Exploration Geophysicists.
- Stewart, R. R., Huddleston, P., and Kan, T. K., 1982, Traveltime analysis and vertical seismic profiles, 52nd Ann. Internat. Mtg: Soc. Of Expl. Geophys., Session:S12.4.
- Tabbi-Annani, A., 1975, Subsurface geology of south central Calcasieu Parish, Louisiana: M.Sc. Thesis, The University of Southern Louisiana.
- Talbot, C. J., 1995, Molding of salt diapirs by stiff overburden, *in* Jackson, M. P. A.,

Roberts, D. G., and Snelson, S., eds., Salt tectonics a global perspective: AAPG Memoir 65, 61-75.

Vendeville, B. C., and Jackson M. P. A., 1992, The rise of diapirs during thin-skinned extension: *Marine and Petroleum Geology*, v. 9, p.331-371.

Winker, C. D., and Buffler, R. T., 1988, Paleogeographic evolution of early deep-water Gulf of Mexico and margins, Jurassic to middle Cretaceous (Comanchean): *Am. Assn. Petr. Geol. Bull.*, **72**, 318-346.

Winker, C. D., 1982, Cenozoic shelf margins, northwestern Gulf of Mexico: *Gulf Coast Assn. Geol. Soc.*, **32**, 427-428.

Yilmaz, O., 1987, Seismic data processing, *in*, Doherty, S. M., ed., *Investigations in Geophysics*, **2**, Society of Exploration Geophysicists.